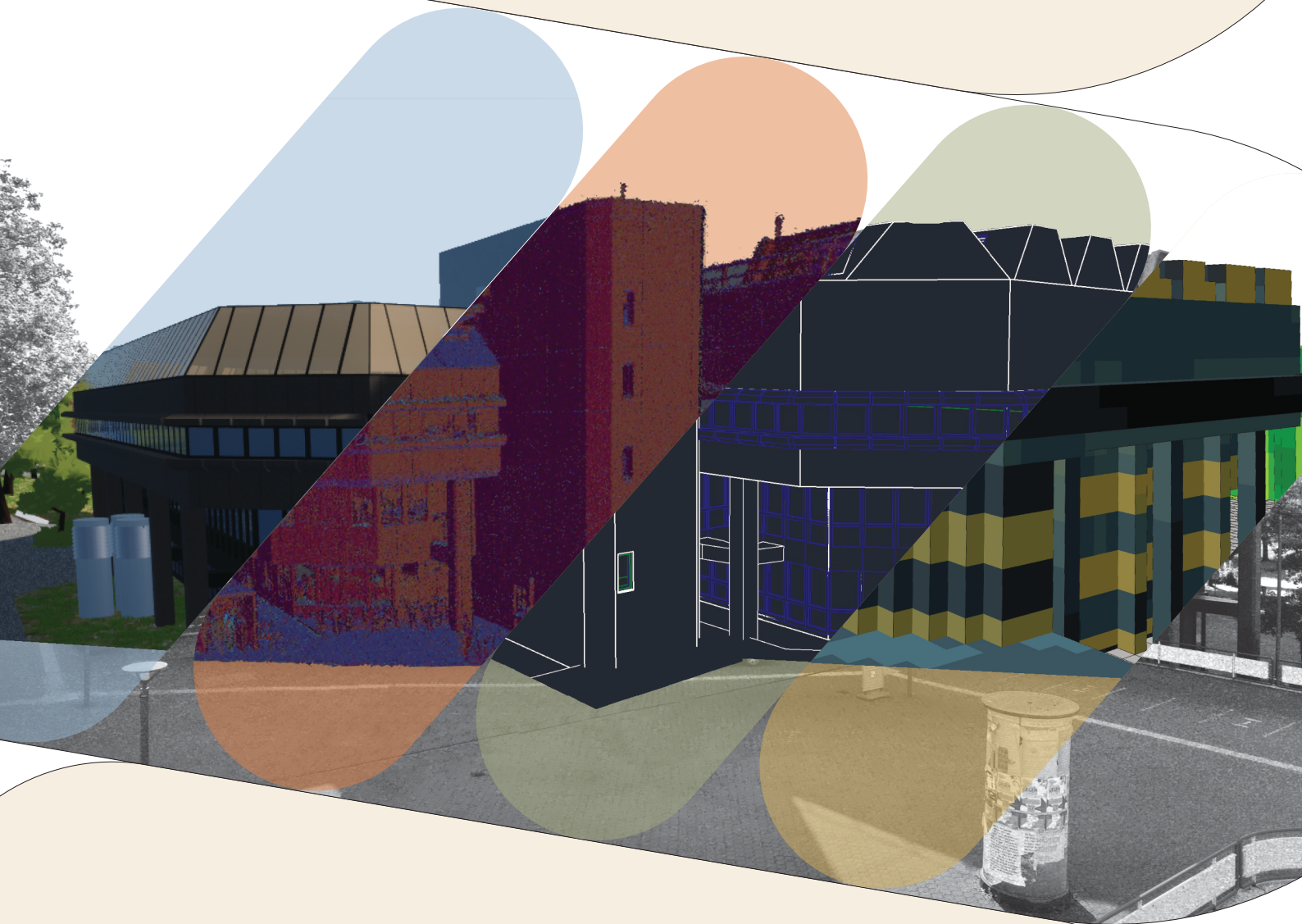


M01

Digital Twin, Microclimate
Simulations, and Dynamic
Visualization of the Central
Library of TU Dortmund
University



Final Report

M01 Digital Twin, Microclimate Simulations, and Dynamic Visualization of the Central Library of TU Dortmund University

Final Report

Jens Kirsten

Nhat Anh Pham

Leonard-Louis Range

Kai Schröer

Konstantin Wickert

Nadine Winter

Supervisors:

Prof. Dr. Thinh Nguyen

Jasmin Latko, M.Sc.

Research Group of Spatial Information Management and
Modelling (RIM)

TU Dortmund University

March 19, 2024

Abstract

The term Digital Twin essentially describes the creation of a virtual replica and its networking with its real physical counterpart. In the context of the digitization efforts of municipalities, the term is now increasingly being used in the context of spatial planning. There, great potential can be assumed, especially against the backdrop of the advancing climate change, for example with regard to the simulation and visualization of climate impacts in urban spaces. Even if this potential seems to be clearly outlined, at least on paper, it is still unclear how this potential can be leveraged in practice. Also unclear is the positive contribution that can be expected from the high spatial detail of digital building models to the accuracy of often coarsely modeled climate simulations.

Therefore, this study aims to identify the application potential of Digital Twins of buildings in the context of spatial planning by means of a literature review and to identify possibilities of combining the process of Digital Twin creation with microclimate simulations in an explorative case study using the example of the Central University Library of the TU Dortmund. One focus of the work is the dynamic visualization of the Digital Twin and the climate simulation results. To this end, a unified conceptual understanding of Digital Twins will be established and practical examples of how the term is understood and its potential applications will be presented. Subsequently, the work process from the creation of a laser scan-based, detailed 3D building model to the execution of various microclimate simulations and dynamic visualization possibilities of the Digital Twin is presented.

The discussion of practical examples of Digital Twins in spatial planning showed that their practical application is still in an early stage. It also became clear that the understanding of the term Digital Twin in practice and research often differs and that in many practical cases, including the results of this work, the term Digital Shadow should rather be used. As for the microclimate simulations, the effects of three variations of the modeling on the simulation results could be illuminated. According to this, the size of the study area, but also the spatial resolution of the whole model seem to have a low influence on the results, while the influence of the LoD could not be clearly clarified. Finally, several tools for dynamic visualization of the results could be successfully applied in the context of the work. However, it became clear that their application requires certain technical knowledge (e.g. programming languages), which in turn may deter many spatial planners from using them.

Keywords: Digital Twin, Dynamic Visualization, ENVI-met, Microclimate Simulations, Virtual Reality

Zusammenfassung

Der Begriff des Digitalen Zwillings beschreibt im Wesentlichen die Erstellung eines virtuellen Abbilds und dessen Vernetzung mit seinem realen, physischen Counterpart. Im Rahmen der Digitalisierungsbestrebungen von Kommunen findet sich der Begriff nun auch vermehrt in raumplanerischen Kontexten wieder. Dort lässt sich insbesondere vor dem Hintergrund des voranschreitenden Klimawandels großes Potenzial vermuten, etwa was die Simulation und Visualisierung von Klimafolgen in Räumen der Stadt betrifft. Auch wenn jenes Potenzial zumindest auf dem Papier klar umrissen scheint, so unklar stellt sich derzeit hingegen noch der konkrete Weg zum Heben jener Potenziale dar. Ungewiss ist indes auch der positive Beitrag, der vom hohen räumlichen Detailgrad digitaler Gebäudemodelle für die Genauigkeit von oftmals grob modellierten Klimasimulationen zu erwarten ist.

Die vorliegende Arbeit verfolgt daher das Ziel, die Anwendungspotenziale von Digitalen Zwillingen von Gebäuden im Kontext der Raumplanung mit Hilfe einer Literaturrecherche aufzudecken und möchte im Rahmen einer explorativen Fallstudie am Beispiel der Universitätsbibliothek der TU Dortmund jene Wege dafür aufzeigen, wie der Erstellungsprozess eines Digitalen Zwillings mit mikroklimatischen Simulationen kombiniert werden kann. Ein Fokus der Arbeit liegt dabei auf der dynamischen Visualisierung des Digitalen Zwillings und der Klimasimulationsergebnisse. Dafür wird zunächst ein einheitliches Begriffsverständnis von Digitalen Zwillingen etabliert und Praxisbeispiele im Selbstverständnis dieses Begriffs sowie deren Anwendungspotenziale vorgestellt. Anschließend wird der Arbeitsprozess von der Erstellung eines laserscan-basierten, detaillierten 3D Gebäudemodells über die Durchführung verschiedener mikroklimatischer Simulationen bis hin zu dynamischen Visualisierungsmöglichkeiten des Digitalen Zwillings dargelegt.

In Auseinandersetzung mit raumplanerischen Praxisbeispielen von Digitalen Zwillingen konnte festgestellt werden, dass deren praktische Anwendung derzeit noch in einem frühen Stadium verhaftet ist. Dabei ist auch deutlich geworden, dass sich das in der Praxis und Forschung angelegte Begriffsverständnis des Digitalen Zwillings oftmals unterscheidet und dass in vielen praktischen Fällen, so auch im Ergebnis dieser Arbeit, eher die Rede von Digitalen Schatten sein sollte. Was die mikroklimatischen Simulationen angeht, so konnten die Auswirkungen von drei Variationen der Modellierung auf die Simulationsergebnisse beleuchtet werden. Demnach scheint die Größe des Untersuchungsgebiets, aber auch die Gitterauflösung des Modells einen gewissen Einfluss auf die Ergebnisse zu haben, wohingegen der Einfluss des LoD der Gebäude nicht eindeutig geklärt werden konnte. Letztlich konnten im Rahmen der Arbeit unterschiedliche Werkzeuge zur dynamischen Visualisierung der Ergebnisse erfolgreich zum Einsatz gebracht werden. Jedoch ist dabei deutlich geworden, dass deren Anwendung ab einem bestimmten Punkt gewisse technische Kenntnisse voraussetzt (bspw. Programmiersprachen), was wiederum viele Raumplaner*innen

von deren Anwendung zurückschrecken lassen könnte.

Schlüsselwörter: Digitaler Zwilling, Dynamische Visualisierung, ENVI-met, Mikroklimasimulationen, Virtuelle Realität

Acknowledgements

The project group would like to thank all the people who helped us during the process of this study and without whom this study could not have been realized. First and foremost, we would like to thank our supervisors, Prof. Dr. Nguyen Xuan Thinh and M.Sc. Jasmin Latko. Through their guidance, professional expertise and organizational support, they were an important part of the success of this project. We would also like to thank Dr. Thomas Schulz for providing the technical equipment and the premises of the Center for Entrepreneurship & Transfer of TU Dortmund University as well as for the mediated contacts. Furthermore, we would like to thank the team of RIM for providing expertise and further help during the process of this study. Also, we would like to thank Andreas Rabe and Frank Demant for granting us access to the roof of the library to install the sensors, which are essential for the creation of a Digital Twin. Finally, we gratefully acknowledge the support of DTN Meteogroup for providing us with the weather data needed for the microclimate simulation.

Contents

Abbreviations	k
1. Introduction	1
2. Research Design	3
2.1. Research Questions	3
2.2. Methodological Approach	4
2.3. Study Area	6
3. Literature Review	11
3.1. Digital Twin	11
3.2. Microclimate Simulations	15
3.3. Dynamic Visualization	20
4. Procedure and Results	25
4.1. Data Overview	25
4.2. Creating a 3D Model of the Central University Library	25
4.2.1. Laser Scanning	25
4.2.2. Clean Up and Merge Point Clouds	28
4.2.3. Revit	35
4.3. LoRaWan and Weather Sensors	38
4.3.1. Installation of Sensors and Gateway	38
4.3.2. Sensor Data Management	39
4.4. Microclimate Simulations with ENVI-met V5.5.1	42
4.4.1. Overview - ENVI-met System and Simulation Models	42
4.4.2. Creating of 3D Models of the Study Areas	44
4.4.3. Preparing and Running the Simulation Files	48
4.4.4. Results of the Microclimate Simulations	52
4.4.5. Verification and Evaluation of Simulation Results	52
4.5. Visualization of Results	66
4.5.1. ArcGIS Online/ArcGIS Dashboard	66
4.5.2. VR Application	70
5. Discussion	77
5.1. Answering the Research Questions	77
5.2. Reflecting on this Study's Findings	78
6. Conclusion and Further Research	83
References	87

A. LoRaWAN and Weather Sensors	II
A.1. Photos of Exact Gateway and Sensor Positions	II
B. ENVI-met Input Data	III
B.1. ENVI-met Grid Rotation	III
B.2. Facade and Roof Materials of the Basic Model (DB Manager)	III
B.3. Soil Materials (DB Manager)	IV
B.4. Simple Plants (DB Manager)	V
B.5. ENVI-guide Forcing Precision	V
B.6. Local Weather Data	VI
C. Grid Cell Coordinates for Verification	VIII
D. ENVI-met Simulation Results	IX

Abbreviations

ABP	Authentication By Personalisation
AI	Artificial Intelligence
AR	Augmented Reality
CFD	Computational Fluid Dynamics
DEM	Digital Elevation Model
FTP	File Transfer Protocol
ICP	Iterative Closest Point
IoT	Internet of Things
LBC	Lateral Boundary Conditions
LiDAR	Light Detection and Ranging
LoD	Level of Detail
LoRaWAN	Long Range Wide Area Network
OTAA	Over The Air Authentication
PLS	Personal Laser Scanning
RIM	Research Group of Spatial Information Management and Modelling
RMSE	Root Mean Square Error
SLAM	Simultaneous Localization and Mapping
SUA	Smart Urban Areas
TLS	Terrestrial Laser Scanning
TTN	The Things Network
UAV	Unmanned Aerial Vehicle
UHI	Urban Heat Island
VR	Virtual Reality
WP	Work Package

List of Figures

1.	Layers of IoT-Integration	2
2.	Research Overview	4
3.	Workflow from 3D Laser Scanning to Dynamic Visualizations	5
4.	Weather Averages Dortmund by Month	6
5.	Locations of the Wwo Campuses North and South as Well as H-Bahn Line	8
6.	Current (left) and Future (right) Central University Library Building . . .	8
7.	Extended Study Area with Narrow Study Area and Walkable Area in VR Highlighted	10
8.	Overview - Level of Detail	12
9.	Simulation of the City of Zurich	13
10.	3D-Mesh of the City of Helsinki	14
11.	Solar Energy Potential of the City of Helsinki	14
12.	Predicted Refurbishment Impact of Buildings of the City of Helsinki	15
13.	Difference Between a Digital Shadow and a Digital Twin	15
14.	Stages of a Digital Model	16
15.	Urban Heat Island	17
16.	ENVI-met Model Architecture	19
17.	AR Application in Vienna	20
18.	VR Application in Herrenberg Study	21
19.	Example Interactive Parameter Control. Text Appears After Pressing a Button	22
20.	Example Dynamic Manipulation. Change in Time of Day	22
21.	Dynamic Point Clusters of Twitter Micro-Posts, in Combination With Path Patterns of Foreign Tourists and Their Temporal Variations in the City of Rotterdam	23
22.	This Project was Conducted Using ZEB-HORIZON & GeoSLAM Hub . . .	27
23.	Schematic Overview of the Library's Division into Seven Partially Over- lapping Parts for the PLS Data Collection Process	28
24.	Data Acquisition by Seven Parts Followed by Red, Purple, Blue, Pink and Yellow Lines and Two Circles on the Roof of the Central University Library	31
25.	Screenshots of the Yellow Point Cloud Section in its Raw Form (left) and Segmented Form (right)	32
26.	Z-axis Rotation of Red Section to Fit Yellow (here displayed in blue)(left) and Almost Overlapping Sections with Need for a Little Rotation (right) .	32
27.	CloudCompare's Cross Section Tool	32
28.	Aligned and Registered Roof Sections with Partly Uncovered Areas	33
29.	The Final Point Cloud with Merged Facades and Roof Sections	33

30.	Detailed Cleanup Process in Autodesk ReCap Pro (top) and its Result (bottom)	34
31.	Floor Plan of Point Cloud/Walls with Measurements (left), Length Measurements of Windows	36
32.	Comparison to the Floor Plan at the Second Level	36
33.	Finished Revit Model	37
34.	LSN50v2-S31 Operates with DLOS8N Outdoor LoRaWAN Gateway in the LoRaWAN Network	39
35.	Locations of the Gateway and Weather Sensors	40
36.	Placement of Gateway and Weather Sensors	40
37.	Configuration of the PHP Script's Config File with Individual Information	41
38.	Excerpt of the Database	42
39.	Difference in Level of Detail - Model in LoD3 (INX1; left) vs. LoD2 (INX2; right), Soil Not Displayed	45
40.	Difference in Study Area Extension - Models of INX3 (left) and INX4 (right)	45
41.	Difference in Grid Resolution - Model in 1 m x 1 m x 1 m (INX 2 ; left) vs. 5 m x 5 m x 5 m (INX 3, right); Soil Not Displayed	45
42.	Difference in Grid Resolution - Model in 5 x 5 x 5 (INX 4 ; left) vs. 2 x 2 x 3 (INX 5, right); Soil Not Displayed	45
43.	Concepts of Vertical Grids	47
44.	Potential Air Temperature of INX 5 at a Z-Height of 2,1 m at 08:00, 14:00 and 20:00	53
45.	Potential Air Temperature of INX 5 at a Z-Height of 13,5 m at 08:00, 14:00 and 20:00	53
46.	Potential Air Temperature of INX 4 at a Z-Height of 2,5 m at 08:00, 14:00 and 20:00	53
47.	Wind Speed of INX 5 at a Z-Height of 2,5 m at 08:00, 14:00 and 20:00	54
48.	Potential Air Temperature of INX 3 at a Z-Height of 2,5 m at 08:00, 14:00 and 20:00	54
49.	Potential Air Temperature of INX 2 at a Z-Height of 2,5 m at 08:00, 14:00 and 20:00	54
50.	Wind Speed of INX 3 at a Z-Height of 2,5 m at 08:00, 14:00 and 20:00	54
51.	Influence of the LoD 2 and LoD 3 of the Central University Library on the Simulation of Air Temperature in the Narrow Study Area, Compared to the Measured Values	58
52.	Influence of the LoD 2 and LoD 3 of the Central University Library on the Simulation of Relative Humidity in the Narrow Study Area, Compared to the Measured Values of All Four Sensors	59

List of Figures

53.	Influence of the Study Area Extent on the Simulation of Air Temperature, Compared to the Measured Values of All Four Sensors	60
54.	Influence of the Study Area Extent on the Simulation of Relative Humidity, Compared to the Measured Values	61
55.	Influence of the Grid Resolution of 1 m x 1 m x 1 m (INX2) vs. 5 m x m 5 m x m 5 (INX3) on the Simulation of Air Temperature, Compared to the Measured Values of All Four Sensors	62
56.	Influence of the Grid Resolution of 1 m x 1 m x 1 m (INX2) vs. 5 m x 5 m x 5 m (INX3) on the Simulation of Relative Humidity, Compared to the Measured Values of All Four Sensors	63
57.	Influence of the Grid Resolution of 2 m x 2 m x 3 m (INX5) vs. 5 m x 5 m x 5 m (INX4) on the Simulation of Air Temperature, Compared to the Measured Values	64
58.	Influence of the Grid Resolution of 2 m x 2 m x 3 m (INX5) vs. 5 m x 5 m x 5 m (INX4) on the Simulation of Relative Humidity, Compared to the Measured Values	65
59.	Content of the .txt File	66
60.	Content of the .txt File for the VR Application	66
61.	Weather Data of the .txt File in .geojson Format	67
62.	Sensors in ArcGIS Online	67
63.	Model Created in ArcGIS Pro	68
64.	Running .py Script for Downloading the .geojson Files	69
65.	Sensors in ArcGIS Dashboard	69
66.	3D-Visualization of the Central University Library With Sensors	70
67.	Mensabrücke and Mensa Building	71
68.	Before (left) and After (right) Landscape Modeling	72
69.	Example of Texture for the Library Building's Facade	72
70.	Before (left) and After (right) the Addition of Props to the Surroundings	72
71.	Structure of the Used .txt Files	73
72.	Running the Python Script via Cmd.exe	74
73.	Basic Blueprint Design for Reading and Writing Sensor Data from a Single .txt File	74
74.	Automatically Updated Display of Sensor Values in the Running VR Application	74
75.	Automatically Played Climate Simulation Videos in the Running VR Application	75
76.	Rotating TU Logo in the Running VR Application	75
77.	Button-Triggered Display of Sensor Values in the Running VR Application	76

List of Tables

1.	Overview of Data	26
2.	Number of Identifiers for Gateway and End Devices	39
3.	Overview of Performed Simulations	43
4.	ENVI-met Software Applications	44
5.	Overview - Model Geometry of Area Input Files	49
6.	Comparison of Units Used by the DTN Weather Station and ENVI-met . .	50
7.	Overview - Simulation Parameters	51
8.	The Correlation Coefficient (R) and Root Mean Square Error (RMSE) for the Verification of the Simulated Air Temperature (T) for Each Model on 31 May 2023	56
9.	The Correlation Coefficient (R) and Root Mean Square Error (RMSE) Between the Measured and Modeled Relative Humidity (RH) for Each Study Area Extent and Selected Day	57

1. Introduction

Digitization is advancing rapidly in many areas of life and around the world. In work, home offices and other remote working concepts are global megatrends. In Germany, 12.9% of the employed population reported working from home in 2019, and this number has almost doubled to 24.8% in 2021 (Statistisches Bundesamt 2023). This trend is not limited to Europe (Felstead & Reuschke 2020; Pénard & Coulanges 2020; STATEC n.d.), but is taking place all over the world (Barrero et al. 2021; Bick et al. 2021). In everyday life, applications based on artificial intelligence (AI) are also likely to become increasingly prevalent due to their free availability and consumer-friendly, easy-to-use interfaces (Chen 2023; Gordijn & ten Have 2023; Kurian et al. 2023). Indeed, AI technology and digitization have made great strides in recent years, and it's not surprising that cities, as the center of most of the world's life, have not been left untouched. Urban areas in particular, where 80% of the world's population is expected to live by 2050 (BMZ n.d.), play a key role in the implementation of digitization efforts due to their quantitative weight, infrastructure and diverse fields of application. In the context of smart city strategies, cities essentially aim to connect urban functions and areas, as well as to collect, integrate, and process a wide range of data in order to enable a more (resource) efficient and higher quality of life and economy in the city (Wiener Stadtwerke 2011: 6).

Depending on the context, possible measures can cover a wide spectrum, ranging, for example, from automatic street light adjustment in Oslo to participatory data visualization in London (Cisco 2014; Kitchin 2013: 7f.). In some cases, urban spaces are reconstructed virtually as so-called Digital Twins.¹ Within this controlled virtual environment, it is possible, for example, to feed in measurements from the real world, to simulate various scenarios virtually on the basis of selected parameters, and finally to derive optimization proposals for the real environment (Kite-Powell 2022). An important component of this is the Internet of Things (IoT), which essentially describes the networking of mostly compact and mobile physical objects equipped with sensors and actuators that can collect data and trigger actions in the interaction between real and virtual environments (Madakam et al. 2015: 165, Figure 1).

Especially in the field of urban planning, Digital Twins seem to offer a wide range of potential applications. For example, 3D building models designed as part of new planning projects can be embedded in the virtual context of the city in order to better assess the potential impacts of the development or to make planning content even more visual and accessible for participation processes (Dembski et al. 2020; Deutscher Städtetag 2017). In view of climate change and the need for mitigation and adaptation, Digital Twins also allow more precise conclusions to be drawn during the planning process about energy efficiency and the energy required to ensure a comfortable indoor climate (e.g., by

¹For a discussion of this paper's understanding of the term Digital Twin, see Chapter 3.1 Digital Twin.

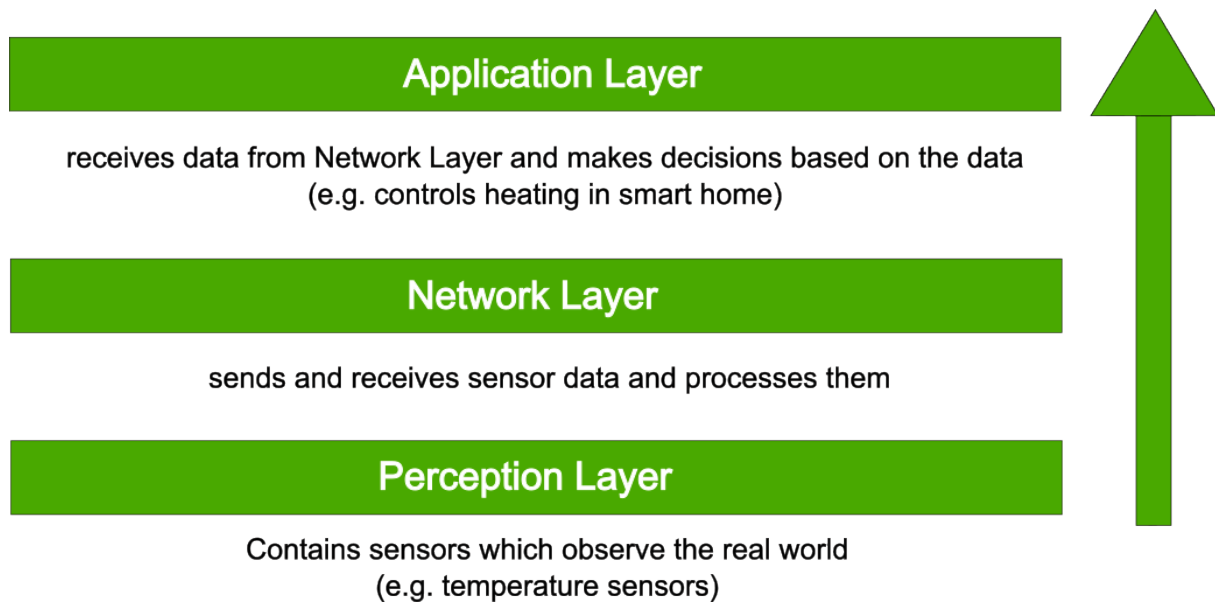


Figure 1: Layers of IoT-Integration (own illustration based on Wang 2022: 72)

the specification of wall and window materials) (Caprari et al. 2022: 14). The issue of energy efficiency in the building sector also plays a central role in Europe’s climate protection strategies due to the enormous potential for reducing CO₂ emissions (Großmann 2020: 199). In addition, climate simulations based on digitized existing buildings offer the opportunity to implement specific optimization measures on the real building or in the building environment that have been evaluated as effective in advance. Unlike new planning projects, where buildings are typically digitally modeled from the outset, the creation of 3D-models in the context of an existing environment occurs after the building is constructed. As this process can be very time-consuming, this project raises questions about its efficiency and return on investment.

This study explores the application potential of Digital Twins in microclimate simulations and their dynamic visualization. Chapter 2, Research Design, presents the objectives and research questions, the methodological approach, and the study area. Subsequently, Chapter 3, Literature Review, offers a review of the current literature on Digital Twins in spatial planning practice, microclimate simulations, and dynamic visualization. Chapter 4, Procedure and Results, provides an overview of the data used in this study, explains each individual work package and programs used, and presents the results obtained. This serves as a basis for the interpretation of the results in Chapter 5, Discussion, as well as for the identified limitations of this study. Finally, the research findings are summarized and reflected in Chapter 6, Conclusion and Further Research.

2. Research Design

2.1. Research Questions

This project is part of a series of studies on the topics of smart urban areas, the greening of buildings, the understanding and application of Digital Twins, and augmented and virtual reality as part of the Research Group of Spatial Information Management and Modelling (RIM) at the TU Dortmund University. This includes the ongoing project *Smart Urban Areas (SUA) – Sustainable System Solutions for Urban Development*², the student project 2022/23 *Development and use of Digital Twins for campuses in Dortmund and Ho Chi Minh City for climate adaptation measures*³, the master student project 2021/22 *Digital Planning: Chances and Limits of Innovative Visualization Technologies for Spatial Planning*⁴ (see Gisa et al. 2022) and the master thesis of Jasmin Latko. Focusing on the Central University Library of the TU Dortmund University, this study addresses the aforementioned context of an already existing environment (in an exploratory manner) by creating a Digital Twin of the library building and using its data for climate simulations of the spatial environment. As the library will be demolished by spring 2024, the Digital Twin will also be used to archive this unique building for posterity (TU Dortmund n.d.-a). Therefore, *the aim of this study is to explore the application potential of a Digital Twin of a building in the context of spatial planning, microclimate simulation, and dynamic visualization of results.* To achieve this aim, the study is further operationalized through three research questions that address the research objectives, the current research gaps in the literature, and help to move the planning and design towards a more interconnected, more efficient, and smarter future.

1. *To what extent are Digital Twins of buildings currently used in practice and what are possible applications in spatial planning?*
2. *What influence does the input 3D model's detail and extent have on the climate simulation and how do simulated and measured values differ at the location of the Central University Library of TU Dortmund University?*
3. *What are possible options for a dynamic visualization of simulated and measured climate data at the location of the Central University Library of TU Dortmund University?*

In addition to the research questions, this paper also aims to provide a kind of working guide on how to create Digital Twins of buildings, how to prepare and conduct microcli-

²<https://www.smarturbanareas.de/>

³<https://rim.raumplanung.tu-dortmund.de/lehre/studentische-projekte/f-projekte/f06-1/>

⁴Original: Digitale Planung: Chancen und Grenzen innovativer Visualisierungstechnologien für die Raumplanung

mate simulations in ENVI-met, and how to dynamically visualize the results of microclimate simulations.

2.2. Methodological Approach

The research process is divided into seven work packages (WP) based on the research questions (Figure 2):

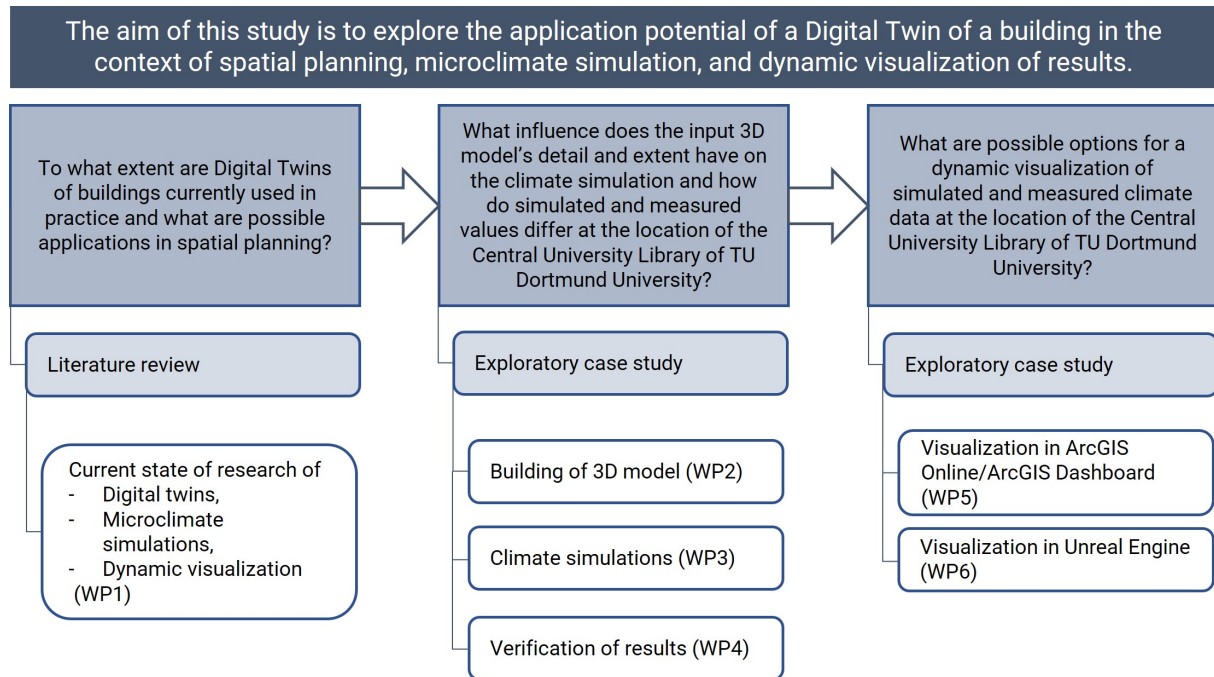


Figure 2: Research Overview (own illustration)

The first research question is addressed in one work package (WP1) based on a literature review and provides the theoretical framework for the project. An overview of the current literature on Digital Twins, climate simulations and dynamic visualizations is given and important keywords are defined. Furthermore, current applications of Digital Twins of buildings in spatial planning are identified. For this purpose, relevant scientific literature as well as practical information sources, e.g. websites of municipalities, are reviewed. This background information is necessary for the evaluation of the final results.

The subsequent case study is based on the Central Library of the TU Dortmund University. The second research question, divided into three main task groups, involves the construction of a detailed 3D model based on point clouds of the library building. Light Detection and Ranging (LiDAR) and Simultaneous Localization and Mapping (SLAM) technologies are used, as well as the software CloudCompare and Autodesk Revit (WP2). Next to that a 3D model is created and a climate simulation is done using SketchUp Pro and ENVI-met (WP3). Furthermore, weather sensors are installed and embedded in a Long Range Wide Area Network (LoRaWAN), while permanent data records are collected in a MySQL database to be used for the verification of the climate simulation. This is

done by using the programming languages R and Python (WP4).

The third research question is divided into two work packages, which include several forms of visualizations of the simulation results and real-time weather data. A static 3D model of the library and the weather sensors is created. A 2D visualization in ArcGIS Online and ArcGIS Dashboard shows a possible way to display Digital Twins dynamically in map format. Since Digital Twins are characterized by dynamic data integration, the data measured by the sensors are embedded in the application and updated in real time. The map is supported by a visualization of the library building's 3D model indicating the locations of the sensors (WP5). With the dynamic visualization of the 3D model in VR using Unreal Engine, the possibilities of integrating simulation results and real-time data into an immersive environment are explored (WP6). Figure 3 gives a diagrammatic overview of the workflow from the 3D laser scanning to the dynamic visualizations.

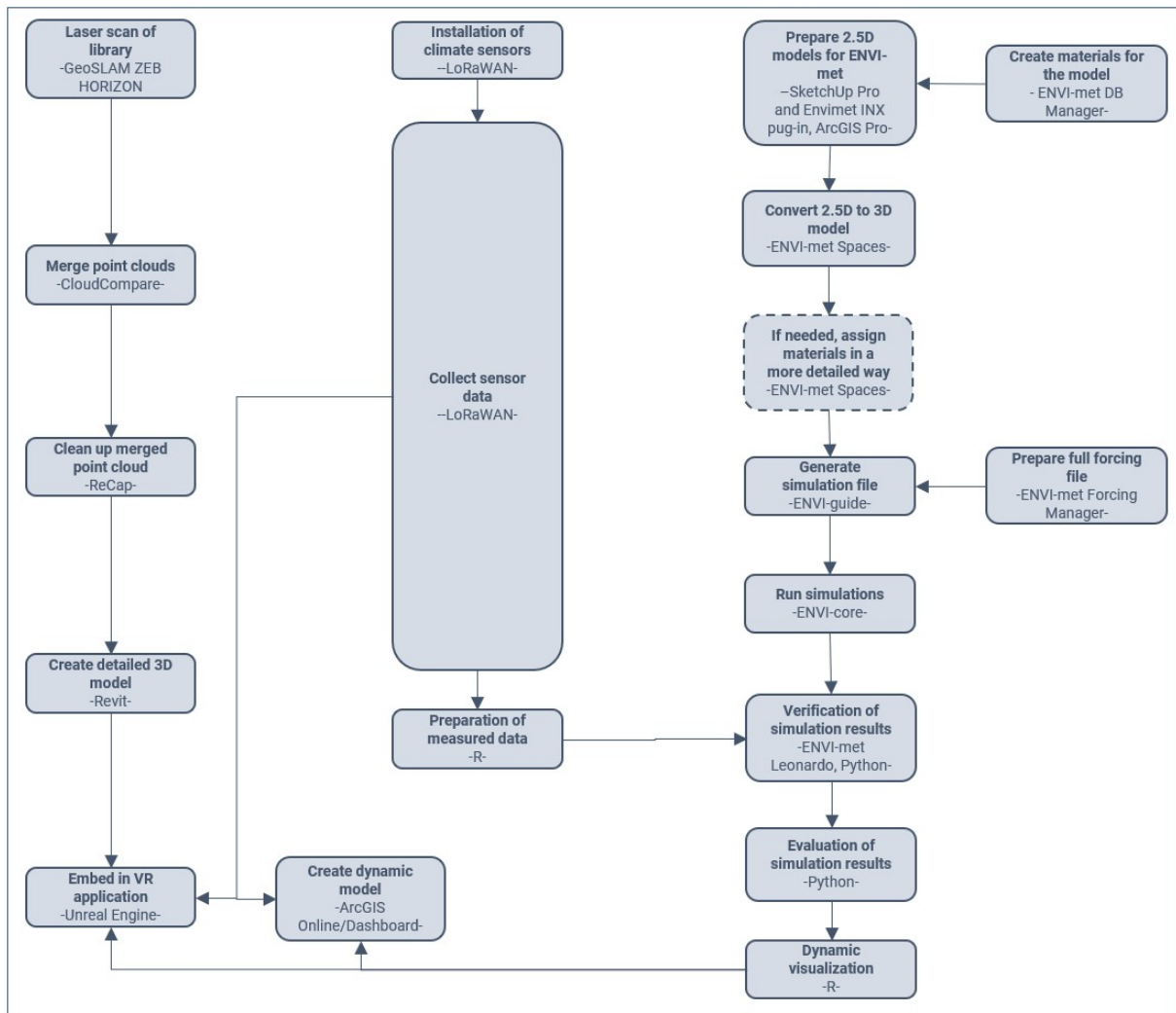


Figure 3: Workflow From 3D Laser Scanning To Dynamic Visualizations (own illustration)

2.3. Study Area

Dortmund is a district-free city in North Rhine-Westphalia and is located in the eastern part of the Ruhr area. The north, east and southeast of the city border on the Unna district, the south and southwest on the city of Hagen and the Ennepe-Ruhr district, the west on the city of Bochum and the northwest on the Recklinghausen district. With around 610.000 inhabitants (as of 31 December 2022) and 280,7 km² Dortmund is ahead of Essen, Duisburg and Bochum both the most populous and the largest city in terms of area in the Ruhr metropolitan region (Statistisches Bundesamt 2022, Dortmunder Statistik 2023).

The city of Dortmund shows varying population densities across its twelve city districts, which can be attributed to the different building structures present in the city area (Stock 2019: 9f.). While the inner-city districts of East, North, and West have densities of between 5.000 and 3.800 inhabitants/km², the districts of Mengede, Scharnhorst, and Hombruch have much lower population densities of less than 1.700 inhabitants/km² (ibid.: 10). According to Stock (ibid.), the local climatic characteristics of a city are significantly influenced by a variety of factors, including building density and land use, as well as other factors such as relief and surface roughness. Dortmund is located in the macroclimatic region known as Northwest Germany, which extends from the North Sea coast to the southern areas of the Eifel and Westerwald regions and the eastern side of the Sauerland region (ibid.). Located in the westerly wind belt and close to the Atlantic Ocean, this region experiences a maritime climate characterized by cool summers and mild winters (Figure 4). Regionally, most of the city of Dortmund is located in the Münsterland climate zone, while the southern and southeastern parts fall under the Sauerland climate zone (ibid.).

	January	February	March	April	May	June	July	August	September	October	November	December
Avg. Temperature °C (°F)	2.3 °C (36.2) °F	2.8 °C (37) °F	5.7 °C (42.2) °F	9.8 °C (49.6) °F	13.7 °C (56.7) °F	16.8 °C (62.2) °F	18.7 °C (65.7) °F	18.2 °C (64.8) °F	15 °C (59.1) °F	11.1 °C (51.9) °F	6.6 °C (43.9) °F	3.4 °C (38.1) °F
Min. Temperature °C (°F)	0.1 °C (32.2) °F	0 °C (32) °F	2 °C (35.5) °F	5.1 °C (41.2) °F	9.1 °C (48.4) °F	12.2 °C (54) °F	14.4 °C (57.9) °F	14.1 °C (57.5) °F	11.4 °C (52.6) °F	8.2 °C (46.8) °F	4.3 °C (39.7) °F	1.3 °C (34.4) °F
Max. Temperature °C (°F)	4.6 °C (40.2) °F	5.7 °C (42.3) °F	9.4 °C (49) °F	14.1 °C (57.5) °F	17.8 °C (64) °F	20.8 °C (69.5) °F	22.7 °C (72.9) °F	22.2 °C (72) °F	18.8 °C (65.8) °F	14.2 °C (57.5) °F	9 °C (48.1) °F	5.5 °C (41.8) °F
Precipitation / Rainfall mm (in)	90 (3)	73 (2)	77 (3)	63 (2)	74 (2)	82 (3)	96 (3)	94 (3)	82 (3)	78 (3)	84 (3)	94 (3)
Humidity(%)	85%	82%	78%	70%	70%	70%	71%	73%	77%	81%	87%	85%
Rainy days (d)	11	10	11	9	10	10	11	11	10	9	11	12
avg. Sun hours (hours)	3.0	3.9	5.4	7.9	8.9	9.5	9.7	8.7	6.7	5.0	3.6	2.8

Figure 4: Weather Averages Dortmund by Month. (climate-Data.org n.d.) Data: 1991 - 2021 Min. Temperature °C (°F), Max. Temperature °C (°F), Precipitation / Rainfall mm (in), Humidity, Rainy Days. Data: 1999 - 2019: avg. Sun Hours

Projected climate change during the 21st century is expected to result in changes in climatic conditions. Moreover, the large-scale and regional climatic characteristics of climate districts at the local level can be significantly influenced by both natural factors, such as relief, and anthropogenic influences, including land use, the extent of soil sealing, emissions of air pollutants, and more (Stock 2019: 11). The ventilation of a city can be significantly influenced by a pronounced relief structure as well as surface roughness, which can be attributed to land use (ibid.: 12). In general, the urban area of Dortmund has a pronounced relief energy, especially in its southern region, which results in well-developed geomorphological structures. Conversely, the expression of surface roughness shows a varied pattern across the city area (ibid.: 13). Land use plays a crucial role in shaping local climatic conditions, as it strongly influences the interactions between a surface and the atmospheric boundary layer (ibid.: 15). In the city of Dortmund, the spatial distribution of different land use types shows a heterogeneous pattern, with open spaces and residential areas scattered throughout. However, the inner city districts are characterized by a relatively dense built-up area. Beyond the downtown districts, there are numerous mosaic-like quarters with small town centers and predominantly scattered development. These areas are interspersed with agricultural land and/or forests, creating an interconnected network of open spaces, woodlands, and green areas (ibid.: 16).

The study area of this project is located in the district of Hombruch. With almost 35 km² and a population of around 58.000 (as of 31 December 2022), this is Dortmund's largest district in terms of area and third largest in terms of population (Stadt Dortmund n.d.). "Extensive hilly forest areas, many agricultural areas and a well-kept residential environment characterize it in large parts" (ibid., own translation⁵). These agricultural open spaces, copses and wooded areas in the district have high values for cold air volume flow almost throughout the area and are also often effective cold air production areas (Stock 2019: 65). Due to the prominent gradient, the cold air flows can reach a high flow velocity and penetrate deep into the built-up areas, where they can have a very positive climate-ecological effect during low-exchange weather conditions (ibid.). Here, due to the presence of the TU Dortmund University campus with around 32.500 students (as of winter semester 2022/2023) in 17 faculties, various research institutions and the TechnologieZentrumDortmund, the district occupies an outstanding position as a research and development location within the city of Dortmund (Stadt Dortmund n.d. TU Dortmund n.d.-c). The university is spread over two campuses, Campus South and Campus North. These areas are characterized by tall and broad building complexes, some with large car parks (Stock 2019: 189), and are separated by extensive green spaces, including the Rahmkeachtal Landscape Park. The campuses are connected by the H-Bahn, a driverless suspension railway system that is still unique in the Ruhr region (Figure 5).

⁵"Ausgedehnte hügelige Waldgebiete, viele landwirtschaftlich genutzte Flächen und ein gepflegtes Wohnumfeld prägen ihn in weiten Teilen."

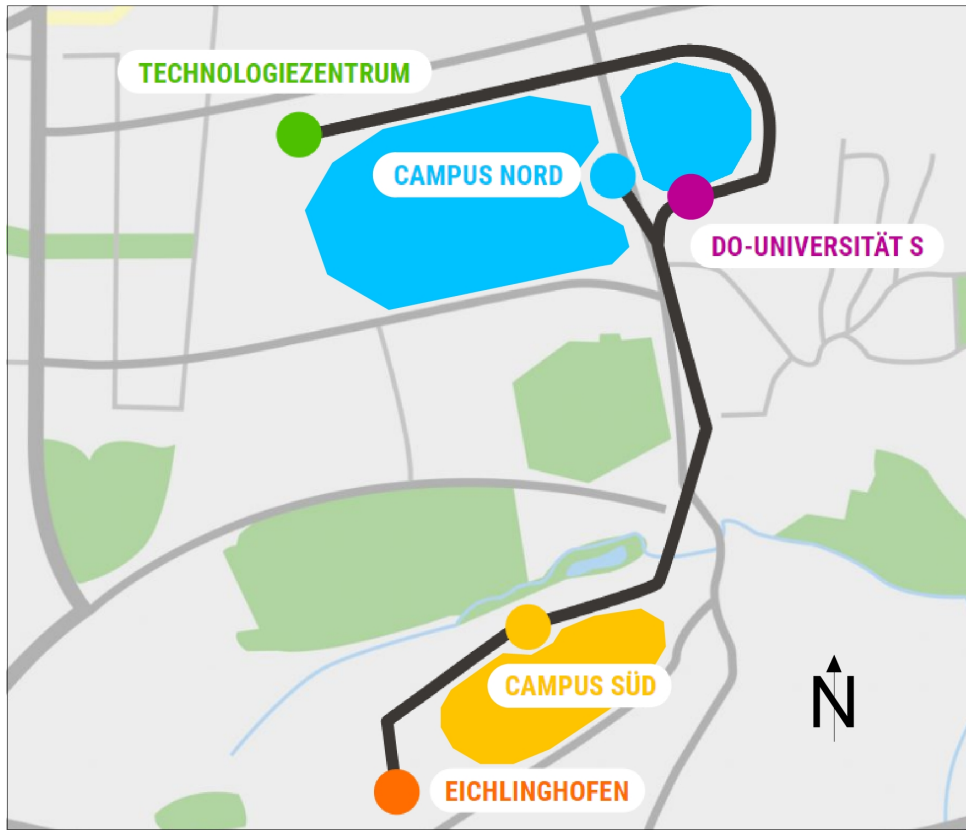


Figure 5: Locations of the Two Campuses North and South as Well as H-Bahn Line (modified based on H-Bahn21 n.d.)



Figure 6: Current (left) and Future (right) Central University Library Building (Rau 2017; TU Dortmund n.d.)

The research object, the Central University Library (Figure 6), has been located on Campus North since 1976 (Lippmann 2015: 2) and has become a building with a high degree of representation for the university. Since then, the library has accumulated almost 1.76 million pieces of media, and an additional 97.000 e-books and over 42.000 e-journals licensed by the library are available on the TU Dortmund campus (TU Dortmund n.d.). Preparations are currently underway for a new Central University Library (Figure 6). The new building will be constructed on the same site as its predecessor. For this purpose, the current library building will be emptied from August 2023 and deconstructed from spring 2024. Construction of the new building will begin in spring 2025 and is scheduled for completion in 2028/2029 (TU Dortmund n.d.-b). The old building is highly energy inefficient (ibid.). However, modernisation of the old building would be uneconomical. Instead, it was decided to construct a new building that meets the changing needs of a library, which is increasingly becoming a central place for learning and meeting, while the space for bookshelves is constantly decreasing (ibid.)

For the micro-scale climate simulation of the Central University Library building in ENVI-met, the area surrounding the building may also be considered (Figure 7). It is important to include significant recreational areas around the library building and to avoid buildings on the edge of the model space in ENVI-met due to wind flow simulation (van Heerden 2021: 7). This extended study area consists of 40% green areas including the rain infiltration biotopes, 36% paved areas including roads, footpaths and car parks and 24% buildings (own calculations based on aerial photographs, RVR 2022). To the north of the library (1), these include the food faculty (2) and the main humanities building (EF 50) (3), and to the east the buildings of the Dortmund University of Applied Sciences (4) and the CDI (5). In between is a green space with meadows, trees and rainwater infiltration areas. To the south and adjacent to the S-Bahn station are the H-Bahn station (6) and the student village (7), as well as a large car park and the Erich Brost Institute (8). To the west, the Mensabrücke (a wide bridge that serves as a connector and as a meeting and lounging area) with the H-Bahn station (9), the Audimax with the adjoining Maths Tower (10) and the main cafeteria building (11) complete the research area. Also worth noting are the differences in height in the area: the southeastern part of the library building is about 4 m lower than the northern part. The narrow study area consists only of the library building itself, part of the Mensabrücke and the vegetation directly adjacent to it. The walkable area in the VR application extends from the Mensabrücke bridge on the north side of the library building to the green space northeast of it, as well as a small area on the library's roof.

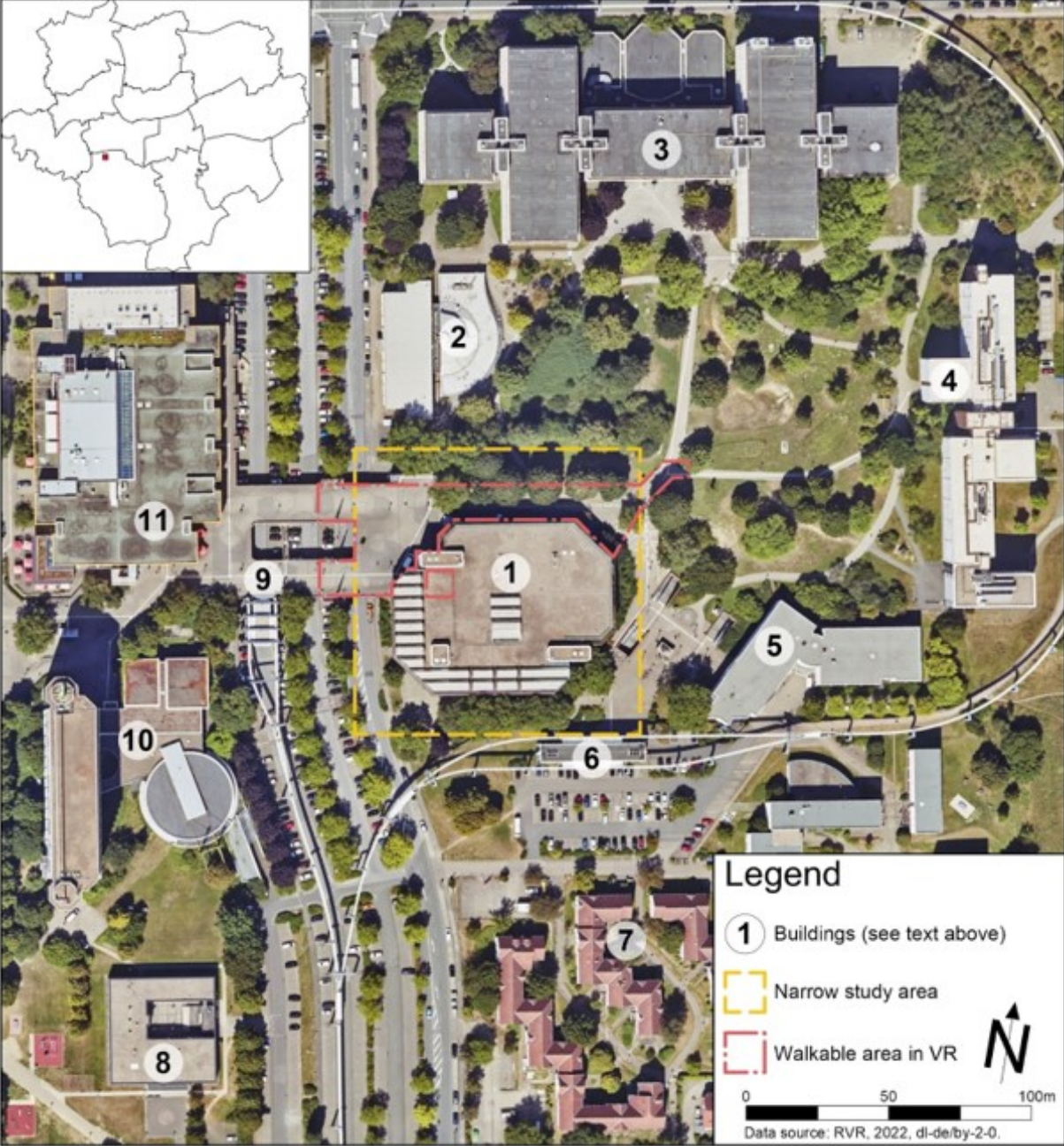


Figure 7: Extended Study Area with Narrow Study Area and Walkable Area in VR Highlighted (RVR 2022)

3. Literature Review

The following chapter highlights the state of research and practice in several areas (WP1). These include the concept and scope of a Digital Twin, the idea of microclimate simulation, and the possibilities of dynamic visualization of data.

3.1. Digital Twin

First, a definition for the concept of a Digital Twin is needed. Klostermeier et al. (2018: 299) state that the definition of a Digital Twin differs depending on the field of application. Despite the different areas in which a Digital Twin is used, there are some common elements. A Digital Twin should be seen as “the individual portrayal of a physical object or process, which makes the data provided by the physical entity intelligently usable for various use cases“ (Klostermeier et al. 2018: 299-300, own translation⁶). The key element of this is that a Digital Twin is a virtual reproduction of a real object. The connection and transfer of data between the physical and the virtual object is also essential. While Klostermeier’s definition focuses on the relation of the physical and virtual object, Batty (2018: 817) sets the focus on the process behind a Digital Twin. He states that a Digital Twin is used “to characterize a variety of digital simulation models that run alongside real-time processes” (ibid.). Both definitions combined highlight the most important aspects of a Digital Twin: the virtual representation of a physical object and the simulations that can be performed with real-time data. In the context of spatial planning Schrotter and Hürzeler (2020: 102) state, that “the Digital Twin means consistent enrichment of the 3D spatial data inventory and, in addition to the modeling and description of the data, a lifecycle management of the individual components as well as the entire data inventory”. The focus lays on the enriched spatial data over the whole lifecycle.

A Digital Twin is not always necessarily based on a 3D model. It is also possible that a 2D model is the basis of a Digital Twin (Al-Ali et al. 2020: 9). In the case that a Digital Twin is based on a 3D model, there are different possible levels of detail, also called Level of Detail (LoD). With increasing LoD, the representation of the geometric detail of the displayed objects also increases (Gröger et al. 2006: 10.; Figure 8). LoD 1 is a model consisting of cuboid blocks without roof structures. LoD 2 is a LoD 1 model extended by roof structures and differentiated surfaces. LoD 3 represents architectural models with detailed wall and roof structures, including e.g. balconies and high-resolution textures. LoD 4 adds inner structures to the objects of an LoD 3 model, e.g. buildings are complemented by rooms and stairs (Gröger et al. 2006: 11).

In the context of urban planning, a Digital Twin offers potential through various appli-

⁶“das individuelle, virtuelle Abbild eines physischen Objektes oder Prozesses, welches die vom physischen Objekt bereitgestellten Daten intelligent für verschiedene Anwendungsfälle nutzbar macht”

3 LITERATURE REVIEW

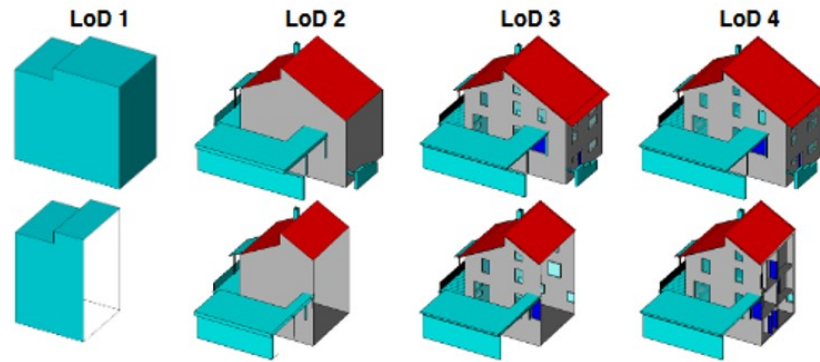


Figure 8: Overview - Level of Detail (Häfele 2011 as cited in Biljecki et al. 2013: 64)

cation possibilities. For example, simulations and predictions based on real-time data can be used to predict events, or the cityscape can be kept in its original state by analyzing historical data. But also the inclusion of citizens through participation and consultation can be simplified by a Digital Twin (Caprari et al. 2022: 11). One use of simulations is to predict the effects of flood events. Particularly in coastal regions with rapid population growth, people and infrastructure are exposed to the hazards of weather events (Ye et al. 2023: 187).

One example of a region strongly affected by climate hazards is India. India has a long coastline of 7517 km, which provides many points of vulnerability. The coastal regions play an important role in the development of the country (Dhiman et al 2019: 1). Also, the monsoon occurs annually in India and can bring flood disasters. For these reasons, it would be important to predict the impact of climate hazards (ibid: 2). A Digital Twin can help simulate climate events such as flooding or inundation, which can determine the impact on the surrounding area. This makes it possible to adjust development to minimize potential damage (Ye et al. 2023: 188). Digital twins in the context of climate change and microclimate simulations are already being used in planning practice: the city of Zurich, Switzerland, uses natural cold air currents to cool the city in summer. However, buildings can act as obstacles to the airflow and influence it negatively. To prevent this, the impact of newly planned buildings on the airflow is simulated. With these simulations, Zurich can maintain its ventilation in the summer (Schrotter & Hürzeler 2020: 108) (Figure 9).

The city of Herrenberg in Germany is also using its Digital Twin for an integrated airflow approach. Factors such as wind, temperature and humidity are considered in order to simulate the distribution and accumulation of traffic-related emissions. These simulations are employed to ensure that future developments in the city do not adversely affect the health of its citizens. However, unlike Zurich's Digital Twin, the one of Herrenberg does not focus directly on climate adaptation (Dembski et al. 2020: 6).

Another city that already uses a Digital Twin in the field of climate is Helsinki. Helsinki has a 3D model of the city, which was created on the basis of aerial photographs. The

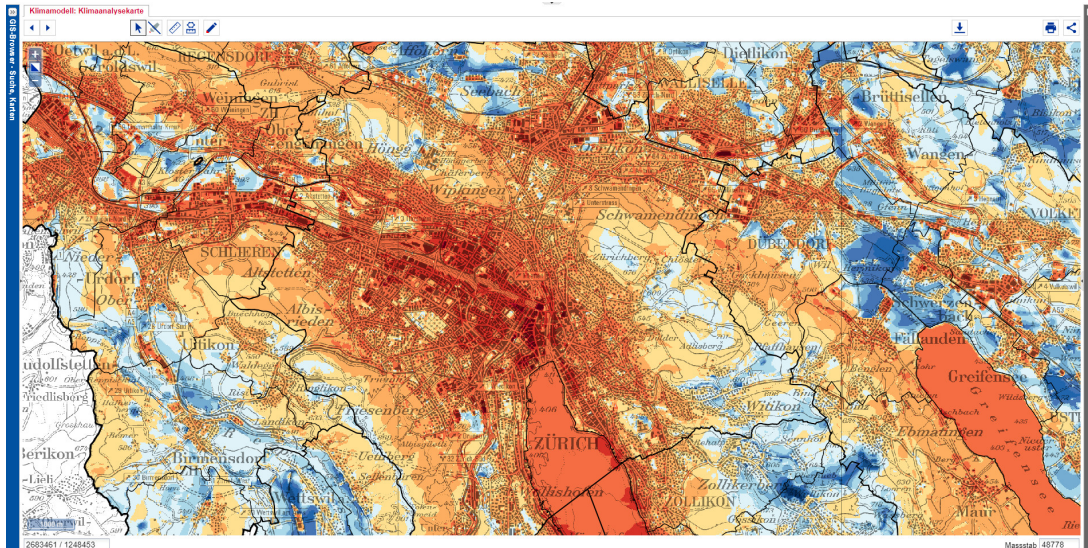


Figure 9: Simulation of the City of Zurich (City of Zurich n.d.)

buildings are completely equipped with textures (Figure 10). This 3D mesh is the basis for, among other things, the Energy and Climate Atlas. The Energy and Climate Atlas is a website that shows the renewable energy sources in Helsinki and their potential locations. For example, the potential for solar energy in the entire city can be viewed on a map (City of Helsinki n.d.c.n.d.; Figure 11).

In addition to solar energy, the City of Helsinki also provides data on the potential for thermal wells for geothermal heat utilization. Thus, there is the possibility to display the potential at a depth of 150 m, at a depth of 300 m as well as at a depth of 1000 m. In addition to the heat production, the heat consumption of the buildings in the City can also be simulated. Finally, the city of Helsinki also provides information on the energy saving potential that can be achieved by energy refurbishment of the buildings (Figure 12).

The figures 10, 11 and 12 show that Helsinki has put a lot of effort into the interactive visualization of the city and climate-related data. The visualizations should not only reach experts, but also be used by other stakeholders such as citizens or housing companies. Helsinki is thus taking an important step towards adapting the city to climate change as effectively as possible. In the future, Helsinki plans to integrate more data into the Energy and Climate Atlas. This will include simulations of the microclimate and the expected costs of the energy-efficient renovation of buildings (City of Helsinki n.d.).

However, the term Digital Twin, which was used in the examples of practical applications presented here, must be viewed critically in one aspect. According to Sepasgozar (2021: 6), the concept of the Digital Shadow exists alongside the concept of the Digital Twin. Yet these two terms are often used as synonyms, also in the literature (ibid.). Liu et al. (2021: 5) conclude that in over half of the literature they reviewed, the term Digital Twin was incorrectly used to refer to a Digital Shadow. There is a crucial difference

3 LITERATURE REVIEW



Figure 10: 3D-Mesh of the City of Helsinki (City of Helsinki n.d.c.)

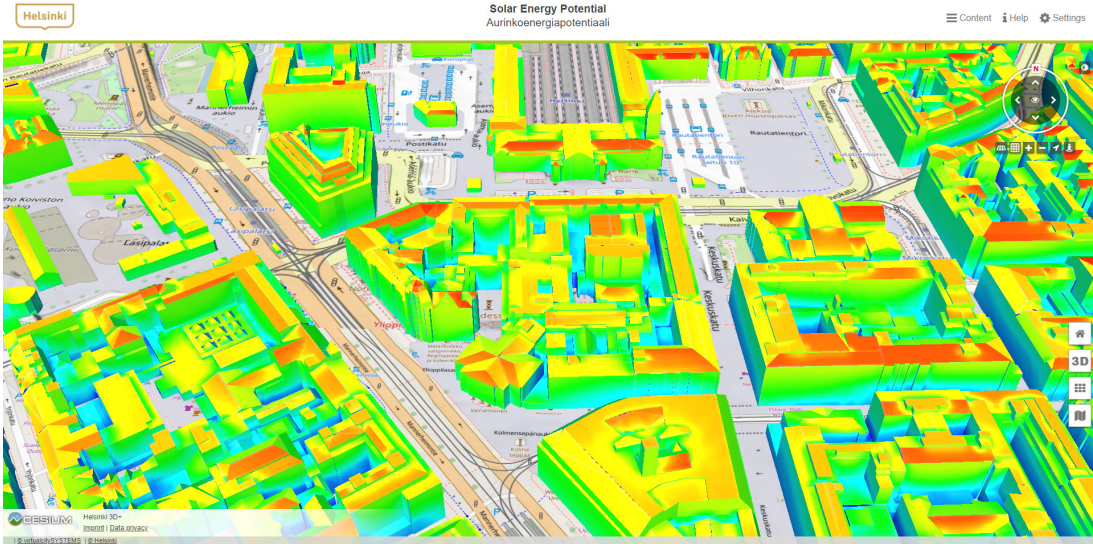


Figure 11: Solar Energy Potential of the City of Helsinki (City of Helsinki n.d.)



Figure 12: Predicted Refurbishment Impact of Buildings of the City of Helsinki (City of Helsinki n.d.b.)

between these two terms: if there is just one model of a real object to which data only flows in one direction, this does not correspond to a Digital Twin (ibid.: 6). While the definitions of Klostermeier (2018) and Batty (2018) have shown the importance of the connectivity of the real and the virtual object, they do not express in which direction the data flows. If the data flow is merely from the real object to the virtual object, it is called a Digital Shadow. Only when the data flow also flows back from the virtual object to the real object is it called a Digital Twin (Figure (Sepasgozar 2021: 6; 13). Tchana (2019: 548) extends the gradations of a Digital Twin by the concept of a Digital Model. This has no automated data transmission in either direction, which means that real-time data cannot be integrated (ibid.) (Figure 14).

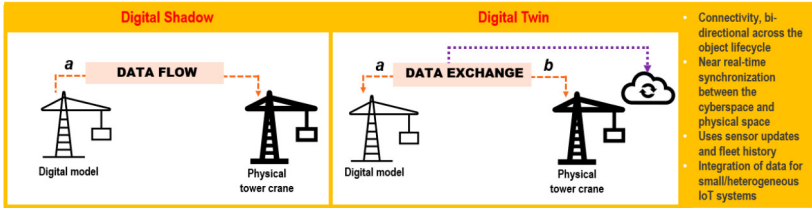


Figure 13: Difference Between a Digital Shadow and a Digital Twin (Sepasgozar 2021: 6)

3.2. Microclimate Simulations

Simulations of the microclimate are one core application of Digital Twin city models. The microclimate is “[the] fine climatic structure of the air space that extends from the very surface of the earth to a height where the effects of the immediate character of the underlying surface no longer can be distinguished from the general local climate”

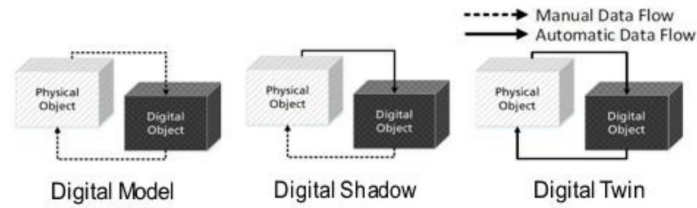


Figure 14: Stages of a Digital Model (Tchana et al. 2019: 548)

(American Meteorological Society 2012a). On a spatial scale this refers to a horizontal extent of up to 2 km (American Meteorological Society 2012b). This extent is of interest because these effects of the surface can significantly impact human well-being and the efficiency of building heating and cooling through effects like the urban heat island (UHI). This study focuses on the basic results and verification of a microclimate simulation, so the human well-being aspect is put aside but these measurements are a critical part of the study of the microclimate.

First, the UHI effect refers to a higher surface temperature in city blocks compared to natural surfaces because of a low albedo and fewer evapotranspiration (Kim 1992: 2334). The large differences in temperatures between grassland, forests and city blocks (Figure 15) can be explained by the fact that solar energy hits buildings and large shaded areas that have a lower albedo, i.e. that absorb more solar energy and reflect less (ibid.: 2333). This heat energy must be transferred back. In forests, evapotranspiration from plants provides cooling, but this is less or not available in built-up areas, so the heat is transferred to the air (ibid.). This effect is exacerbated by a larger urban and thus sealed area (Ward et al. 2016: 535) as well as reduced wind flow within the urban canopy layer that traps anthropogenic heat and emissions (DWD n.d.). Still, these impacts do not have to be negative. A higher temperature can reduce the energy demand of buildings depending on the location and the season (Toparlak et al. 2017: 1614, 1631). This can be addressed with urban design that is optimized for cool air flow into the city like in Zurich (see Chapter 3.1). Cities in southern Europe also seem to be better adapted to heat waves (Ward et al. 2016: 535). A good coordination between the building energy demand and the human well-being is necessary.

As mentioned in the introduction, more energy efficient buildings, especially considering heating and cooling are a goal of city planners and policymakers. For this purpose build applications like EnergyPlus by the U.S. Department of Energy model buildings, their materials and HVAC applications in detail (Yang et al. 2012: 243). While the energy demand of the Central University Library is one area of interest, a specific building energy modeling is part of a different project. The results of a microclimate simulation however can be incorporated into the building energy model for a more detailed result (ibid.). Here, simulations of the microclimate are needed to better understand the im-

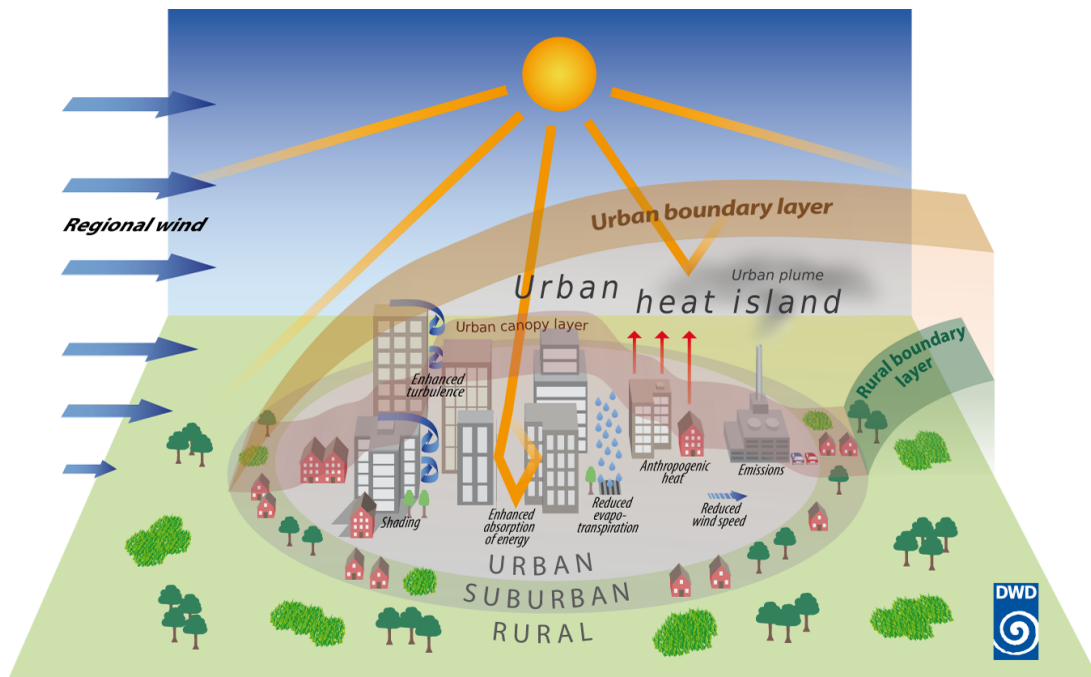


Figure 15: Urban Heat Island (DWD n.d.)

pacts of the climate, building materials, trees, and foliage on the temperature. Because of advancements in simulation software and computational resources a numerical simulation approach based on a Computational Fluid Dynamics (CFD) model can be applied (Toparlar et al. 2017: 1615). In the past, the measurement of the microclimate was limited to weather stations at singular points in space. Climate simulations allow for a continuous depiction of data across the entire surface while data from weather stations may be used to prepare and verify the simulated data (ibid.: 1614). Numerical simulations allow a comprehensive and detailed coverage of the study area and the possibility to try out different scenarios in comparison to simple observations (ibid.: 1615). In this case a simulation could indicate hot- or cold-spots on a building that could be addressed either with better insulation or foliage. The effect on the indoor temperatures could be assessed with a specific building energy simulation model that incorporates wall materials and thicknesses as well as the heat convection inside the building. The results of a numerical simulation of the microclimate are an ideal basis for such a simulation.

The numerical simulation applied here is a CFD model. As the name suggests, fluid dynamics models understand the heat convection, wind fields, dispersion, and air pollution as fluids that can move around complex building shapes and within urban canyons (Souch & Grimmond 2006: 274). CFD offers the integration of wind velocity, temperature, humidity, and air pollution on a fine scale that allows measurements on buildings or humans (Toparlar et al. 2017: 1615). For this, a fine model of the building geometry and surrounding area is needed (ibid.). One well-used application of CFD is the program ENVI-met (first introduced by Bruse & Fler 1998, Toparlar et al. 2017: 1621). ENVI-met is a

3 LITERATURE REVIEW

holistic 4D system, consisting of 3D space and time, which allows a comprehensive analysis of the parameters relevant for the urban climate (Bruse 2000: 3). A non-hydrostatic 3D numerical flow and energy balance model is used to simulate the microclimate. This model is based on the laws of thermodynamics, fluid mechanics and atmospheric physics, but also plant physiology and soil science (ENVI-met 2017b: 6; ENVI-met 2023a). ENVI-met consists of multiple models that describe the atmosphere, soil, vegetation as well as ground and building surfaces (Bruse 2004). For the purposes of the simulation the study area is approximated into a 3D raster so that all variables can be calculated on every raster block (ibid.: 1). The scientific basis of all models is now touched upon.

The atmosphere model consists of variables of the “main wind flow, temperature, humidity and turbulence” (ibid.: 1). The wind flow is calculated using “non-hydrostatic incompressible Navier-Stokes equations” (ibid.: 1). “In the [Navier-Stokes] formulation, the fluid is treated as a continuous material [...] with local physical properties that can be represented by continuous functions of space and time” (McLean 2012: 13). This means that the air flow can be predicted based on the larger scale meteorological conditions (Bruse 2004: 1). The model used to approximate the exact variables for each block (since an exact simulation for every time point would be very demanding) are Reynolds-averaged Navier-Stokes equations where a time-averaged result of the variables is calculated, specifically with the Yamada and Mellor $E-\epsilon$ model (Toparlar et al. 2017: 1627). Another model basis that is finding more application because of more precise results in turbulent airflows while having a larger computational demand are Large-Eddy-Simulations (ibid.).

Additionally to the wind field, there are further calculations included in the model, such as air temperature, humidity, shading, soil and vegetation geometries (Figure 16, ENVI-met 2023a). The wind field is updated at regular intervals and takes restraining forces of plants and facades/roofs into account (ibid.). The air temperature and specific humidity include the convection in the air and existing sources and sinks of sensible heat and vapor, e.g. ground surfaces and leaves of vegetation (ibid.). Shading, that is calculated with the location and date of the simulation, has an effect on the air and surface temperatures (ibid.). The soil is simulated to a depth of 4 m and considers the heat and water conductivity as well as water sources like ponds and evaporation and intake of water from plant roots (ibid.). Simple and complex vegetation geometries are included that can also simulate the effect of roof and facade greening (ibid.).

Furthermore, the model architecture includes a 1D boundary model with an extent from 0 m, ground level, up to a height of 2.500 m (Huttner 2012: 5). It is required for initializing the simulation and as a basis for the lateral boundary conditions (LBC) of the 3D atmospheric model (ibid.). The LBC define the model’s behavior at its lateral limits and have a strong impact on the development of atmospheric variables during the execution of the simulation (ENVI-met 2017c; Huttner 2012: 53). The 1D model represents the vertical profiles of the atmospheric variables (wind speed, turbulence, air

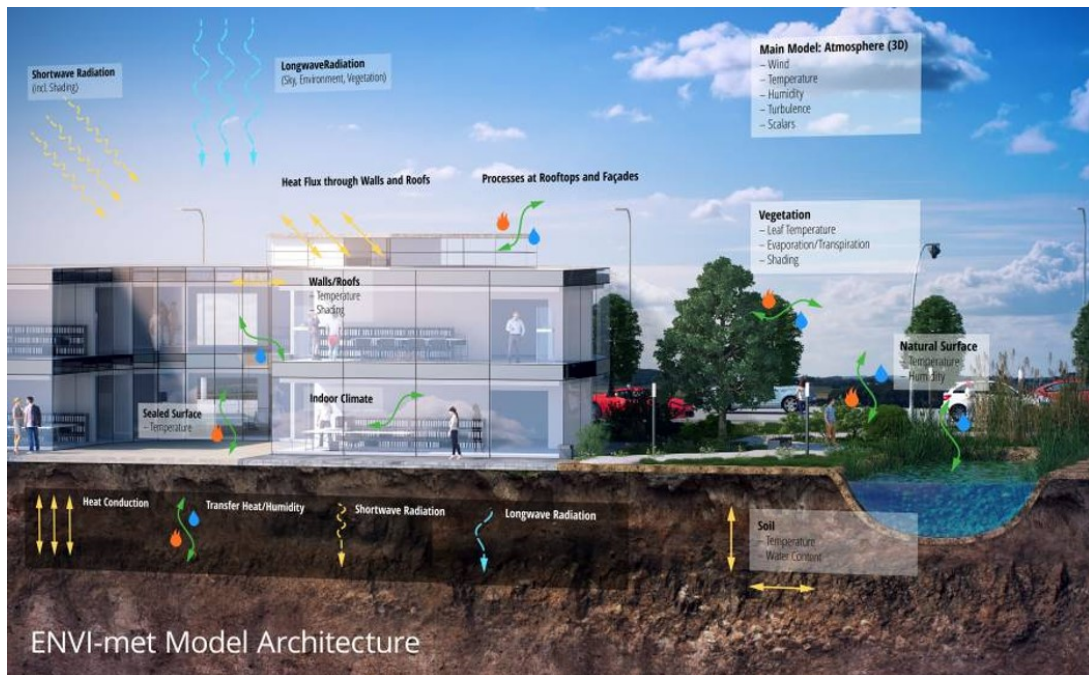


Figure 16: ENVI-met Model Architecture (ENVI-met 2023a)

temperature, humidity) in a quasi-stationary state (Huttner 2012: 52). With these profiles at the inflow boundary of the 3D model, the simulation is initialized (ibid.: 56).

Microclimate models are already in use for city planning purposes. The presented city-wide models focus on cold air influx or the distribution of emissions (see Chapter 3.1). Smaller scale models can take a broader approach and investigate case comparisons between “different urban geometries, [...] vegetation patterns, building materials and building forms” (Toparlar et al. 2017: 1624). Examples for this are studies that compare the effects of greening on thermal comfort at different scales and climate zones (e.g. Herath et al. 2018 for Colombo, Sri Lanka, Choi et al. 2021 for Seoul, South Korea, and Schaefer 2022 for Dortmund-Marten).

An integral part of any simulation is the verification process. The results of microclimate simulations should only be considered reliable if there is a verification with measured data, “according to several CFD best practice guidelines” (Toparlar et al. 2017: 1630). Measurements of surface temperatures can be obtained with satellite data and thermal cameras while smaller temperature sensors can sense air temperature and humidity. Additionally to the real-world measurements in this study multiple simulations of different detail are executed. This approach can also assess the variation of simulations (ibid.: 1630). Yet, even with the validation using real-world data there is always some degree of uncertainty. Even measurements with intervals of up to 10 min show such a variability that these conditions cannot be properly reproduced (Schatzmann & Leitl 2011: 185). This limitation is especially important because this study only assesses the data from one day. In an ideal scenario, long-term observations and simulations would be used with ad-

ditional laboratory measurements in wind tunnels (*ibid.*). However, a thorough validation using multiple sensors is an important part of this study.

3.3. Dynamic Visualization

Climate simulations are among the most challenging problems in scientific computing due to their size and complexity. Leading-edge simulations at one km resolution require some 80 billion grid cells (NVIDIA Developer 2020: Min 00'02"-00'13"). Each of these cells contains dozens of parameters such as temperature, pressure, wind and moisture. Once all of the data have been generated, the next step is to determine how to turn that data into valuable information.

“Finding the right way to represent data has been an active topic of much thought and discussion since the beginnings of visualization” (Rheingans 2002: 6). Visualization is an incredibly useful tool for identifying patterns and trends and gaining meaningful insights from massive data sets. Lowe (2004: 258) found that diagrammatic representations enhance comprehension by eliminating the mental burden of manipulating information that would otherwise be required in text-based presentations. Seeing the data in ways people can intuitively understand allows stakeholders, e.g., scientists, policymakers, or the general public, to use the information and take action when needed. Over time, advancements in the field of information technology and computer graphics have opened up new possibilities for creating visual representations of scientific phenomena and abstract data (Hegarty 2004: 343). These breakthroughs help scientists to showcase their data not only in static⁷ formats, but now to even immerse viewers in dynamic⁸ displays, some even combined with real time data, such as augmented reality (AR) or virtual reality (VR) (Caprari et al. 2022: 9f., Nijhuis et al. 2023: 12, Tinh 2022) (Figure 17 & 18). In this study, the latter will be the primary focus: “The term virtual reality refers to the use of three-dimensional displays and interaction devices to explore real-time computer-generated environments” (Bryson 1993: 495).



Figure 17: AR Application in Vienna (fluxguide n.d.)

⁷Static means stationary or fixed and these systems are not interactive (Lewis n.d.)

⁸Dynamic means energetic and these systems are capable of action or change (Lewis n.d.)

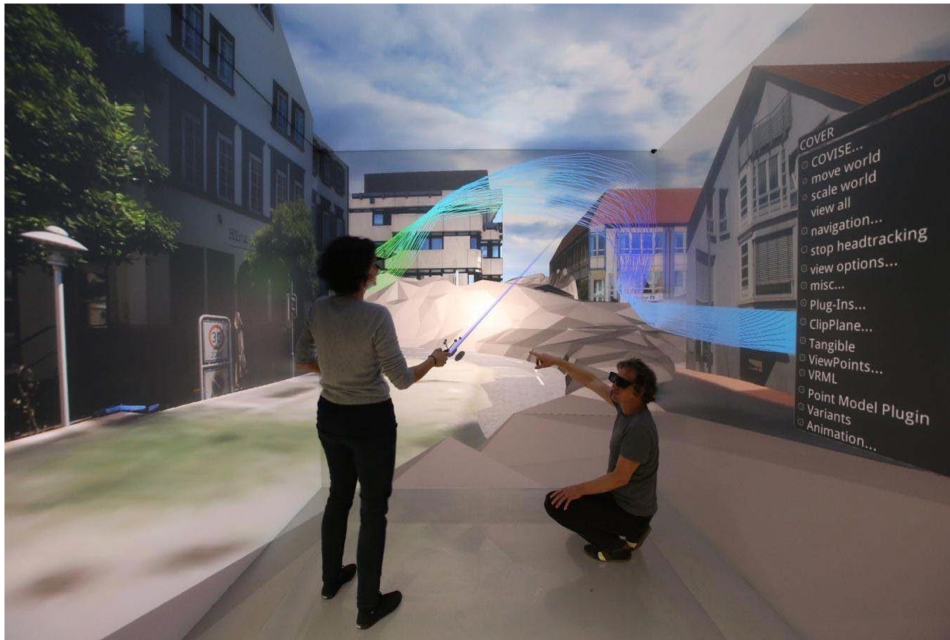


Figure 18: VR Application in Herrenberg Study (Dembski et al. 2020: 11)

Taking a step back, Hegarty (2004) distinguishes between different types of dynamic displays. First, there is the classic example of an animation of a visible phenomenon, such as a machine in motion. These displays are known for their realism, as they showcase a sequence of events in real time (ibid.: 345). Then, there are the dynamic representations, where space is used as a metaphor for some more abstract information, i.e., entities that are not directly observable but are spread out in space, such as changes in pressure or temperature on a weather map (ibid.). Finally, dynamic displays can distort reality in various ways, such as slowing down some processes and speeding up others or showing an object or phenomenon from different or changing viewpoints (ibid.). AR and VR technologies show characteristics of each of these three categories, with their strengths lying particularly in the latter, as it provides the ability to view a virtual object by dynamically controlling the viewpoint. “Dynamic manipulation engages a viewer’s kinesthetic sense in addition to his visual sense, adding an immediacy to the exploration experience” (Rheingans 2002: 6). When discussing the power of interaction, Rheingans (ibid.) distinguishes between dynamic and interactive control. “With interactive parameter control, the displayed image only updates periodically, such as when the user releases a button or selects a menu . With dynamic manipulation, a displayed image changes as the viewer moves a continuous input device, such as a slider, joystick, mouse, or tracker” (ibid.). In contrast to interactive parameter control (Figure 19), dynamic manipulation allows you to see not only the start and end points, but also the states in between (Figure 20). This gives the impression of directly interacting with the object, bypassing the need to rely on invisible entities to modify it, and contributes to the researcher’s understanding of the data (ibid.).

3 LITERATURE REVIEW

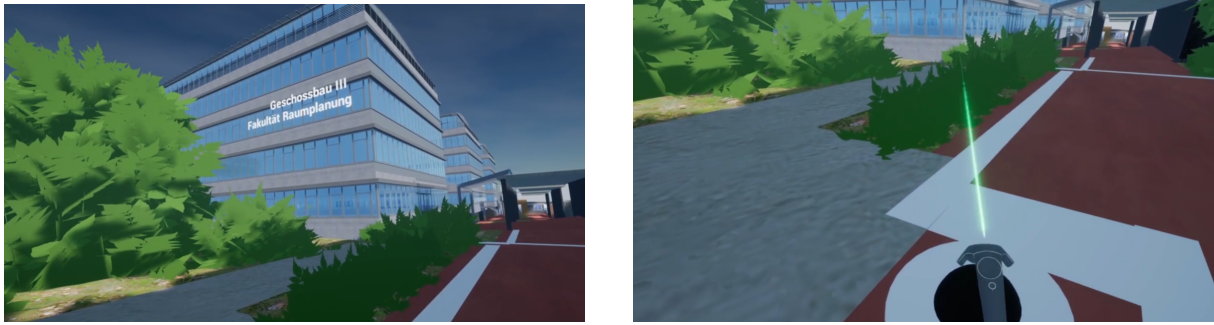


Figure 19: Example Interactive Parameter Control. Text Appears After Pressing a Button (Gisa et al. 2022)

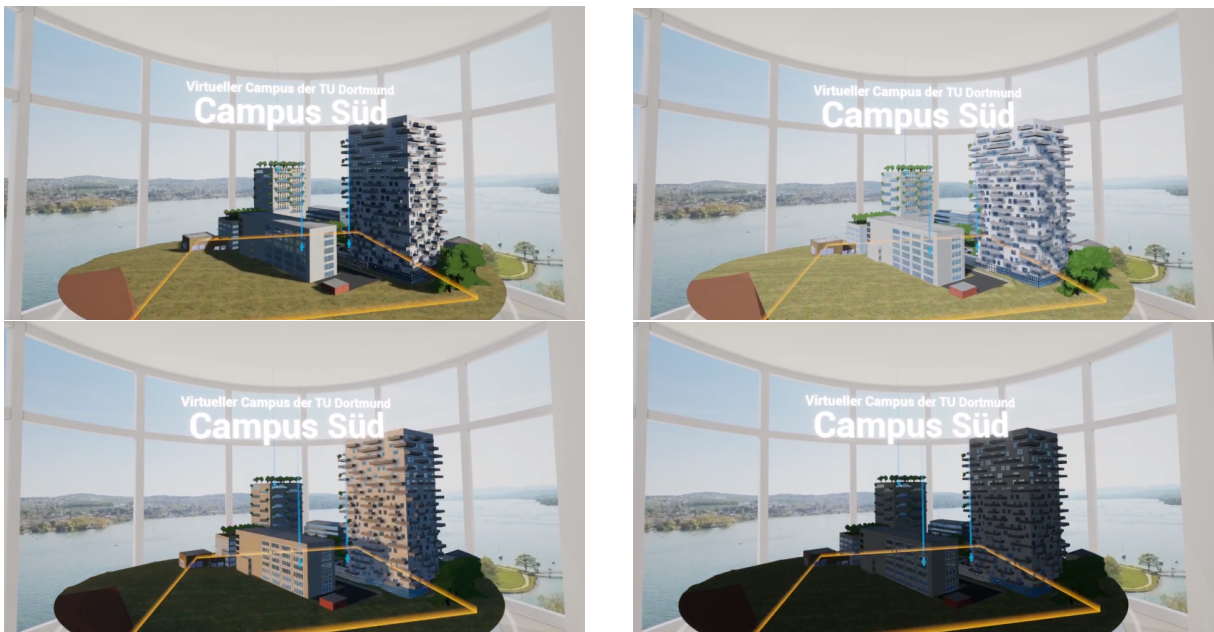


Figure 20: Example Dynamic Manipulation. Change in Time of Day (Gisa et al. 2022)

For microclimate simulations and Digital Twins, the visualization and understanding of the results is becoming increasingly important, especially given technological advances such as the 5G mobile communication standard and the accessibility of AR and VR applications (Nguyen et al. 2016: 724; Thinh 2022: 95). Through the use of software such as ArcGIS online or Unreal Engine these visualizations can be used, e.g. for a more tangible development and communication of new constructions in a city, with a Digital Twin growing alongside the original (Nguyen et al. 2016: 733). Combined in 3D digital city models, maps can be enriched with municipal data sets, real-time weather data, or visitors' opinions published on social media, and much more (Psyllidis et al. 2015: 21) (Figure 21).

Beside their general visualization potential, AR and VR are also used as a tool for digital visualization and digital participation in spatial planning. They offer a high level of immersion and no dependence on being on site, time and weather. This way they can improve the basis for decision-making by linking and visualizing different data sets and

illustrating the future effects of possible decisions (Engel & Döllner 2012: 170; Tomkins & Lange 2020). They enable the representation of possible future developments and alternatives before intervening in the environment (Imottesjo & Kain 2022). And they serve as a tool to involve interested stakeholders in the planning process (Caprari et al. 2022, Dembski et al. 2020).



Figure 21: Dynamic Point Clusters of Twitter Micro-Posts, in Combination With Path Patterns of Foreign Tourists and Their Temporal Variations in the City of Rotterdam (Psyllidis et al. 2015: 31)

4. Procedure and Results

This chapter outlines the workflow used in this study to address the research questions. First, a comprehensive overview of the data used is provided. Next, the process of creating the 3D model of the library is detailed, including laser scanning and post-processing procedures. The installation and management of the weather sensors used in the study are then explained. Next, the microclimate simulation involves the creation of a 3D model of the extended study area, followed by the execution of the simulation. To ensure accuracy, a verification step is performed to assess the quality of the simulated data. The results of the simulation and the weather data collected from the sensors are dynamically visualized and augmented with real-time data using ArcGIS Online/Dashboard and a VR application.

4.1. Data Overview

This project uses a plethora of programs and data, so it is important to keep track of all the data. All primary data, i.e. data that the project has obtained and measured itself, are listed in Table 1. Since the origin of the data plays an important role in the feasibility of such a project, the data are grouped by source. Much of this project would not have been possible without the data provided specifically for this project.

4.2. Creating a 3D Model of the Central University Library

This chapter details the procedure of WP2. It begins with a discussion of the laser scanning process and outlines the steps taken to clean and merge the captured data effectively. Finally, the chapter explains the creation of the 3D model in Revit.

4.2.1. Laser Scanning

Laser Scanning or more specifically 3D Laser Scanning is a process of using a 3D laser scanner to capture a real-world object or environment and collect 3D digital model data about the shape and properties of the object which compose of thousands of points in 3D space (Vosselman et al. 2004; Cheng et al. 2018; Dong et al. 2020). These point clouds can be used in a wide variety of fields, primarily those in construction and civil engineering (Tang et al.2011). Additionally, the 3D laser scanning technology can be utilized for the creation of Digital Twins and their subsequent visualization in VR or AR, among other fields of application (Tang et al. 2011; Dembski et al. 2020).

In recent years, when it comes to creating 3D images of architectural scenes from point cloud data, the use of Terrestrial Laser Scanning (TLS) or Personal Laser Scanning (PLS) has made significant progress (Sanchez & Zakhor 2012). While TLS is usually mounted on a fixed tripod, scanning and capturing 360-degree images, PLS requires the user to

Table 1: Overview of Data

Data	Type	Resolution	Source	Used in
Publicly available data				
Digital elevation model (DEM)	Raster Image	1m x 1m	GeoBasis NRW 2023b	SketchUp Pro, Unreal Engine
Topographical Satellite Image	Raster Image	-	GeoBasis NRW 2023a	SketchUp Pro, Unreal Engine
Topographical Satellite Image	Raster Image	-	RVR 2022	Unreal Engine
Private data, specific to this project				
UAV-Footage	Raster Images (Perspective)	-	RIM, Grützner 2022	Revit
Data of a weather station	Temperature, Dew Point, Wind Speed, Wind Direction	10 min	DTM	ENVI-met
Floor Plans	Raster Image, .dwg	-	TU Dortmund University Library Archive	Revit
Own survey data				
LiDAR-Scan	Point Cloud	<1cm	Own survey	CloudCompare, Revit
Weather sensors	Air Temperature, Rel. Humidity	10 min	Own Survey	ENVI-met Verification
Tree position, extent and type	Feature Class	-	Own Survey	ENVI-met

move around the object to collect point cloud data. In this project, the Central University Library’s facades and roof were scanned at the beginning of May 2023 using a GeoSLAM ZEB HORIZON personal mobile laser scanner (PLS) (Figure 22). The GeoSLAM ZEB HORIZON used in this project captures point cloud data rapidly and easily, at a rate of 300.000 points/s and 160 lines/s (16 lines at 10Hz). The user captures data while walking through the area of interest. ZEB-HORIZON’s unique scanning technology eliminates the need for space-intensive scanner setups and data registrations associated with terrestrial laser scanning (Gollob et al. 2020). Additionally, PLS has LiDAR technology that enables users to measure the distance to objects by illuminating them with a laser pulse in an extremely fast and accurate way in a wide range of environmental circumstances (GeoSLAM 2020).

For the walking path, an optimum solution was found after some initial trials: The library’s facade and roof have been divided into seven partly overlapping pieces (Figure 23), which are scanned separately in order to keep the file sizes small, avoid long post-processing times and minimize the severity of file loss in the event of technical problems with the scanner.

In order to establish the coordinate reference system, the inertial measurement unit

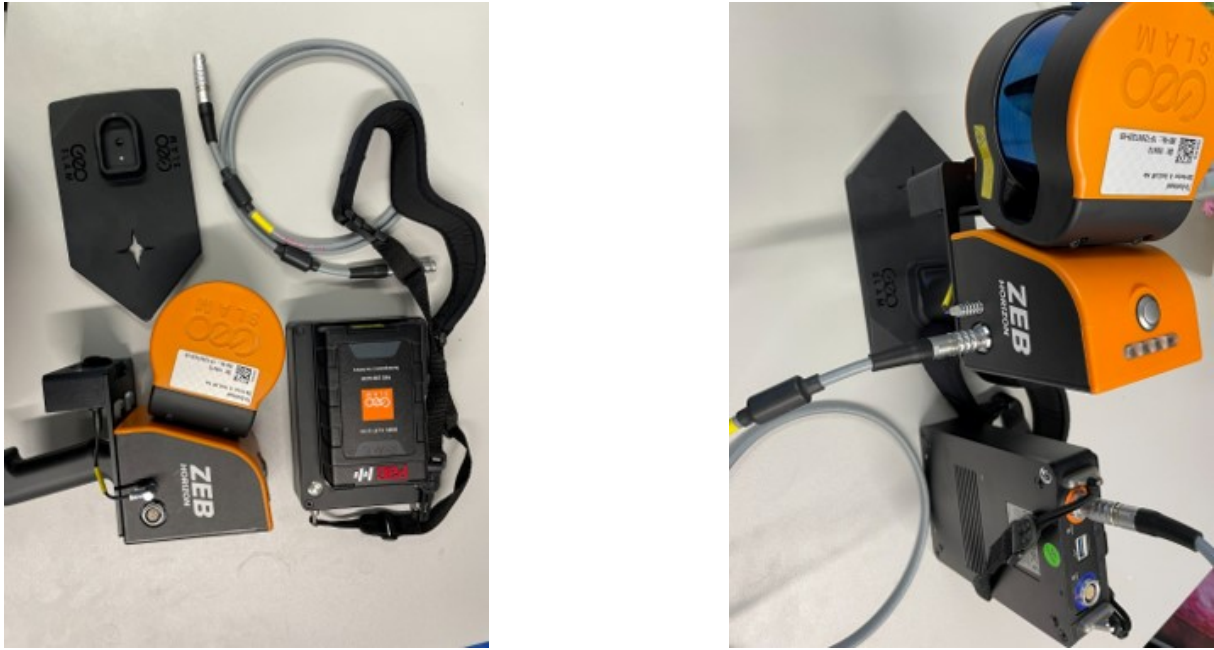


Figure 22: This Project was Conducted Using ZEB-HORIZON & GeoSLAM Hub (own illustrations)

(IMU) is initialized with ZEB HORIZON (GeoSLAM 2020). To carry the scanner single-handedly along the walking path, the scanner was mounted from the reference base plate with approximately 15-20 seconds of initialization. Data from the 3D measurements were stored in highly compressed format on the portable data logger's hard drive during the scanning process. When performing a laser scan of a 3D environment, it is important to view objects, e.g. pillars, from multiple angles (GeoSLAM 2020: 12). This way, enough information can be gathered about each object and gaps in the point cloud, so-called 'shadows', can be avoided (ibid.). Consequently, the surveyor walked his path from the start of the red line (near purple) to its end (near yellow) and back again to the previous starting point, varying the distance to the facade along the way, to capture as much detail as possible. The surveyor then repeated this process for each path, scanning the entire facade and roof of the library to collect the necessary point cloud data. It took approximately three to four hours to complete the entire walk, including the scanning process and the recording of the data. By using a USB flash drive, measurement data were transferred from the data logger onto a computer subsequent to each performed scan. From there, data pre-processing was carried out using GeoSLAM Connect Viewer (Figure 24).

By default, each point is colored based on its elevation value with a gradient from blue (low values) to red (high values). According to the manufacturer, coordinates of the registered point cloud are given by a local reference system, with the start of the walking path occurring at triple zero in all three dimensions (x, y, z). LAZ format is compatible with several point cloud software programs, and it was used to export PLS data for the

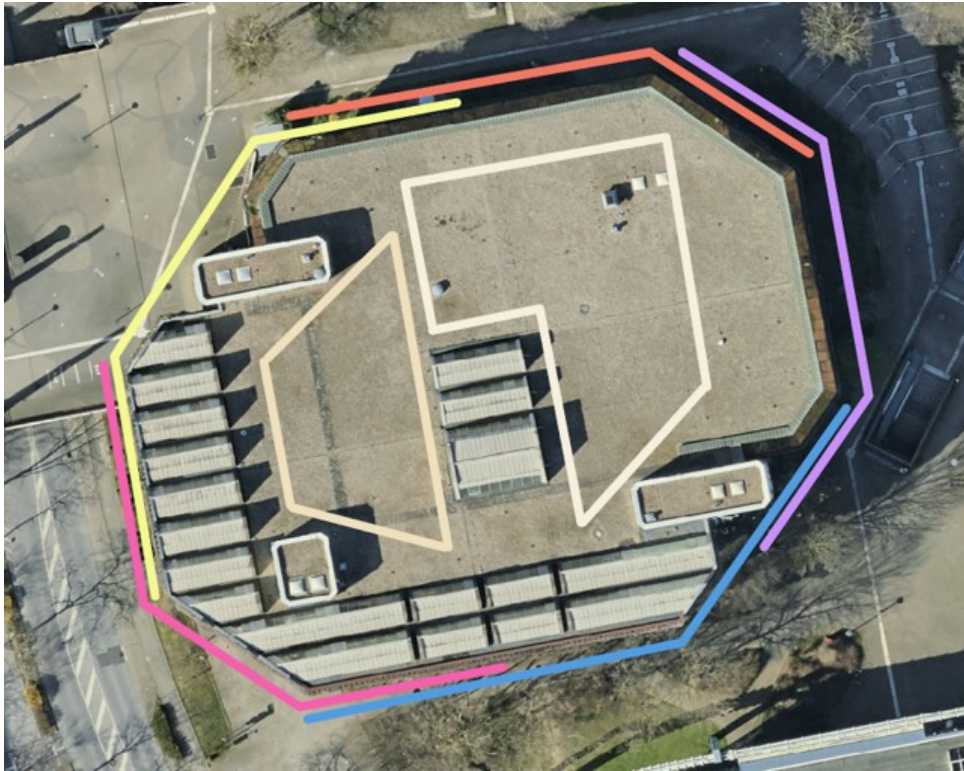


Figure 23: Schematic Overview of the Library’s Division into Seven Partially Overlapping Parts for the PLS Data Collection Process (own illustration based on RVR 2022)

library’s facade and roof.

4.2.2. Clean Up and Merge Point Clouds

In order to further process the laser scan data, first of all, it has to be reduced to the area of interest. The used ZEB HORIZON laser scanner, with its rotating head, also captures much of the library’s surroundings, i.e. the datasets contain a lot of additional spatial information that is not needed for the creation of the library’s 3D model (e.g. points of people, trees and bushes). Since the library’s facade scans have been separated into five sections, as already mentioned in the previous chapter, it is also required to overlay the individual scans and put them together as one merged point cloud. This is why it is important to have an overlap between adjacent scans to get reference points for the overlaying process.

To achieve this, the project group decided on using the software CloudCompare and Autodesk ReCap Pro. CloudCompare is an open-source 3D point cloud and mesh processing software with a good self-learning infrastructure, which provides a good handling and performance, even with larger amounts of data (CloudCompare n.d.). ReCap Pro on the other hand offers an easy-to-understand and reduced user interface, reminiscent of CAD programs, which makes it easier to navigate and process the data in detail. Since

the program also belongs to the Autodesk software family, it provides interoperability with Revit, which will be used in later work steps to build the detailed 3D model of the library building. While CloudCompare is utilized in the project to roughly clean the data and to align and merge the separate scans, ReCap Pro shall be used to clean the data in detail.

With the LAZ files from the separate scan locations imported, the workflow in CloudCompare begins with the segmentation of each file. This means that essential information, e.g. the library's facade, is isolated from additional information, e.g. trees and people (Figure 25).

Here, it is recommended to pursue a non-destructive workflow, i.e. keeping the additional information in order to be able to refer to it later in case of need. The segmentation process is repeated for each separate scan file. Subsequently, the segmented scans are rotated and their overlapping parts aligned with the rotate/translate tool to form one construction as a whole. Since the scans of the yellow, red and purple section (Figure 23). had essentially the same starting point, only little elevation adjustments for the alignment of these three sections need to be made. The most effort is required for each section's incremental rotation around the z-axis and their point clouds best possible alignment to each other (Figure 26).

CloudCompare offers an automatic registration tool called finely register, which can be leveraged to achieve a higher alignment precision. The tool is based on the Iterative Closest Point (ICP) algorithm (CloudCompare 2015), which is one of the most widely used algorithms for point cloud matching (Rajendra et al. 2014: 891). The ICP algorithm aims at finding pairs of nearest points in two adjacent scans and minimizing their distance. On this basis it calculates the required transformation and applies it, which brings the advantage that no target points need to be set manually (ibid.). However, this tool can only handle a pair of two point cloud sections at a time, which is why for this application it had to be applied four times. Thereby, it was found that CloudCompare's automatic registration tool does not work too well in the given context of application. Each time of use there has been an error distance (RMS) ranging up to 0,24, successively adding imprecision to the aligned construction. After three runs this led to the problem that the last section did either fit its left or right neighbor, but not both. This approach would probably have worked more reliably with more overlap between the scans (Cheng et al. 2018: 9) and fewer sections. However, to stay on schedule, the existing scans of the facade were used and manually matched as best as possible, e.g. using CloudCompare's cross section tool for more visual control (Figure 27).

After aligning the separate facade point clouds, they are then merged into one single point cloud. Before finalizing the building, the two separate, overlapping roof scans are as well segmented, rotated and translated manually. This time, using the finely register tool for the two roof sections produces better results, potentially because of the lower number

4 PROCEDURE AND RESULTS

of sections, more overlap between the sections and overall simpler geometries. However, because a safety distance had to be kept while scanning, it was not possible to scan every angle of the roof, especially leaving the southern edge uncovered (Figure 28).

The final step in CloudCompare is to place the roof in the correct location. Therefore the edges of the library's stairs provide important reference points for correctly aligning the roof to the facade (Figure 29). To ensure maximum flexibility for further work steps, the final aligned point cloud is then exported as two .e57 files. One file containing the merged library's facades and one containing the merged roof. This way, the appropriate file can be imported on demand during the working process and the performance can be improved because instead of one large file, there will be two smaller files.

After the processing in CloudCompare, the original workflow planned to clean up the two files in more detail using ReCap Pro. Although this was done meticulously (Figure 30), there were problems with saving the final product. This was because the program took multiple days to export and at the end of the export process it shut down, losing all the progress. To save time and work, the project group therefore decided to proceed with the rough cleanup from CloudCompare.

4.2 Creating a 3D Model of the Central University Library

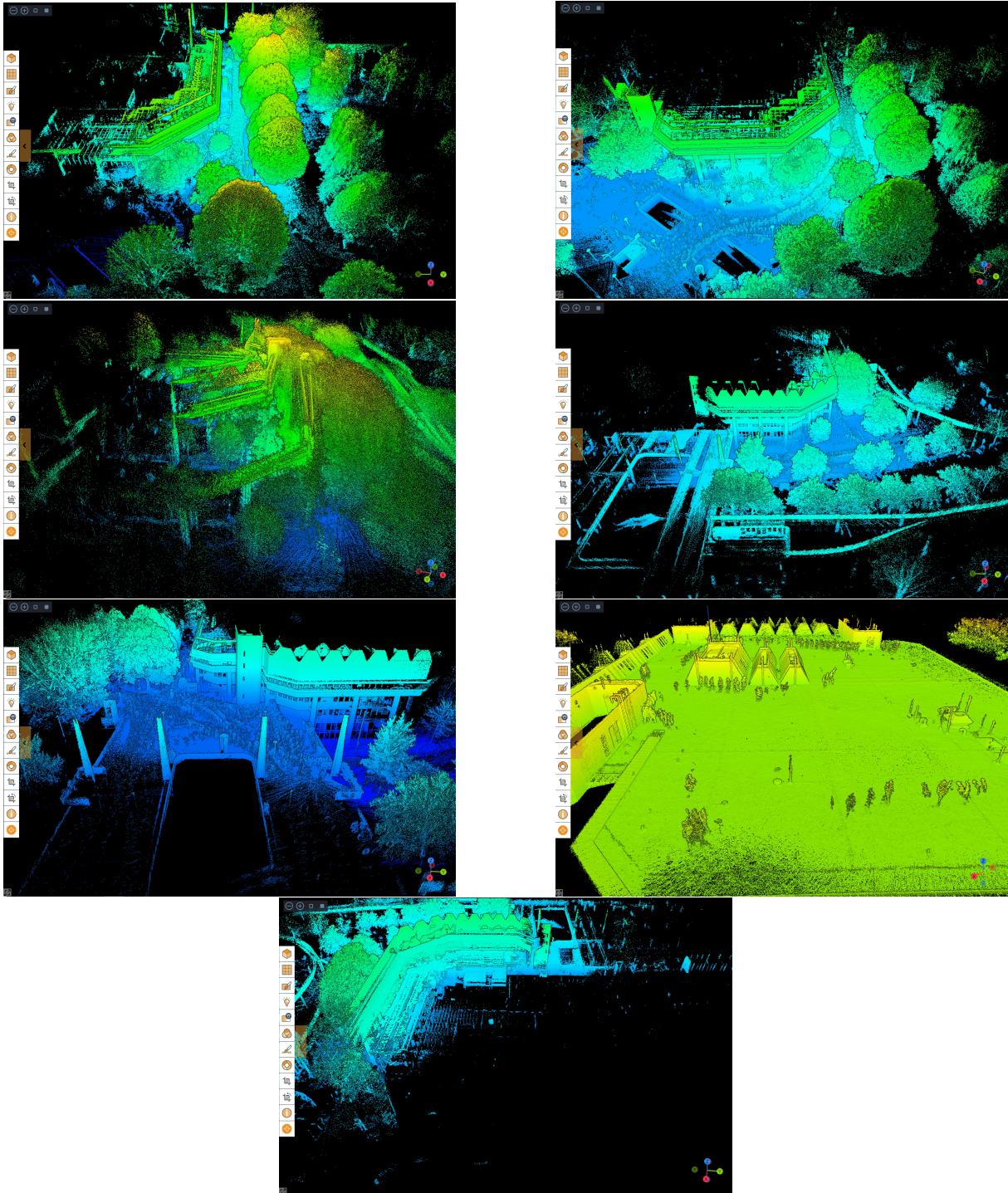


Figure 24: Data Acquisition by Seven Parts Followed by Red, Purple, Blue, Pink and Yellow Lines and Two Circles on the Roof of the Central University Library (own illustration)

4 PROCEDURE AND RESULTS

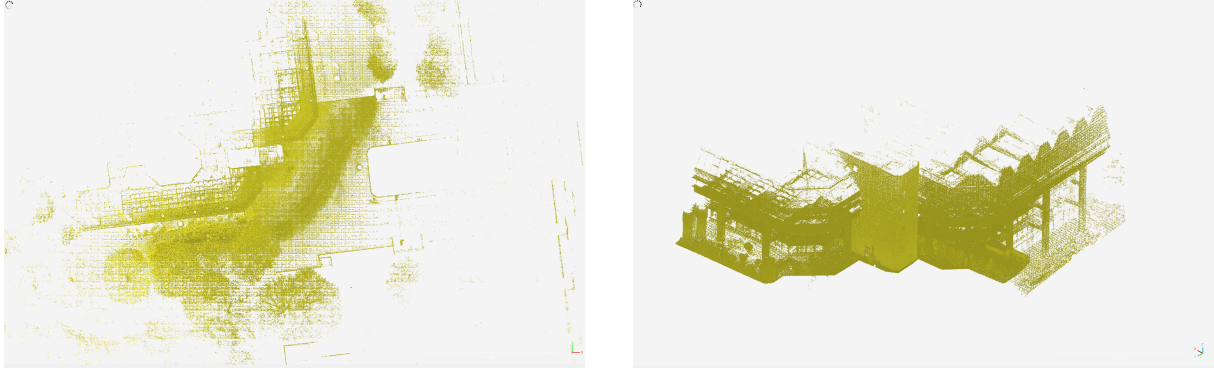


Figure 25: Screenshots of the Yellow Point Cloud Section in its Raw Form (left) and Segmented Form (right) (own illustrations)

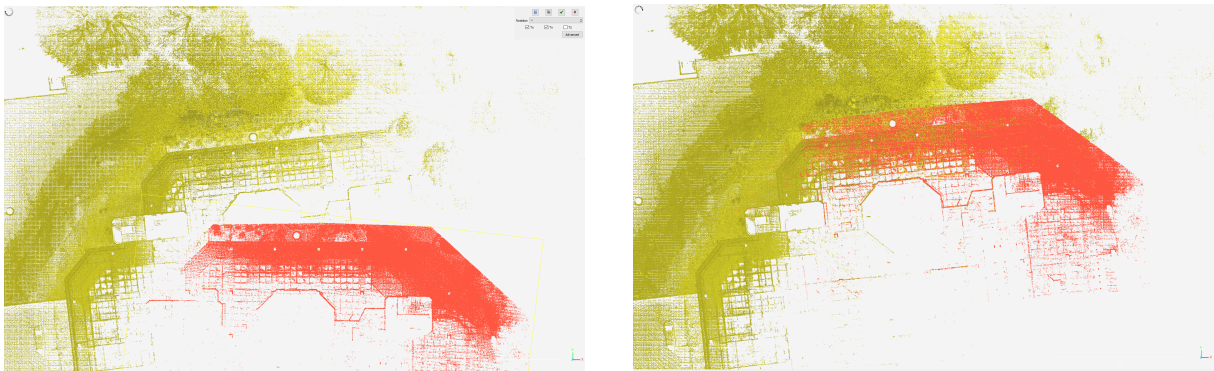


Figure 26: Z-axis Rotation of Red Section to Fit Yellow (here displayed in blue)(left) and Almost Overlapping Sections with Need for a Little Rotation (right) (own illustrations)

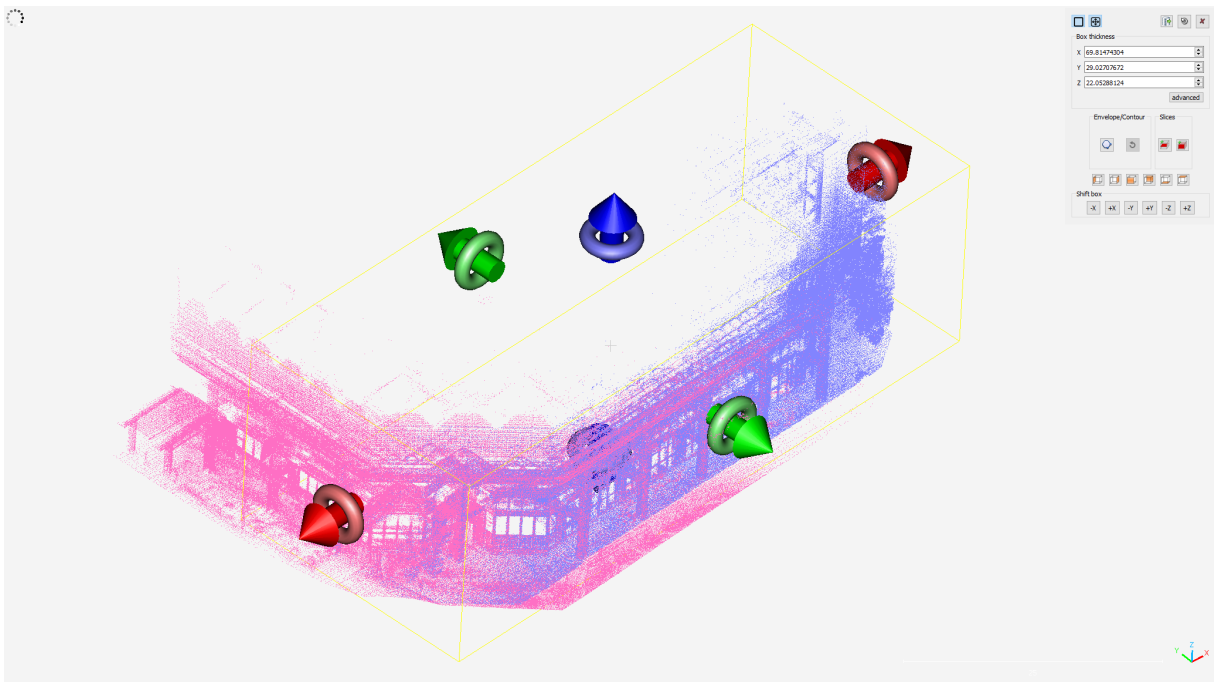


Figure 27: CloudCompare's Cross Section Tool (own illustration)

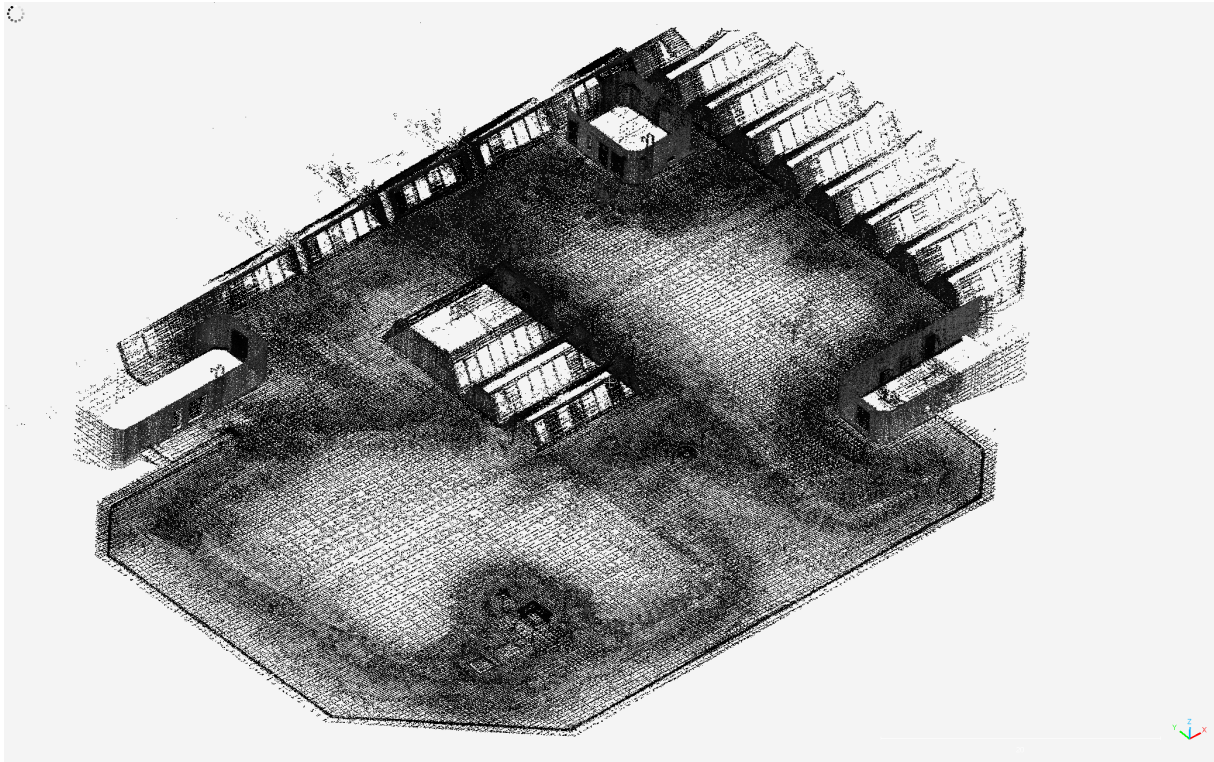


Figure 28: Aligned and Registered Roof Sections with Partly Uncovered Areas (left edge)
(own illustration)

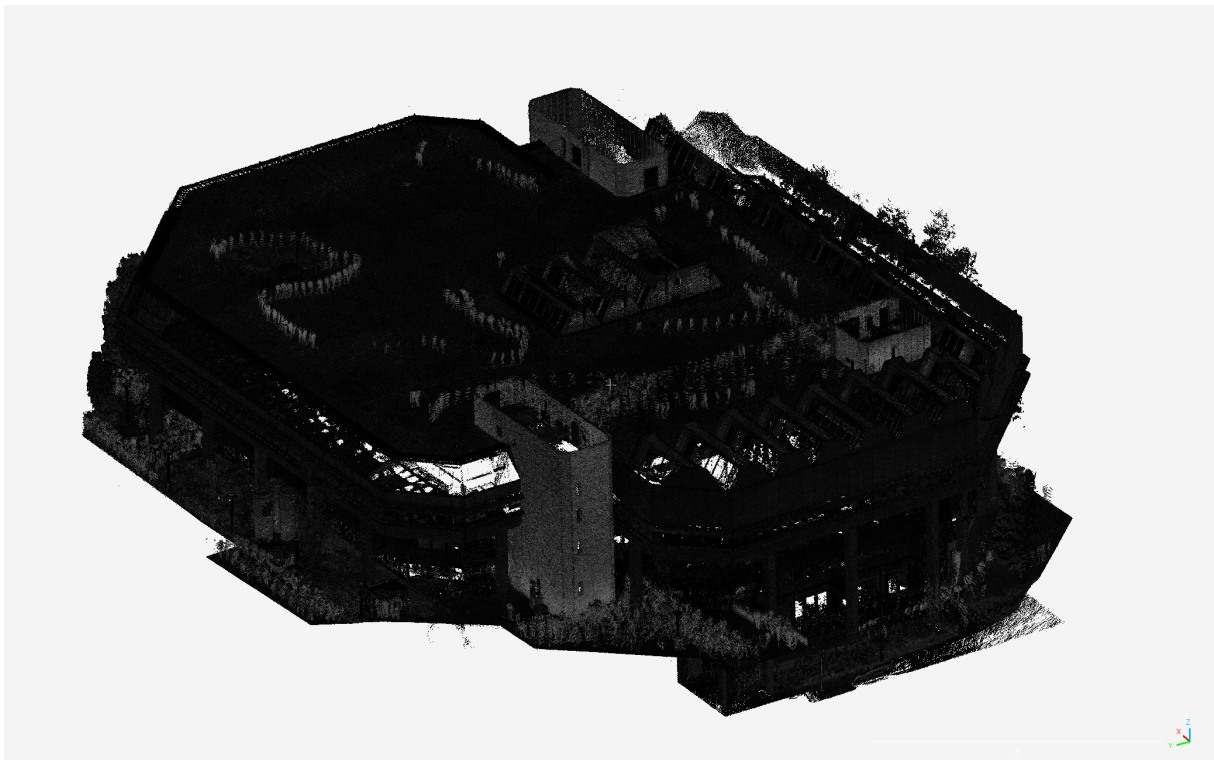


Figure 29: The Final Point Cloud with Merged Facades and Roof Sections (own illustration)

4 PROCEDURE AND RESULTS

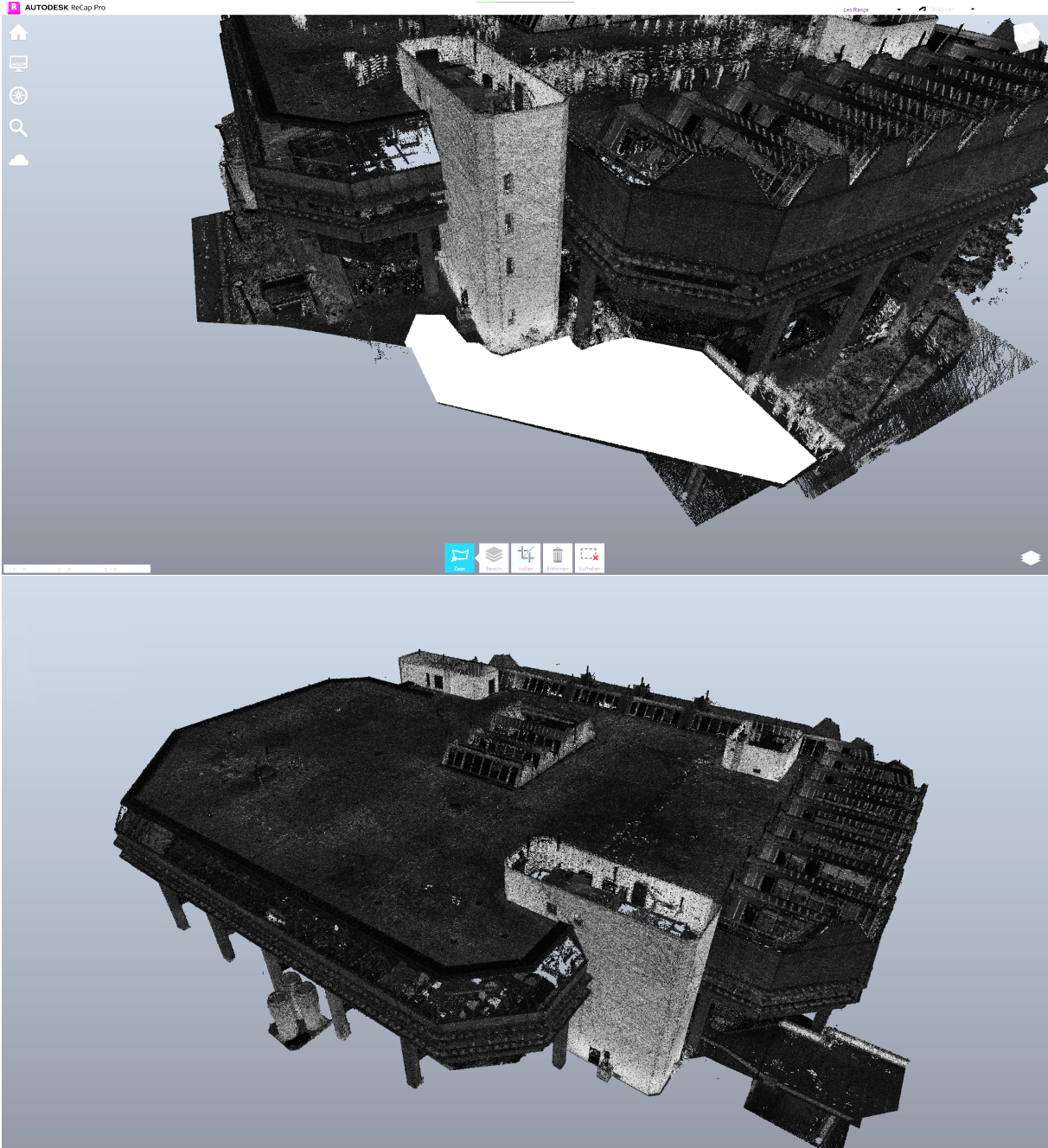


Figure 30: Detailed Cleanup Process in Autodesk ReCap Pro (top) and its Result (bottom) (own illustration)

4.2.3. Revit

After obtaining the merged point cloud, the next step is the modeling of the building facade, roof and other features like windows and doors with Revit. The 3D modeling of existing buildings via point clouds has played an important role in the cultural heritage field that this study and further studies of existing buildings can draw upon (Tommasi et al. 2016). First the point cloud needs to be exported in a file format that can be handled by Revit and then the building is modeled using family libraries and (limited) parametric modeling.

First, in ReCap Pro the combined .e57 point cloud file is imported. Here some of the same functionality as in CloudCompare can be applied. Because the point cloud was already cleaned up and cut back in CloudCompare as described in Chapter 4.2.2, the data only had to be saved as a .rcp file for import in Revit, which was achieved without significant processing time. In Revit, the .rcp file is embedded into a new project. After this, the point cloud is rotated so that the longest walls are orthogonal to the grid for ease of use and to keep consistency to the other modeling steps.

Revit is a parametric object-oriented software, i.e. components can be defined by fixed and editable parameters (Tommasi et al. 2016: 434). This is especially useful when there are repeating elements like windows or facade structures. Windows for example can be defined by their width, height and width of frame while other elements like the depth and the materials are fixed. This family logic applies to every element that is not unique in the building.

The basic workflow looks like this: First the horizontal and vertical cross sections that describe important points in the structure like floor bottoms and ceilings are defined. Viewing the floor plans now reveals usable slices of the point cloud with which the walls and windows can be modeled (Figure 31). Here, the Revit Family modules are used. Walls are drawn atop the lines in the point cloud. Windows and other facade elements are drawn using the sectional planes. Here, two additional types of data are used: UAV footage of the outside as well as existing architectural floor plans. Because of the repeating elements, especially windows, length measurements can be extrapolated from these elements (Figure 31). After that, the walls are compared with the floor plans. Because of inaccuracies in the point cloud (see Chapter 4.2.2) as well as in the floor plans a combination of all data is used to model the building. The overall difference between the model and the provided floor plans does not exceed 0,5 m (Figure 32). With this approach a fairly detailed model of the library building is achieved (Figure 33) that can be used for further climate modeling in ENVI-met as well as visualization in Unreal Engine.

4 PROCEDURE AND RESULTS



Figure 31: Floor Plan of Point Cloud/Walls with Measurements (left), Length Measurements of Windows (right) (own illustration)

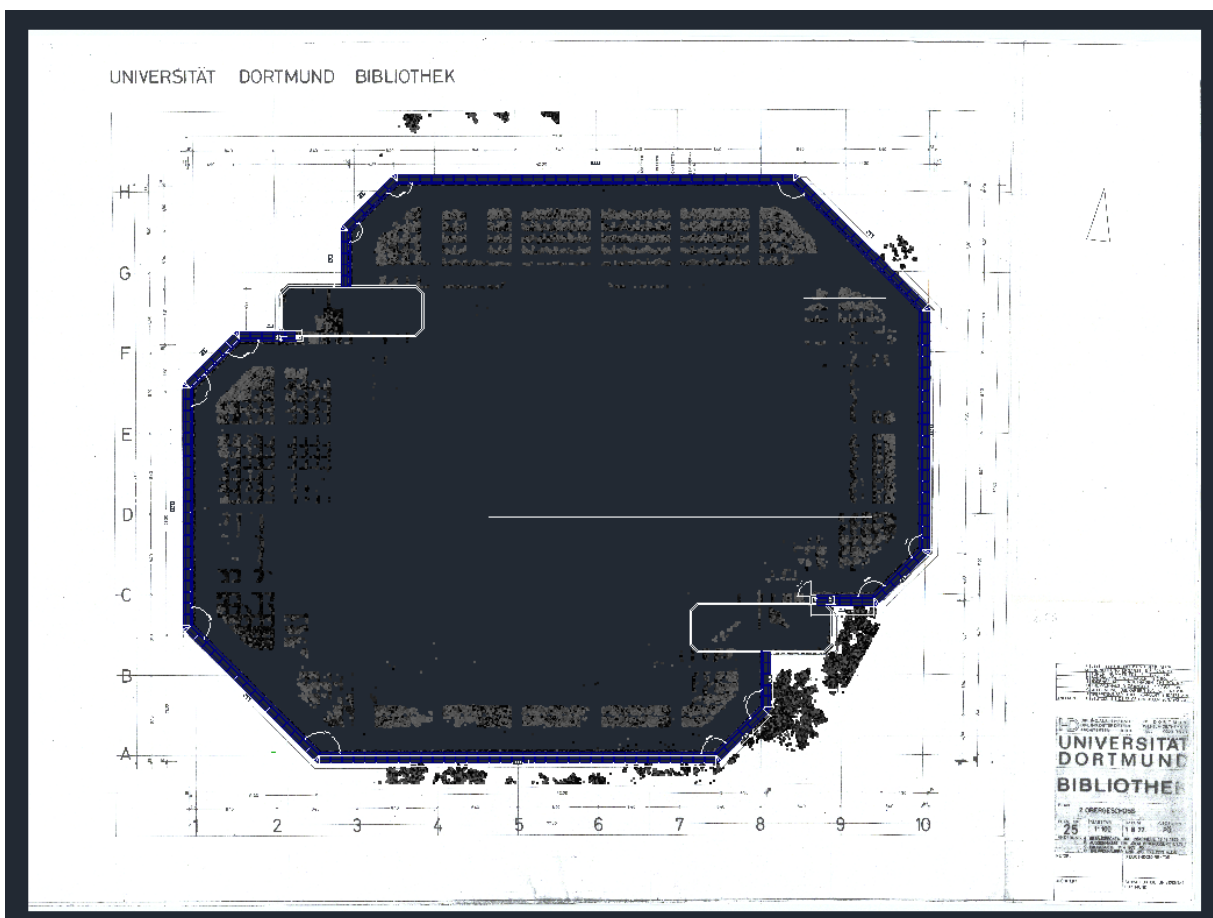


Figure 32: Comparison to the Floor Plan at the Second Level (own illustration)

4.2 Creating a 3D Model of the Central University Library

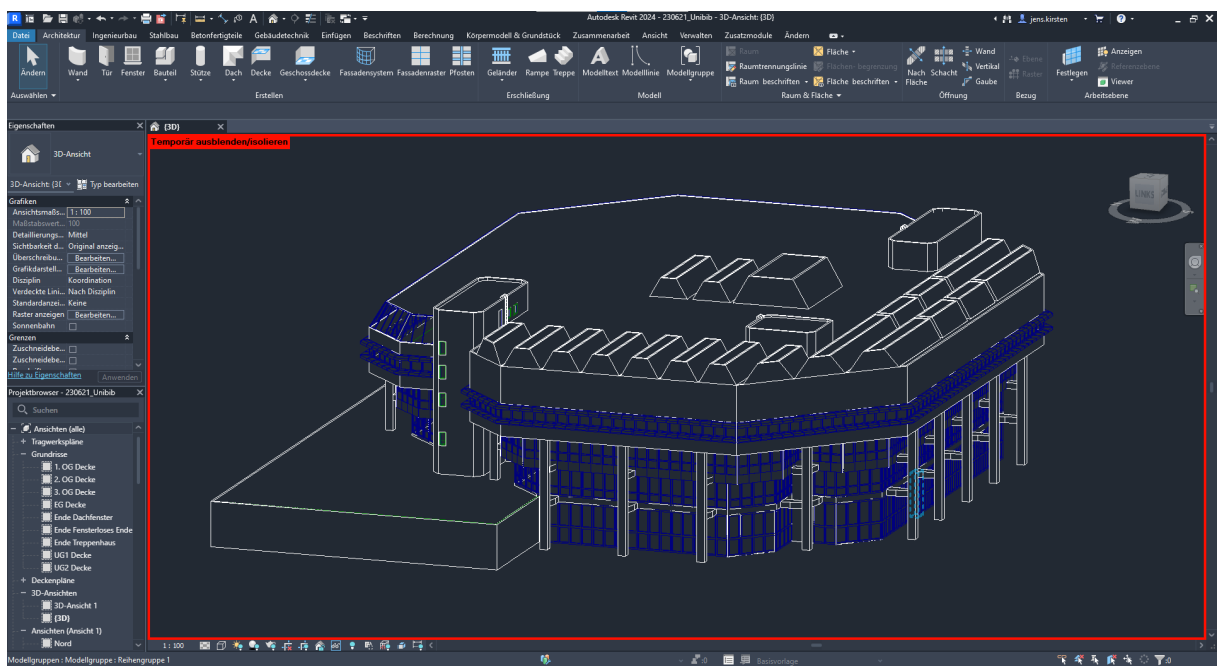


Figure 33: Finished Revit Model (own illustration)

4.3. LoRaWan and Weather Sensors

In this chapter, first the technical and physical installation of the weather sensors and the gateway, as part of WP4, is described. Also the way of managing and storing the weather data which are sent by the sensors is highlighted.

4.3.1. Installation of Sensors and Gateway

In recent years, The Things Network (TTN) has provided a global collaborative device ecosystem with LoRaWAN to support the IoT by facilitating long-distance wireless communication. In addition to a set of open tools, it offers a global, open network at a low cost, allowing for maximum security and scalability (Khoa et al. 2019: 1). An interactive map of all established gateways around the world, which can be found on the TTN website, underlines its broad use. In particular, TTN is operated through The Things Stack, which is a LoRaWAN network server for managing, monitoring, and connecting devices, gateways, and end-user applications. The data routing is secured, scalable, and reliable due to it (The Things Industries n.d.-a). Due to the outstanding and user-friendly features mentioned above, TTN/The Things Stack was used for setting up the gateway and sensors in the project.

This project utilized the DLOS8N Outdoor LoRaWAN Gateway, which is an open source outdoor LoRaWAN gateway. In order to support applications in different countries, DLOS8N has pre-configured LoRaWAN frequency bands. During this project, the frequency is EU_863.870 MHz. In addition to the gateway, four LoRaWAN weather sensors (LSN50v2-S31B) are used, which measure the surrounding air temperature and relative humidity precisely. At a given time interval, the sensors keep pushing their data via LoRaWAN to the gateway, from where it is then forwarded to the IoT server (Figure 34). The built-in sensor SHT31 offers a highly reliable and stable digital output with fully calibrated, linearized and temperature compensated output. Further, the SHT31 is equipped with an anti-condensation waterproof casing for long-term use, as well as eight 1000 mAh Li-SOCI2 batteries, designed for long-term use up to ten years (Dragino 2023).

Within LoRaWAN, it is a requirement that every LSN50v2-S31 end device registers with a network before it can send and receive messages. The LSN50v2-S31 end devices perform a join procedure with a LoRaWAN network using keys including AppEUI, DevEUI, and AppKey that are unique globally which users need for registering activated by an Over The Air Authentication (OTAA) or Authentication By Personalisation (ABP) (The Things Network n.d.). When the LSN50v2-S31 is powered on, it will join the LoRaWAN network and begin transmitting data. In this project, the uplink period, i.e. the data transfer interval, has been set to 10 minutes.

A *DLOS8N Outdoor LoRaWAN Gateway with an inserted SIM Card* to bridge an IP network server to the LoRa network and four end devices LSN50 vs-S31B were configured

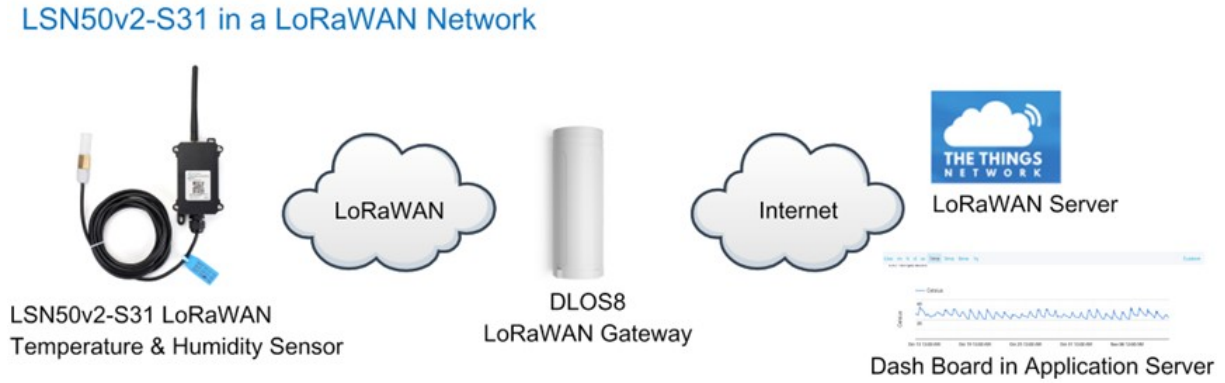


Figure 34: LSN50v2-S31 Operates with DLOS8N Outdoor LoRaWAN Gateway in the LoRaWAN Network (Dragino 2023)

according to number of identifiers for end devices (DevEUI - 64 bit end-device identifier, EUI-64 (unique)) and gateway (GatewayEUI - 64 bit gateway identifier, EUI-64 (unique)) (Table 2)

Table 2: Number of Identifiers for Gateway and End Devices

Devices	GatewayEUI/ DevEUI
Gateway	A8 40 41 FF FF 23 A5 C8
Sensor 1	A8 40 41 2E A1 86 CB 27
Sensor 2	A8 40 41 3A 21 86 CB 29
Sensor 3	A8 40 41 33 31 86 CB 1A
Sensor 4	A8 40 41 6D 01 86 CB 22

The four sensors were installed in different locations to represent different weather conditions. It was also important to be able to access them from inside the library building for future maintenance, but to protect them as much as possible against theft from outside. The gateway was installed on the roof (Figure 35 & 36, Appendix A.1).

4.3.2. Sensor Data Management

At this point the weather sensors were embedded in the established LoRaWAN environment, physically attached to the library and since then have been sending their data to the The Things Stack application server (see Chapter 4.3.1). Here the sensors can be managed and their data values can be displayed right after receiving and decoding their uplink data message. However, the data values are not stored permanently on The Things Stack (Egger 2021).

In order to build up a dataset to use for the microclimate simulation it is therefore required to have the data forwarded from the network and stored somewhere permanently. For this, as a first step, a webspace has to be registered. The provider bplaced.net for example offers a free web hosting service including up to two MySQL databases and hosts

4 PROCEDURE AND RESULTS



Figure 35: Locations of the Gateway and Weather Sensors (own illustration based on Grützner 2022)

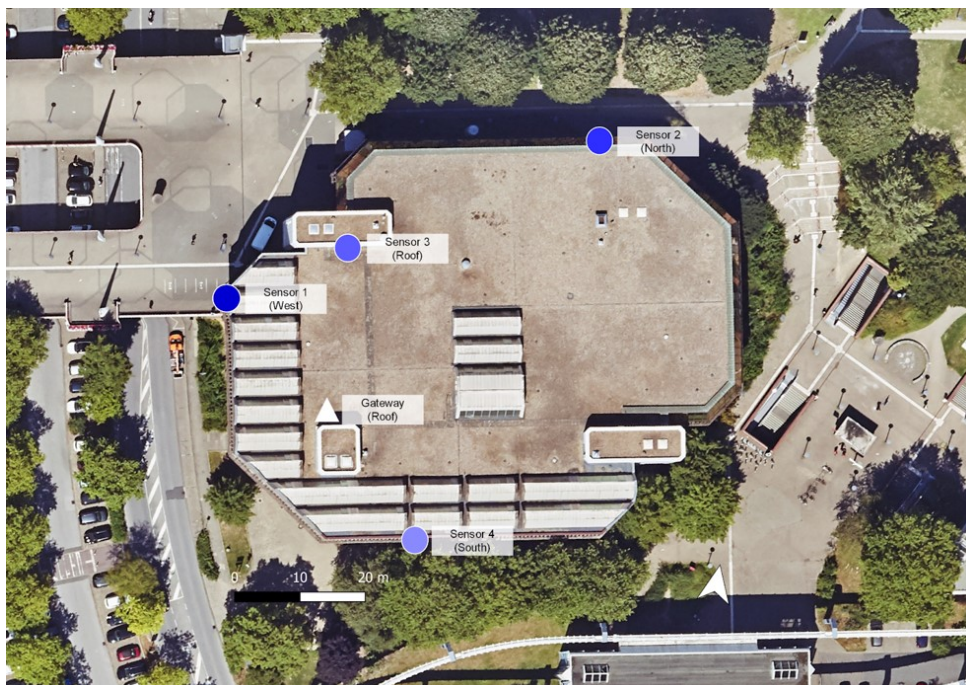


Figure 36: Placement of Gateway and Weather Sensors (own illustration based on DOP BY RVR 2022)

his servers in Austria and Germany, which is beneficial for data privacy. After registration, a MySQL database has to be added, which will later contain the data values of the sensors. SQL stands for structured query language and marks a standard that is used to interact with databases and retrieve particular information needed (Rohland 2008). MySQL on the other hand is an open source database that builds upon that standard and enables the actual interaction with the database, e.g. via data queries (MySQL n.d.).

A free .php script helps to get the data values automatically written into the database (see Egger 2021). PHP as a programming language is well suited due to its simple syntax and the possibility to be used on the bplaced FTP server (Powers 2022: 1; bplaced n.d.). However, in order to function properly this script first has to be filled with individual information such as the database's username and password (Figure 37). In a next step the .php script files have to be uploaded via file transfer protocol (FTP) to the webspace's FTP server with the help of a FTP client / program such as FileZilla. FTP allows the efficient file transfer between client and server and storage of data on the FTP server (Bhushan 1972). As a last configuration step concerning the bplaced webspace, a stylesheet preset has to be imported into the database, so the sensor data are later on structured (see Egger 2021).

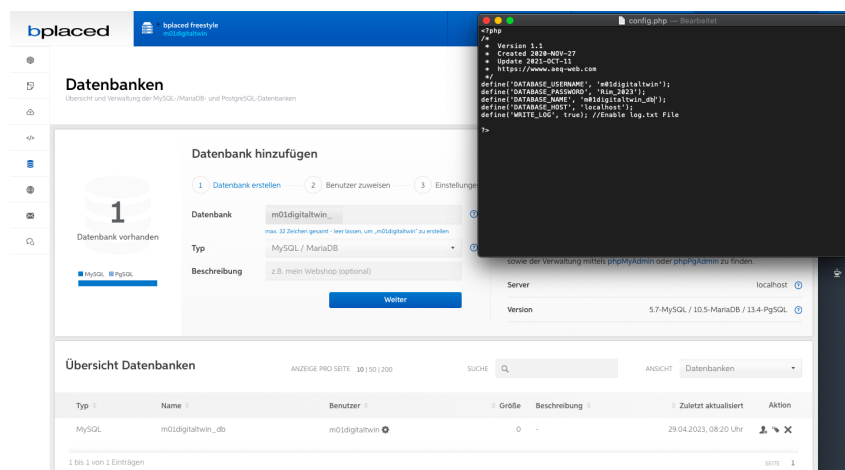
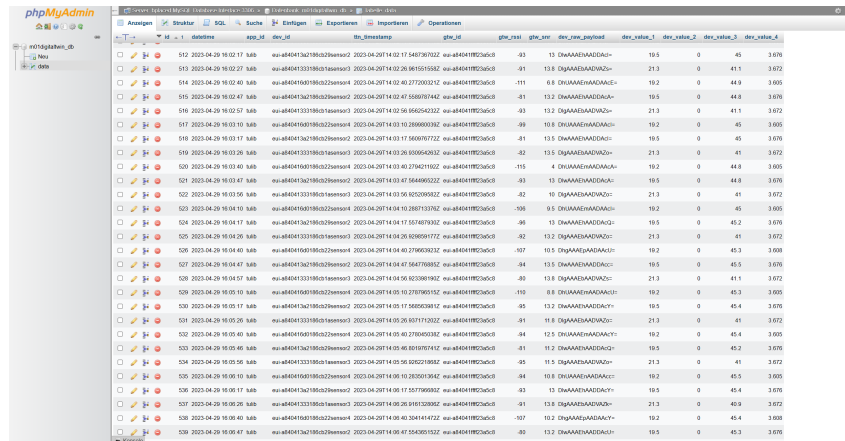


Figure 37: Configuration of the PHP Script's Config File with Individual Information (own illustration)

Now that the webspace and database have been configured and the .php script files have been uploaded to the webspace, it needs sensor data that can be written into the database. To achieve this, the data from The Things Stack are forwarded to the .php script using a webhook. Webhooks allow servers to communicate with each other and to build an integration with third party services like the bplaced webspace and its .php script (The Things Industries n.d.-b). With the sensors sending their data to the database, it is now possible, but also necessary, to keep track of the data from time to time using the phpMyAdmin database dashboard. phpMyAdmin is a webtool and gives the possibility to visually manage the database and to use different tools, e.g. creation of simple graphs,

4 PROCEDURE AND RESULTS

while still granting the ability to directly execute SQL statements (phpMyAdmin n.d.). Each database row represents a single measurement and contains information about e.g. the sensor name, the date and time as well as the air temperature and relative humidity of measurement (Figure 38).



id	date	time	sensor	temp	humid	...				
512	2023-04-29	16:02:11	484043307386032sensor0	17.54873032	484041883608	03	13	0	45	3.676
513	2023-04-29	16:02:27	484043307386032sensor0	17.54873032	484041883608	03	13	0	45	3.676
514	2023-04-29	16:02:43	484043307386032sensor0	17.54873032	484041883608	03	13	0	45	3.676
515	2023-04-29	16:02:59	484043307386032sensor0	17.54873032	484041883608	03	13	0	45	3.676
516	2023-04-29	16:03:15	484043307386032sensor0	17.54873032	484041883608	03	13	0	45	3.676
517	2023-04-29	16:03:31	484043307386032sensor0	17.54873032	484041883608	03	13	0	45	3.676
518	2023-04-29	16:03:47	484043307386032sensor0	17.54873032	484041883608	03	13	0	45	3.676
519	2023-04-29	16:04:03	484043307386032sensor0	17.54873032	484041883608	03	13	0	45	3.676
520	2023-04-29	16:04:19	484043307386032sensor0	17.54873032	484041883608	03	13	0	45	3.676
521	2023-04-29	16:04:35	484043307386032sensor0	17.54873032	484041883608	03	13	0	45	3.676
522	2023-04-29	16:04:51	484043307386032sensor0	17.54873032	484041883608	03	13	0	45	3.676
523	2023-04-29	16:05:07	484043307386032sensor0	17.54873032	484041883608	03	13	0	45	3.676
524	2023-04-29	16:05:23	484043307386032sensor0	17.54873032	484041883608	03	13	0	45	3.676
525	2023-04-29	16:05:39	484043307386032sensor0	17.54873032	484041883608	03	13	0	45	3.676
526	2023-04-29	16:05:55	484043307386032sensor0	17.54873032	484041883608	03	13	0	45	3.676
527	2023-04-29	16:06:11	484043307386032sensor0	17.54873032	484041883608	03	13	0	45	3.676
528	2023-04-29	16:06:27	484043307386032sensor0	17.54873032	484041883608	03	13	0	45	3.676
529	2023-04-29	16:06:43	484043307386032sensor0	17.54873032	484041883608	03	13	0	45	3.676
530	2023-04-29	16:06:59	484043307386032sensor0	17.54873032	484041883608	03	13	0	45	3.676
531	2023-04-29	16:07:15	484043307386032sensor0	17.54873032	484041883608	03	13	0	45	3.676
532	2023-04-29	16:07:31	484043307386032sensor0	17.54873032	484041883608	03	13	0	45	3.676
533	2023-04-29	16:07:47	484043307386032sensor0	17.54873032	484041883608	03	13	0	45	3.676
534	2023-04-29	16:08:03	484043307386032sensor0	17.54873032	484041883608	03	13	0	45	3.676
535	2023-04-29	16:08:19	484043307386032sensor0	17.54873032	484041883608	03	13	0	45	3.676
536	2023-04-29	16:08:35	484043307386032sensor0	17.54873032	484041883608	03	13	0	45	3.676
537	2023-04-29	16:08:51	484043307386032sensor0	17.54873032	484041883608	03	13	0	45	3.676
538	2023-04-29	16:09:07	484043307386032sensor0	17.54873032	484041883608	03	13	0	45	3.676
539	2023-04-29	16:09:23	484043307386032sensor0	17.54873032	484041883608	03	13	0	45	3.676

Figure 38: Excerpt of the Database (at this point without sensor 1) (own illustration)

In the early stages of the project, each sensor worked properly and the data were reliably sent to the database. At a later stage, it was noticed that individual data packets were occasionally missing, manifesting e.g. in missing transmission intervals in the data records. The reason for this could not be found. However, instead of one exact reason, there may be several reasons presumably causing this. From downtime caused by temporary attempts to process and export the data in multiple formats for different work packages of the project (e.g. WP5 & 6), over failures on the sensor's end (expectable packet loss (The Things Industries n.d.a) and re-integration issues with sensor 1), to multiple possibly conflicting webhooks for different application areas (bplaced MySQL database, ArcGIS Online / Dashboard and VR). The database entries were regularly archived in tables to prevent data loss and finally used for the microclimate simulation.

4.4. Microclimate Simulations with ENVI-met V5.5.1

This chapter presents the procedures for WP3 and WP4. This includes the creation of 3D models of the two study areas, the preparation and execution of the simulation file, and the presentation of the results with their verification and evaluation.

4.4.1. Overview - ENVI-met System and Simulation Models

ENVI-met is a software designed for predicting urban microclimate for small sections of urban areas. Common fields of application include architecture, landscape architecture, building design, and environmental planning (ENVI-met 2021a). Unlike several other environmental simulation models, it not only calculates e.g. the airflow between buildings

or the solar radiation on facades, but consists of a variety of dynamic sub-systems taking into account different interactions between buildings, surfaces, vegetation and air, including its synergies (ENVI-met 2017b: 6; ENVI-met 2021a; see Chapter 3.2). Because of this holistic approach and its well-featured and approachable program suite, it is used in this study. The software has been continuously improved since 1994 (ENVI-met 2017b: 6) and each update offers improvements in the handling of the software and in the simulation calculations (ENVI-met 2023b). Therefore, this study is realized with the latest version, V5.5.1.

Several simulations are performed to investigate the influence of the input 3D model, focusing on the extension of the study area, the LoD and the grid resolution (Table 3). Therefore, different simulation models are exported from a base model in LoD2 that covers the extended area. The narrow area is defined by limiting the extended area to a smaller size. This ensures that the objects in the simulation models are placed in the same size and position. For the narrow area, some building parts and plants needed to be eliminated due to the required free space between objects and model borders. The grid resolution is chosen when exporting the model. For a better overview, IDs are assigned to the individual simulation models (Table 3). They are named after the respective Area Input File (.INX-file) used for the simulation. All other settings remain the same for the simulations.

For the analysis of the influence of the LoD (Figure 39) two models of the narrow area with a grid resolution of 1 m on each axis are compared (INX1 and INX2). In one model, the Central University Library building, which in the base model is in LoD2, is replaced by the 3D model built in Revit (see Chapter 4.2.3). The influence of the extent of the study area is investigated by comparing a model of the narrow area (INX3) with a model of the extended area (INX5) with a grid resolution of 5 m on the x, y, and z axes (Figure 40). Furthermore, the influence of the grid resolution is analyzed with two models of the narrow area (INX2 and INX3) (Figure 41), and with two models of the extended area (INX4 and INX5) (Figure 42). The comparison for the narrow area focuses on a grid resolution of 1 m or 5 m on each axis. For the extended area, grid resolutions of 2 m x 2 m x 3 m and 5 m x 5 m x 5 m, respectively, are compared. As part of the analysis, the simulation results are verified with the collected values measured by the weather sensors

Table 3: Overview of Performed Simulations

Model ID	Study Area	LoD	Grid resolution (x-y-z)
INX1	narrow area	LoD3	1 m x 1 m x 1 m
INX2	narrow area	LoD2	1 m x 1 m x 1 m
INX3	narrow area	LoD2	5 m x 5 m x 5 m
INX4	extended area	LoD2	5 m x 5 m x 5 m
INX5	extended area	LoD2	2 m x 2 m x 3 m

(see Chapter 4.3.2).

The ENVI-met software is divided into several applications that complement each other and structure the process from model creation to simulation and result evaluation (Table 4). BIO-met and Albero were not used in this study. Monde was replaced by SketchUp.

Table 4: ENVI-met Software Applications (own illustration based on ENVI-met 2022)

Software Application	Description
Headquarter	Provision of quick access to all ENVI-met applications
Projects/Workspace	Definition of workspace and organization of projects
Monde	Digitizing model area (2.5D), Generation of provisional Area Input File
Spaces	Digitizing model area (2.5D and conversion to 3D model), Generation of final Area Input File
Forcing Manager	Generation of Full Forcing Files from measured data or common weather file for the simulation file
ENVI-guide	Definition of general and meteorological simulation settings and creation of simulation file
ENVI-core	Execution of the simulation
BIO-met	Calculation of Human Thermal Comfort Indices from ENVI-met model output files
Leonardo	2D and 3D analysis of results
DB Manager	Database of all elements (wall materials, soils, simple plants, sources etc.) and their attributes available for digitizing the model area, includes creation and modification of customized materials
Albero	3D modeling of plants for digitizing the model area

4.4.2. Creating of 3D Models of the Study Areas

For the numerical calculation of the urban microclimate, a computational image in the form of a 3D model of the area of interest is required (Bruse 2000: 4, 6). The simulation model consists of different elements: Buildings, soils, plants and terrain, which are assigned different elements such as materials or plant types that are stored in a database. These elements contain different attributes relevant for the microclimate, e.g. the albedo

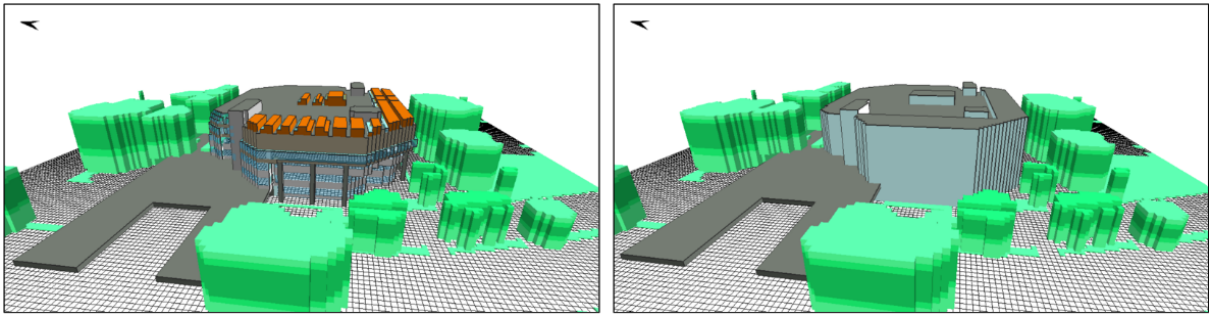


Figure 39: Difference in Level of Detail - Model in LoD3 (INX1; left) vs. LoD2 (INX2; right), Soil Not Displayed (own illustration)

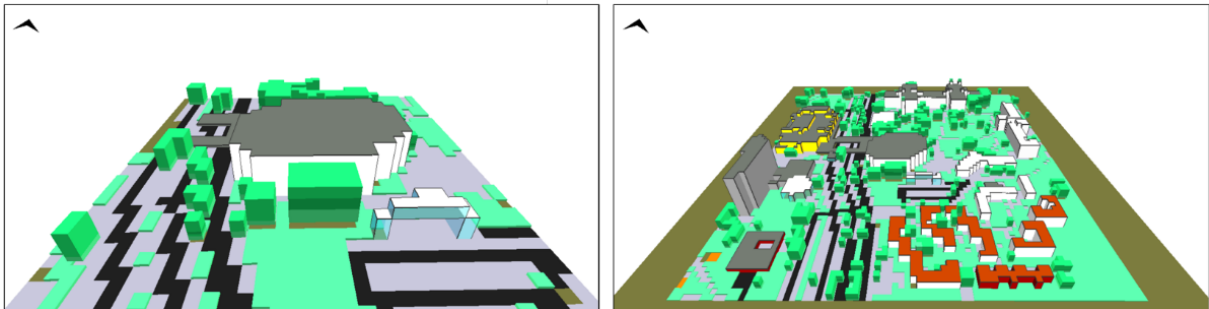


Figure 40: Difference in Study Area Extension - Models of INX3 (left) and INX4 (right) (own illustration)

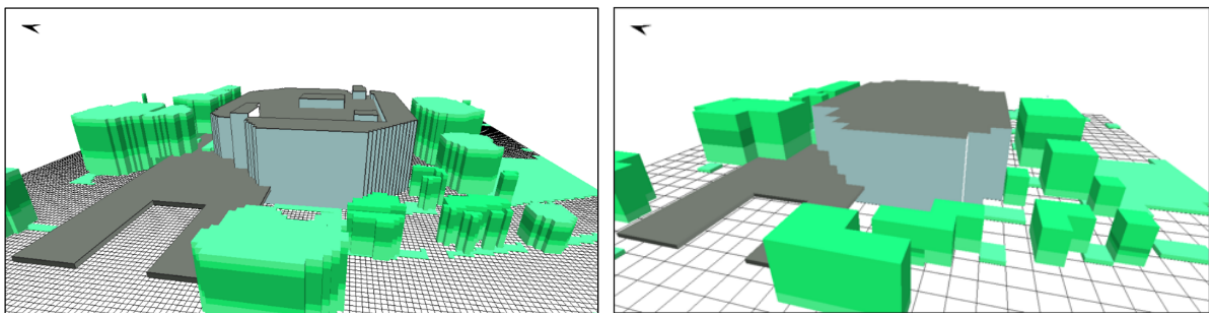


Figure 41: Difference in Grid Resolution - Model in 1 m x 1 m x 1 m (INX 2 ; left) vs. 5 m x 5 m x 5 m (INX 3, right); Soil Not Displayed (own illustration)

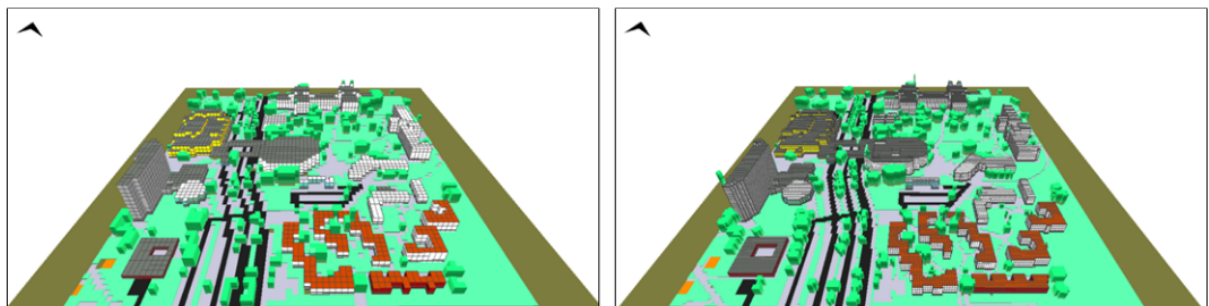


Figure 42: Difference in Grid Resolution - Model in 5 x 5 x 5 (INX 4 ; left) vs. 2 x 2 x 3 (INX 5, right); Soil Not Displayed (own illustration)

of surfaces. The 3D simulation model is created in several steps in the form of a rectangular grid-based cuboid consisting of basic volume elements (Bruse 2000: 4). By combining these grid blocks, complex structures can be approximated (ibid.). The model architecture is therefore constrained by the boundaries of the individual grid blocks and angled edges are represented in a stair-like pattern. The higher the resolution of the grid, the more accurately the microclimatic parameters are calculated (ibid.: 6). However, a high accuracy is accompanied by a high computational effort, which is mainly reflected in long calculation times (ibid.). The typical horizontal model resolution ranges from 1 m to 10 m (ENVI-met n. d.). The recommended dimensions for the overall size of the model range from 50 x 50 to 500 × 500 grid cells in the x-y plane and 20 to 50 grid cells along the z-axis (ibid.)

For generating the 3D model, first, a 2,5D model of the study area must be created. A 2,5D model is a 2D model that implicitly stores height information in addition to the x-y plane information (ENVI-met 2018: Min 00'30"-01'38"). This allows a 3D view of the model, but limits the possibilities of material assignment: only one material type per cell of the x-y plane can be assigned (ibid.). For specifying the material of each grid block, 3D coordinates are required (ibid.). These are only generated with the conversion from the 2,5D to a 3D model (ibid.). However, the advantage of the 2,5D model is the possibility to adjust the resolution of the model grid after the model has been built (ibid.).

The 2,5D model can be built either in ENVI-met Monde or using the QGIS plugin (ENVI-met 2023c) or SketchUp Pro and the Envimet INX plugin (Di Nunzio 2022). The Envimet INX plugin allows building the 2,5D models for ENVI-met Spaces in SketchUp (ibid.). For this study, the plugin for SketchUp Pro was chosen because it allows the modeling of the variety of roof structures in the study area relatively easily. The tool is based on vector data and helps setting up most parts of the model such as grids, buildings, soils, terrain, 2D and 3D plants, resources and sources (Di Nunzio 2022). Before modeling, all necessary data, such as building footprints, heights, and materials, ground surfaces, and existing vegetation, must be gathered. (Aerial) photographs and digital orthophotos, including those from Google Maps and Google Earth, as well as site visits are helpful. Based on the spatial data collected, georeferenced modeling of the study area was mainly done using SketchUp Pro software, supported by data preparation in ArcGIS Pro and SketchUp Pro Eneroth Face Creator plugin.

In SketchUp Pro, the model's geolocation has to be defined since the geographical location is relevant for the simulation results. ENVI-met uses the UTM coordinate system based on the World Geodetic System 84 ellipsoid. To better fit the structure of the study area to the rectangular grid, it is possible to rotate the area counterclockwise (Appendix B.1). In this case, it is rotated by 349,1 degrees. The grid is created using the Envimet INX plugin. It is possible to create multiple grids for exporting various Area Input Files (.INX files), which are needed for the further processing of the model. As a method of

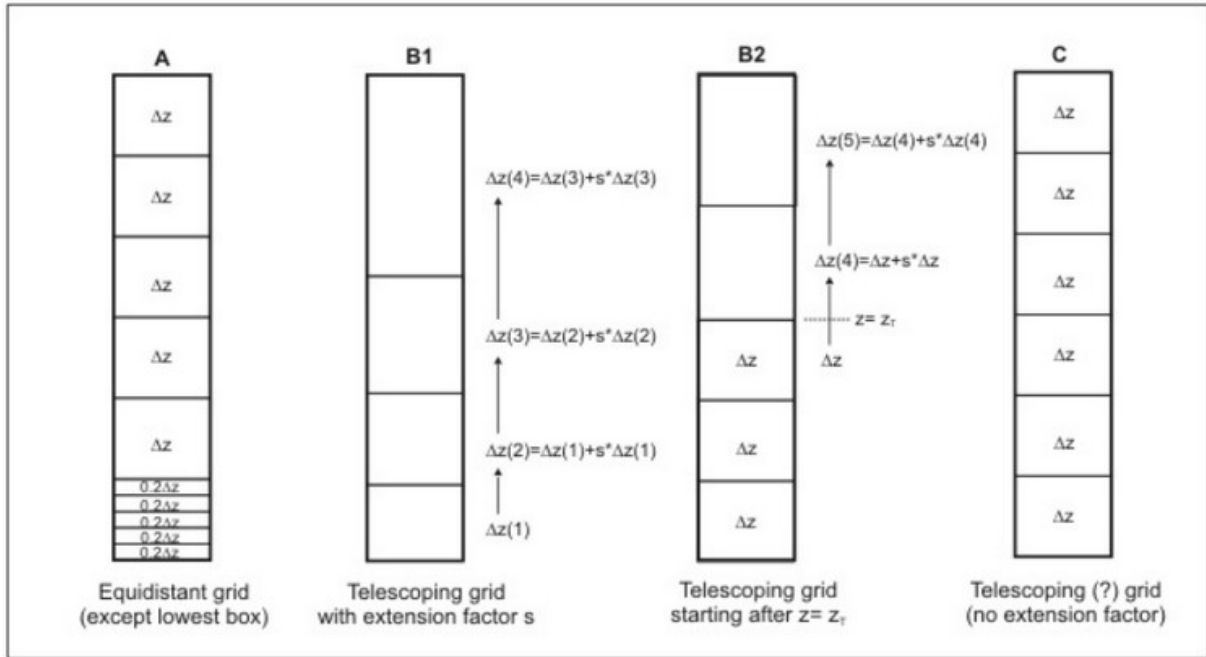


Figure 43: Concepts of Vertical Grids (ENVI-met 2021a)

vertical gridding (Figure 43), a combination of telescoping and equidistant grid is chosen in order to reduce the computational effort. Equidistant means that the height Δz of the lowest grid cell is split into 5 subcells (ENVI-met 2021b). Telescoping means that the size of Δz increases exponentially with increasing height (ibid.). It is recommended to start telescoping above the highest object of the model to prevent distortions (ENVI-met Admin Tim 2020). According to the developers, telescoping factors up to 30% are reasonable and up to 20% are recommended if the cells should not be stretched too extremely (ibid.). In this study, telescoping of 20% will start above the Central University Library in the models for the narrow study area and above the Maths Building in the models with extended study area at 21 m and 60 m, respectively.

In SketchUp Pro, all buildings are drawn as closed 3D solids. It is important to keep the geometry of all elements as clean and simple as possible (Di Nunzio 2022). Due to the resolution of the analysis grid, roofs are represented as flat roofs, windows are excluded, but larger cuboid roof structures are taken into account. The buildings are then converted individually into SketchUp Pro groups via the Envimet INX plugin, indicating the appropriate facade and roof materials from the DB Manager (Appendix B.2). It is important that each element is assigned its own ID. Otherwise, errors may occur. For easier modeling of the soil surfaces, a shapefile is created for each soil material in ArcGIS Pro and imported into SketchUp Pro. These individual layers can each be easily converted into skp groups in SketchUp Pro and assigned the appropriate soil material, in this model Asphalt and Pavement (Appendix B.3). The procedure for modeling vegetation is the same as for soil surfaces. Grass areas and trees with different heights were each created as a shapefile, imported into SketchUp Pro and defined as a skp group with the

matching element from DB Manager (Appendix B.4). Terrain modeling is also possible. According to the developers, the development of terrain calculation is in progress and they do not recommend it for general simulations or study areas with relatively flat topography including changes up to 10 m of terrain height as it complicates the analysis (ENVI-met Admin Tim 2023). Due to the relatively small height differences of about 4 m in the study area (see Chapter 2.3) as well as the complex geometry of DEM and the resulting difficulty of processing it in SketchUp Pro, this was not included.

The final 2,5D model is exported as an ENVI-met Area Input file (.INX file) and further processed in the application Spaces. In Spaces, the geographical location and model geometry such as the size of grid cells or the method of vertical grid generation can be adapted. There is also a function to adapt the grid resolution, which did not work in this study. Changing the resolution after exporting the .INX file from SketchUp Pro led to misaligned building IDs. In addition, final details of the model or materials can be edited before the model is converted into a 3D simulation model. In the case of model INX2, no adjustments are made. The building's materials are a concrete to glass ratio 50 to 50 for the facade and default concrete for the roof. In contrast to this, the materials of the LoD3 library building (INX1) are adapted to reality on a small scale (Figure 39). For comparability of the results, the models share the same model geometry or study extent, depending on the focus (Table 5).

4.4.3. Preparing and Running the Simulation Files

Following the creation of the .INX file, the respective Area Input File for the investigation of the urban climate is transferred to the application ENVI-guide to generate the simulation file. Here, general simulation settings such as date, time and duration as well as meteorological settings must be defined. A typical time frame is 24-48 h, with a minimum of 6 h (ENVI-met 2017a). With sufficient hardware simulations of several months or a whole year are also possible. As numerical models need a certain initialisation time, the simulation start time should be at night or during sunrise (ENVI-met 2017a). It can then follow the atmospheric processes (ibid.). Initiating a simulation at noon results in wrong start conditions (ibid.). Therefore, all simulations are carried out for the 31st of May 2023 from 00:00 to 24:00 o'clock. Since the simulated values are verified with the measured values (see Chapter 4.3), the selection of the day had to be adjusted to the schedule for the installation of the weather sensors and the subsequent data availability. Up to this point, the measured weather data were available in the MySQL database without any gaps. Additionally, on this day there was a relatively large temperature difference from 8,85 °C to 23,85 °C.

Since the atmospheric model is the main model (see Chapter 3.2), the meteorological settings are crucial for the simulation. They have a strong influence on the results (Salvati & Kolokotroni 2019: 3367). The choice of the initial meteorological conditions and the

Table 5: Overview - Model Geometry of Area Input Files

	INX1	INX2	INX3	INX4	INX5
Study area*	narrow area	narrow area	narrow area	extended area	extended area
LoD	LoD3	LoD2	LoD2	LoD2	LoD2
Total model size (x, y, z)	171 m x 171 m x 45,96 m	171 m x 171 m x 45,96 m	170 m x 170 m x 46,84 m	470 m x 520 m x 158,99 m	494 m x 524 m x 134,88 m
Model dimensions (x, y, z)	171 x 171 x 30 grid cells	171 x 171 x 30 grid cells	34 x 34 x 8 grid cells	94 x 100 x 20 grid cells	247 x 262 x 29
Size of grid cells (dx, dy, dz)	1 m x 1 m x 1 m (base height)	1 m x 1 m x 1 m (base height)	5 m x 5 m x 5 m (base height)	5 m x 5 m x 5 m (base height)	2 m x 2 m x 3 m (base height)
Minimum distance between model border and buildings	24 grids cells = 24m	24 grids cells = 24m	5 grid cells = 45m	9 grid cells = 45m	32 grid cells = 64 m
Total number of grid cells (x*y*z)	877.230	877.230	9.248	188.000	1.876.706
Method of Vertical Grid Generation	Combined telescoping and equidistant	Combined telescoping and equidistant	Combined telescoping and equidistant	Telescoping	Telescoping
Highest Building	21 m	21 m	21 m	52 m	52 m
Start of telescoping height	21 m	21 m	21 m	60 m	60 m
Telescoping factor	20%	20%	20%	20%	20%
Model rotation out of Grid North Geographical	349,1 degrees	349,1 degrees	349,1 degrees	349,1 degrees	349,1 degrees
Location (UTM; Latitude, longitude)	51.49, 7.42	51.49, 7.42	51.49, 7.42	51.49, 7.42	51.49, 7.42
Reference Time Zone	CET/ GMT+1	CET/ GMT+1	CET/ GMT+1	CET/ GMT+1	CET/ GMT+1
Total simulation time needed**	Did not finish	39 h 7 min 12s	1 h 40 min 55 s	8 h 32 min 50 s	256 h 40 min 17 s

* For Study Area see Chapter 2.3

** Different types of hardware were used so the comparison is not exact

lateral boundary conditions (LBC) are especially important (ibid.; Huttner 2012: 53). ENVI-met provides non-forced and forced LBC (ibid.). A forced LBC means that the boundary conditions of the limited 3D model area, which are defined by the 1D model, the temporal and spatial development of the atmospheric data can be defined by the user (Huttner 2012: 52, 56). According to Huttner (2012: 56) it is necessary to force the simulation for a comparison of the results of a numerical simulation with measured data. Additionally, due to their simplicity, non-forced LBC are not recommended anymore (Appendix B.5). Therefore, this study is conducted with forced LBC.

Compared to non-forced LBC, the forced ones are the most stable (ibid.: 53, 56; 2017c). However, numerical instability can be easily caused by abrupt changes in the variables, especially wind speed and wind direction (Huttner 2012: 57). Furthermore, errors may occur if the 1D vertical profile does not represent the average conditions of the model (ENVI-met 2017c). These instabilities were also experienced in this project work, as some simulation attempts were terminated due to unstable temperature, humidity or CO₂ fields due to too drastic changes in wind speed or direction. Depending on the available data, simple or full forcing is chosen. While simple forcing only includes data on temperature and humidity, full forcing can include wind, air temperature, radiation/clouds, relative humidity and precipitation. Therefore, it provides the highest precision (Appendix B.5). However, forcing precipitation is only recommended when simulating very long periods of time (ENVI-met 2017b). The data used for forcing must be local, either measured or calculated e.g. with a validated urban energy model (Salvati & Kolokotroni 2019: 3367).

For this study, a full forcing file is prepared in the Forcing File Manager using local weather data (Appendix B.6). The weather data was obtained from the company DTN, which operates a large number of weather stations in Europe, including one at TU Dortmund University on Campus North (DTN/MeteoGroup Nederland 2023). The data of the weather station must be converted into the units necessary for ENVI-met (see Table 6). Due to the lack of data for radiation/clouds, the simulation is made with the assumption of a cloudless day. The simulations for this study are performed forcing air temperature, humidity and wind speed.

Table 6: Comparison of Units Used by the DTN Weather Station and ENVI-met

Data	Weather station unit	ENVI-met unit
Abs. Air Temperature	°C	°K
Rel. Humidity	°C (dewpoint)	percent
Wind speed	Beaufort scale	m/s
Wind direction	degree	degree

The Conversion of the relative humidity is done according to the following formulas (Mal-

berg 2007: 104, 11):

$$r = 100 \cdot \frac{\text{SDD}(T_D)}{\text{SDD}(T)}$$

And:

$$\text{SDD} = 6,1078 \cdot 10^{\frac{a \cdot T}{b+T}}$$

Where

r: relative humidity

SDD: Saturation vapor pressure in hPa

T: Temperature in °C

T_D: Dewpoint in °C

With the parameters:

$$a = 7,5 \text{ and } b = 237,3 \text{ for } T \geq 0$$

The windspeed is converted with the following formula (Kraus 2004: 39):

$$v = 0,8360 \text{m/s} \cdot B^{3/2}$$

Where:

v: Windspeed in m/s

B: Beaufort strength

Lastly, the simulation settings and the .INX file are merged into a .simx file. This file contains all relevant simulation parameters (Table 7) and is loaded into the application ENVI-core to check for errors or warnings and finally run the simulation. Depending on the model size and the computer's hardware, the process of simulation may take a few hours up to a few days (ENVI-met 2022).

Table 7: Overview - Simulation Parameters

Simulation parameters (Simulation Task File)	
Simulation Date (dd.mm.yyyy)	31.05.2023
Simulation Start Time (hh:mm)	00:00
Total Simulation Time (h)	24
CPU Cores to be used	Multi Core (parallel)
Forcing Method	Full Forcing
Forced Data	Wind, air temperature, relative humidity

4.4.4. Results of the Microclimate Simulations

After the successful simulations (INX1 aborted with an error after 8 simulated hours), the results can be evaluated and visualized in ENVI-met Leonardo or via single data sheet export in other statistics software. Here, visualizations were created with R and Python. Additionally to the images provided in this work, dynamic visualizations of the climate data can be viewed in this Microsoft Sway Presentation⁹. Of the large amount of data and variables that are exported by ENVI-met, this study focuses on the potential air temperature with some exploration of other variables. The dynamic visualizations use linear interpolation of the raster values for a ten-minute interval for a clearer picture, the figures in this study all use the data directly exported from ENVI-met.

The temperature is depicted across three different times (8:00, 14:00 and 20:00). Differences between a z-height of 2,5 m and 12,5 m (approximately the height of the weather sensors on the facade) are highlighted. Every simulation follows a very similar pattern. The maximum temperature does not exceed 27°C in any simulation and the diurnal variation is similar across the simulations. Overall, the temperature to the north of the library building is a few degrees below the rest of the area and especially the southwestern points (Figures 44, 46, 48, 49). This temperature difference could be explained by the north side of the library being shaded and the extensive vegetation in this part of the study area. One southeastern corner of the EF50 building has an especially low temperature that might be caused by higher airspeeds or turbulence (Figure 47).

The z-height also has an effect on the temperature. In Figure 45, at a height of 13,5 m, a slightly lower overall temperature especially in the morning and noon can be observed. Here, wind might be able to pass more easily through the area since it is not influenced by the ground and vegetation. In Figure 47 the wind is coming from the northeast since there is a recognizable lee at the southwest of buildings, even in the narrow extent of the simulation (Figure 50). Faster air speeds are especially simulated at the edges of the study area where the incoming wind encounters the first buildings which can be observed in both the wide and narrow extent of the study area. Other important variables like the surface temperature of the ground or the relative humidity are illustrated in the dynamic visualizations.

4.4.5. Verification and Evaluation of Simulation Results

The accuracy of the performed microclimate simulations is investigated by examining two parameters that are commonly used for the verification of forecast models: The correlation coefficient (R) and Root Mean Square Error (RMSE) (Barnston 1992: 699). The correlation coefficient R describes the strength of the linear relationship between two variables (ibid.). The correlation coefficient takes values between -1 and 1, where zero is

⁹<https://sway.office.com/7XxDyfntWACIagbk?ref=Link>

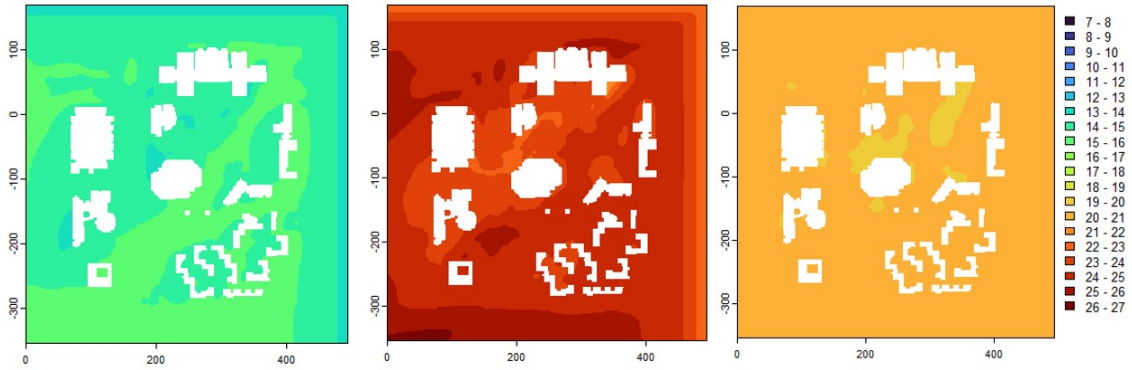


Figure 44: Potential Air Temperature of INX 5 at a Z-Height of 2,1 m at 08:00, 14:00 and 20:00 (own illustration)

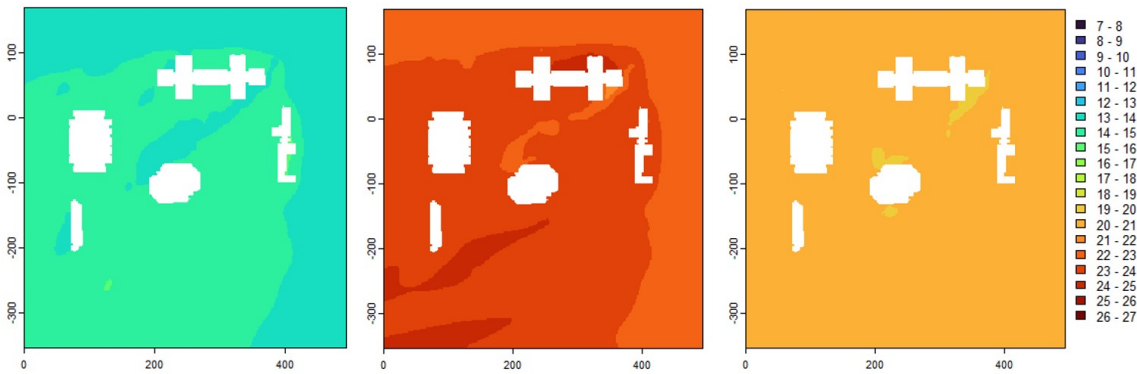


Figure 45: Potential Air Temperature of INX 5 at a Z-Height of 13,5 m at 08:00, 14:00 and 20:00 (own illustration)

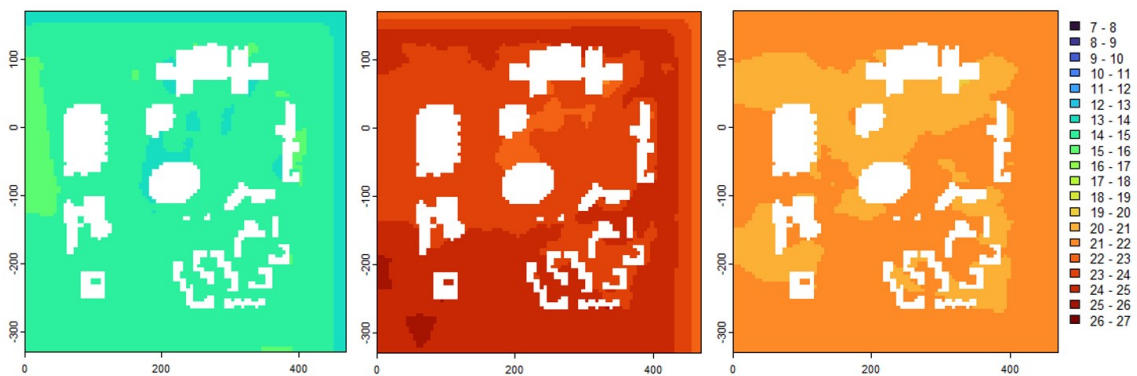


Figure 46: Potential Air Temperature of INX 4 at a Z-Height of 2,5 m at 08:00, 14:00 and 20:00 (own illustration)

4 PROCEDURE AND RESULTS

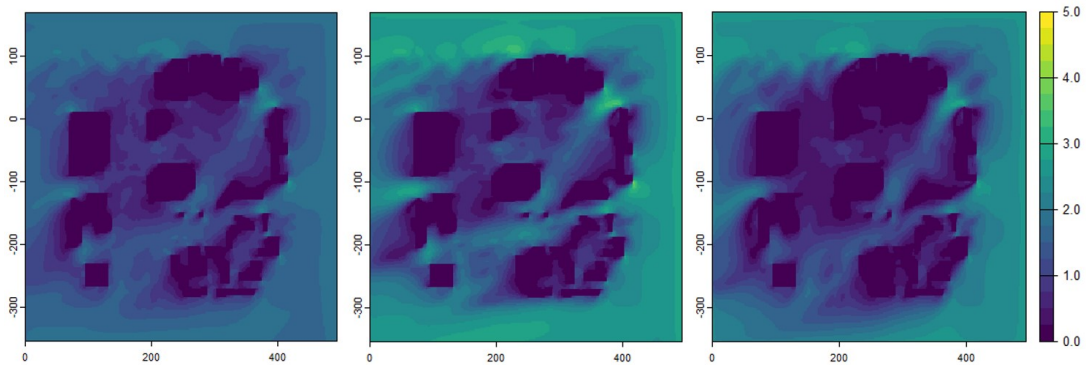


Figure 47: Wind Speed of INX 5 at a Z-Height of 2,5 m at 08:00, 14:00 and 20:00 (own illustration)

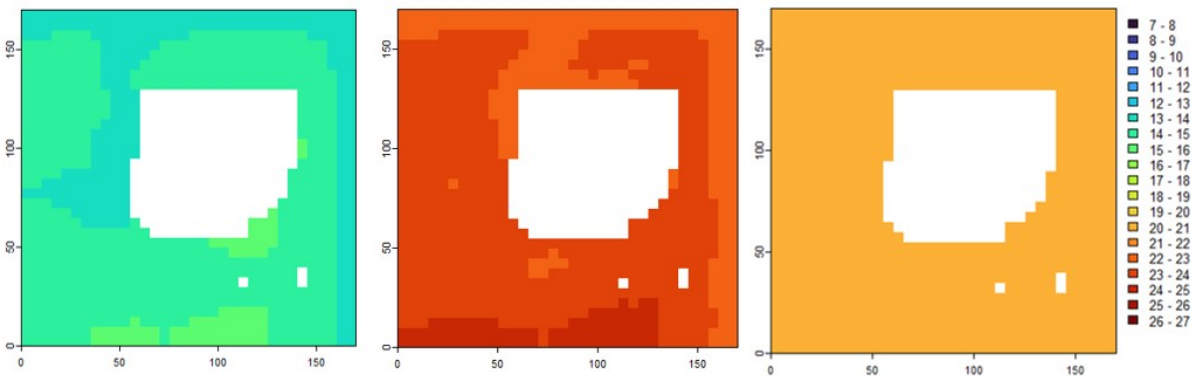


Figure 48: Potential Air Temperature of INX 3 at a Z-Height of 2,5 m at 08:00, 14:00 and 20:00 (own illustration)

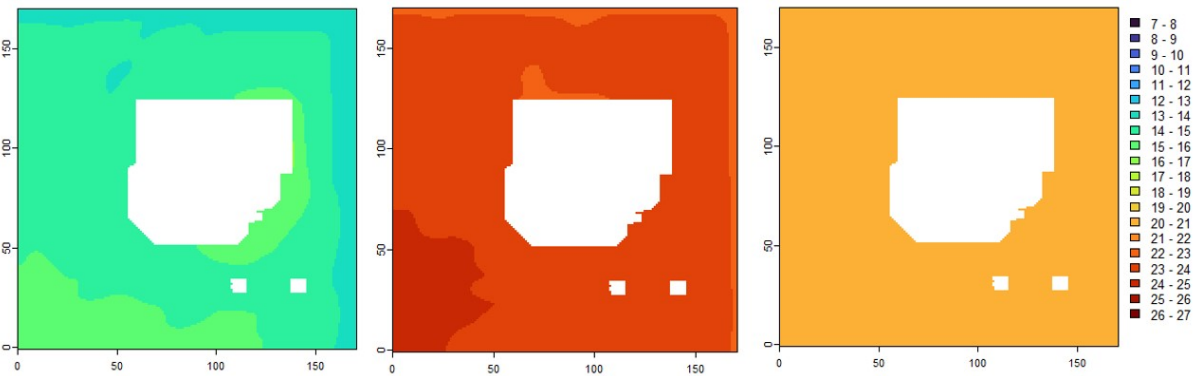


Figure 49: Potential Air Temperature of INX 2 at a Z-Height of 2,5 m at 08:00, 14:00 and 20:00 (own illustration)

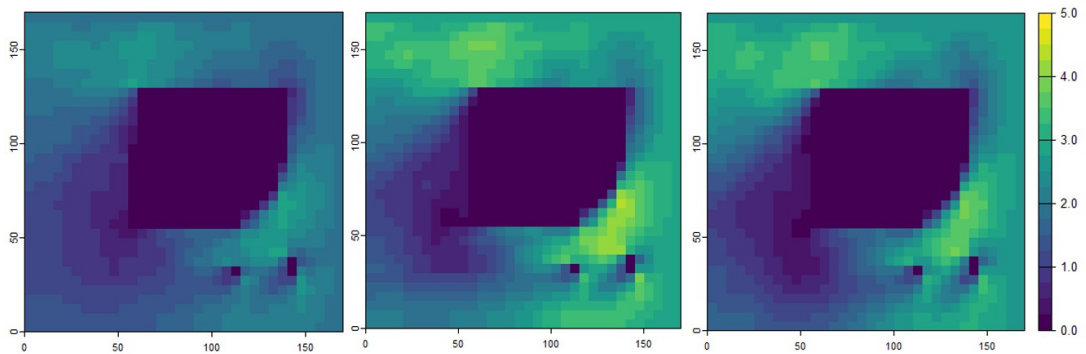


Figure 50: Wind Speed of INX 3 at a Z-Height of 2,5 m at 08:00, 14:00 and 20:00 (own illustration)

no correlation, -1 a perfect negative and +1 a perfect positive linear correlation (von der Hude 2020: 35). For a reliable model the following applies: $R \rightarrow 1$. R is calculated as follows:

$$R = \frac{\sum_{t=1}^n (X_t^{Obs} - \bar{X}^{Obs})(X_t^{Sim} - \bar{X}^{Sim})}{\sqrt{\sum_{t=1}^n (X_t^{Obs} - \bar{X}^{Obs})^2 \sum_{t=1}^n (X_t^{Sim} - \bar{X}^{Sim})^2}}$$

Where

- X_t^{Obs} : Observed values
- \bar{X}^{Obs} : Average of observed values
- X_t^{Sim} : Simulated values
- \bar{X}^{Sim} : Average of simulated values
- n : total number of time elements
- t : index of element

Moreover, the RMSE is used to determine the forecast quality (von der Hude 2020: 104). For this, the actual measured value is compared with the forecast value for each element (ibid.). The RMSE is calculated from the square root of the average forecast error (ibid.):

$$RMSE = \sqrt{\frac{1}{n} \sum_{t=1}^n (X_t^{Obs} - X_t^{Sim})^2}$$

The smaller the RMSE, the better the simulated values fit to the measured values (Barnston 1992: 700). For a model to be considered reliable, this parameter should tend towards the following value: $RMSE \rightarrow 0$ (Salata et al. 2016: 322). Experimental verifications carried out in other studies showed RMSE values ranging from 0,66 to 4,83, including values such as 1,61, 1,39, 1,47 and 2,9 for air temperature (Lee et al. 2016, Song & Park 2015, Duarte et al. 2015, Jänicke et al. 2015, Middel et al. 2014, Hedquist & Brazel 2014, all as cited in Salata et al. 2016: 18).

In this study, the simulated values of air temperature and relative humidity at the Central University Library are evaluated, comparing them to the values measured by the sensors. Due to the sensors' technical features, the verification and evaluation of the simulation results focuses on the air temperature and the relative humidity which is an important factor when estimating the building's energy needs and human well-being, respectively. The simulated values are available for each full hour from 01:00 to 23:00 o'clock, respectively 01:00 to 08:00 o'clock for INX1 (Appendix D), and the measured values in intervals of ten minutes. Therefore, hourly averages were calculated from the measured ten-minute values (Appendix D).

Table 8 lists the correlation coefficients and RMSE for verification of the simulated air temperature. Overall, the models show correlation coefficients of $R \geq 0,93$, excluding INX1, indicating that the simulations highly correlate with the real-world data. The

4 PROCEDURE AND RESULTS

RMSEs range from 1,99 to 5,58, which means that the simulated air temperature values deviate on average 1,99°C to 5,58°C from the measured values. The deviations are slightly higher than in other experimental studies (Salata et. al 2016: 335).

Furthermore, it is noticeable that the simulation results for the sensor location on the roof show the highest RMSE with values between 5,37 and 5,58, excluding the RMSE of 3,12 of INX1. Here, the simulated values deviate averagely the most from the measured ones. Across models, the measured values from sensor 2 on the north facade were predicted most accurately. Here, the RMSEs range from 1,99 and 2,47.

Table 8: The Correlation Coefficient (R) and Root Mean Square Error (RMSE) for the Verification of the Simulated Air Temperature (T) for Each Model on 31 May 2023 (own illustration)

	R					RMSE				
	INX1	INX2	INX3	INX4	INX5	INX1	INX2	INX3	INX4	INX5
Sensor1	0,50	0,94	0,95	0,94	0,94	3,02	3,68	3,88	3,84	3,81
Sensor2	0,86	0,95	0,96	0,94	0,93	2,47	1,99	2,08	2,31	2,34
Sensor3	0,93	0,93	0,93	0,94	0,94	3,02	5,47	5,58	5,51	5,37
Sensor4	0,88	0,98	0,99	0,99	0,98	2,71	2,57	2,71	2,70	2,66

The correlation coefficients and the Root Mean Square Error for the simulation of relative humidity are displayed in Table 9. Generally, the percentage of relative humidity is overestimated by the simulations. Again, INX1 has the broadest span of R values (0,16 to 0,94) showing slightly less correlation than for air temperature. The other models indicate very strong positive linear correlations with the real-world data, shown by correlation coefficients of $0,94 \leq R \leq 0,99$, excluding INX1. The RMSEs vary from 11,07 to 18,92, which are high values given that RMSE tends to zero for reliable models. Consequently, the calculated relative humidity shows a high average deviation from the observed values.

There is again a difference between the sensors. For sensor 4, the models shows the strongest linear positive correlation. In addition, sensor 2 shows comparatively the lowest RMSE, with values between 11,07 and 15,24 which still indicate a high average deviation. Comparatively, the models performed least accurately at the location of sensor 3.

Table 9: The Correlation Coefficient (R) and Root Mean Square Error (RMSE) Between the Measured and Modeled Relative Humidity (RH) for Each Study Area Extent and Selected Day (own illustration)

	R					RMSE				
	INX1	INX2	INX3	INX4	INX5	INX1	INX2	INX3	INX4	INX5
Sensor1	0,38	0,96	0,96	0,96	0,96	18,05	15,82	16,73	16,45	16,34
Sensor2	0,80	0,98	0,98	0,98	0,98	15,24	11,07	11,91	12,35	12,23
Sensor3	0,96	0,94	0,93	0,93	0,93	13,47	18,32	18,50	18,92	18,60
Sensor4	0,85	0,98	0,99	0,99	0,99	15,56	14,55	15,04	15,53	15,49

Influence of Level of Detail In order to evaluate the influence of the LoD, the simulation results of INX1 and INX2 are compared. Both models cover the narrow study area with a relatively high grid resolution of 1 m x 1 m x 1 m and differ only in the LoD. INX1 is modeled in LoD3 and INX2 in LoD2. It is important to note that due to an error in running the INX1 simulation, the data is only available from 01:00 to 08:00 o'clock. It is not known if the error affected the simulation results before the termination. Therefore, the comparison is restricted.

Figure 51 shows the graphs of the measured air temperature and the values of the two simulations. The curves of both simulations are approximately the same, except for sensor 1 where the values of INX1 are little closer to the measured ones. Comparing the RMSE of each model, this impression is confirmed. Although INX1 values are not more accurate for all 4 sensors, overall the average deviation ranging from 2,47°C to 3,02°C is slightly smaller than that of INX2. Humidity, on the other hand, is underestimated by both models (Figure 52). Again, both models perform about equally well and show similar curves to the measured values. Looking at the RMSE values, no model can be identified

4 PROCEDURE AND RESULTS

that performs more accurately. The LoD2 model shows the largest average deviation at sensor 3, with 18,32. Here, INX1 has a smaller average deviation of 13,47.

Overall, comparing these simulations, the LoD does not have any strong positive or negative impact on the model's performance. The creation of a model in LoD3 takes significantly more time than in LoD2 and the difference is rather low. In this case, the effort was not reflected in more accurate simulation results.

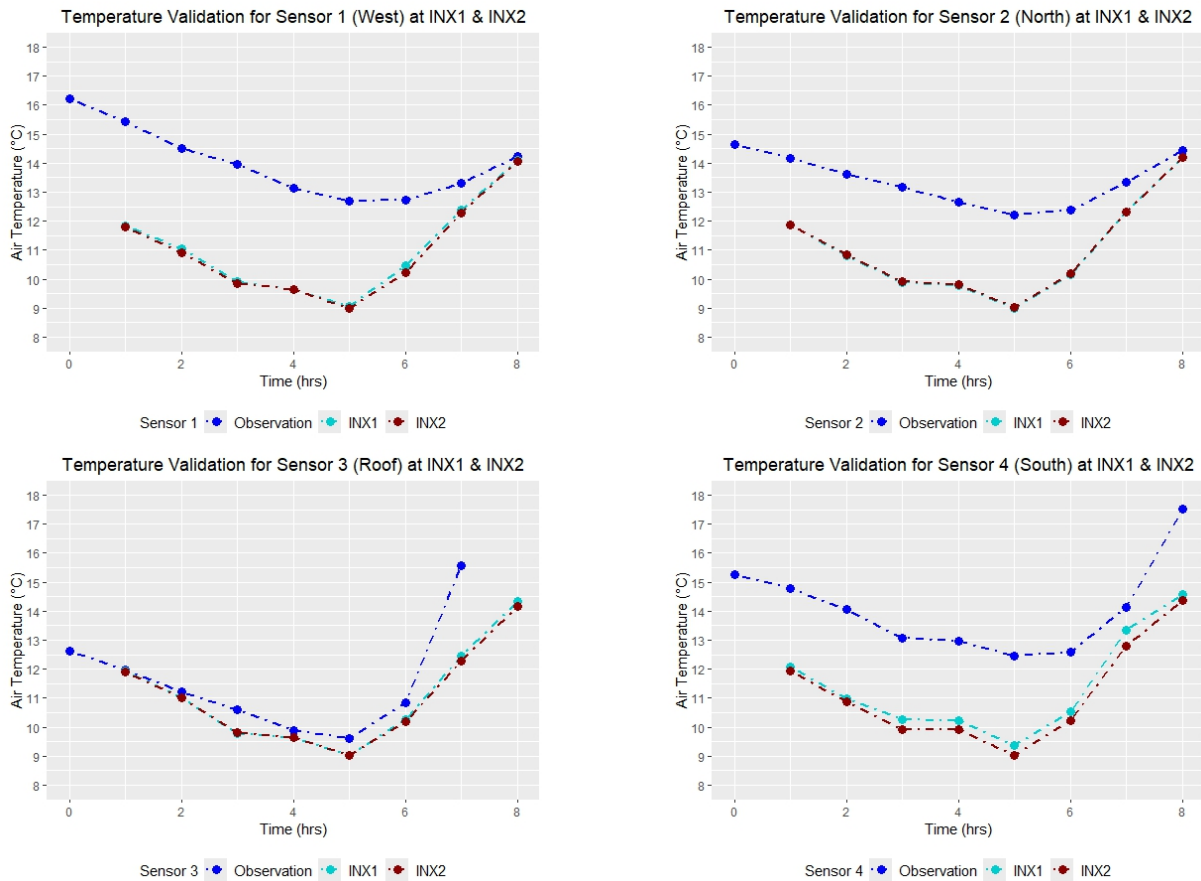


Figure 51: Influence of the LoD 2 and LoD 3 of the Central University Library on the Simulation of Air Temperature in the Narrow Study Area, Compared to the Measured Values (own illustration)

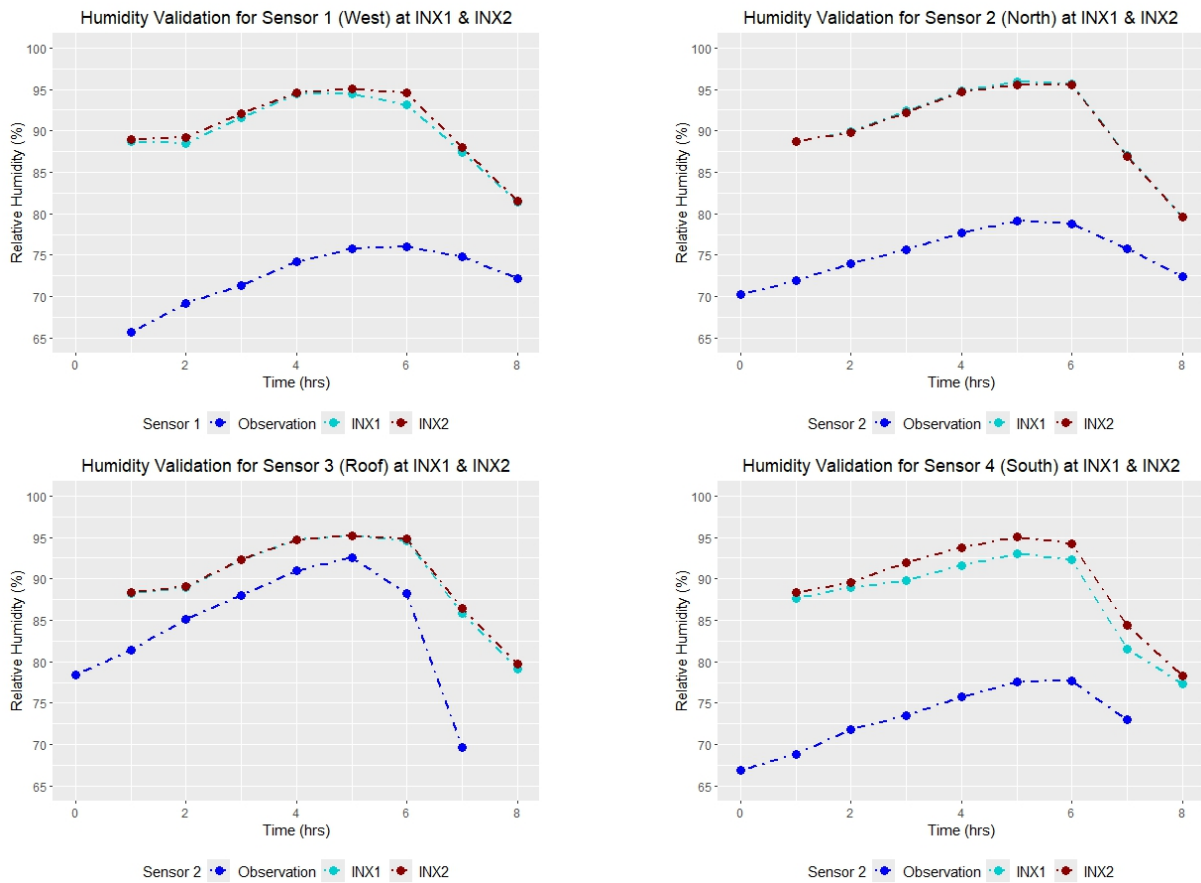


Figure 52: Influence of the LoD 2 and LoD 3 of the Central University Library on the Simulation of Relative Humidity in the Narrow Study Area, Compared to the Measured Values of All Four Sensors (own illustration)

Influence of Study Area The influence of the study area is analyzed by comparing INX3, covering the narrow study area, and INX4, the extended area (see Chapter 4.4.1). Both models have a grid resolution of 5 m on each axis and the same LoD, which is LoD2. Again, the curves of both models are very similar for the computed values of air temperature (Figure 53) and relative humidity (Figure 54).

For the air temperature, the difference of the correlation coefficients of both models ranges from zero to 0,02. Both models perform about equally well. For the average deviations, both models also perform similarly well. For sensor 1, 3 and 4, the simulated values of INX4 deviate on average 0,01°C to 0,07°C less from the measured values than the ones of INX3. For sensor 2, INX3 computes better, with a difference of 0,23°C compared to INX4. Overall, the results of INX3, the narrow study area model, are slightly better for the four comparison points in terms of the strong positive linear correlation and average error deviation.

A comparison of the linear correlation for humidity shows that both models again show equally good performance. With regard to the RMSE, INX3 shows better values for comparison point 2,3 and 4, deviating from 0,36 to 0,49 less than INX4 depending on

4 PROCEDURE AND RESULTS

sensor location. INX4 performs better at sensor 1 with 0,28 less deviation. Overall, INX3 also provides better results for the calculation of the relative humidity. The positive linear relationship is about the same and the average value deviation is slightly lower than INX4.

Overall, the results of both models are very similar, with the tendency that the model for the narrow area performs slightly better. For the simulation of the microclimate at the Central University Library, this model's area extent should be used, because it takes significantly less time to model a small study area in SketchUp and the computation time of the simulation with 1 h 41 min were significantly lower than for the extended area model area with 8 h 33 min.

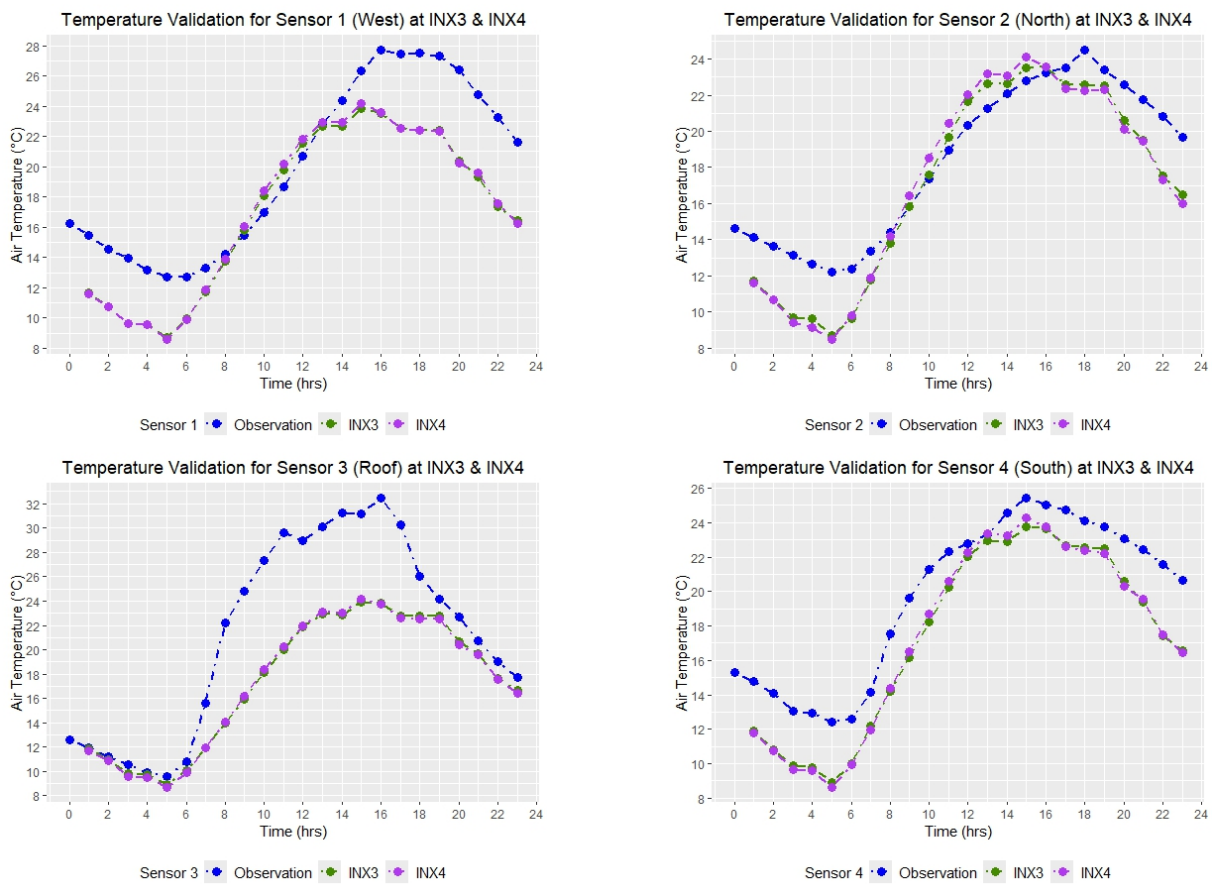


Figure 53: Influence of the Study Area Extent on the Simulation of Air Temperature, Compared to the Measured Values of All Four Sensors (own illustration)

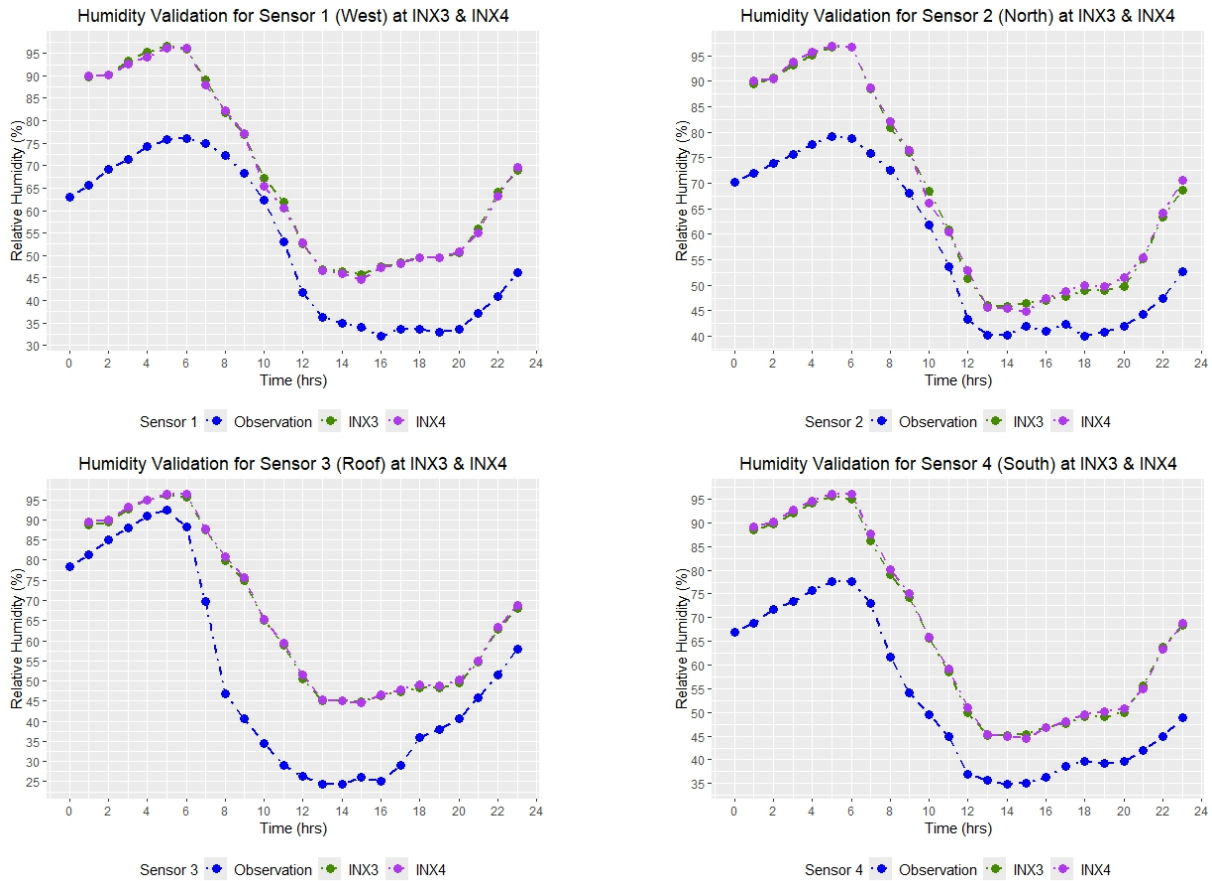


Figure 54: Influence of the Study Area Extent on the Simulation of Relative Humidity, Compared to the Measured Values

Influence of Grid Resolution The analysis of the influence of the grid resolution is based on two comparisons: one of the narrow and one of the extended study area. A grid resolution of 1 m or 5 m on each axis is compared for the narrow area and a resolution of 5 m x 5 m x 5 m or 2 m x 2 m x 3 m for the extended area. All models have LoD2. As for the study area, the curves of both models are very similar for the calculated values of air temperature (Figure 55 for the narrow area; Figure 57 for the extended area) and relative humidity (Figure 56 for the narrow area; Figure 58 for the extended area).

Looking at the air temperature and relative humidity in the narrow area models, they show a similar strong linear positive correlation. Depending on the sensor location, the R value of INX2 or INX3 is 0,01 points better. Overall, the R values range between 0,93 and 0,99, which is very high. The differences between the models are minimal (depending on the sensor location $\leq 0,01$).

The average deviation between predicted and observed values is also very similar, with INX2 being slightly less deviant for air temperature. The average deviation of the values of INX2 is 0,09 to 0,21 lower than in INX3. Looking at relative humidity, the error values for INX2, the high grid resolution, are also slightly lower, ranging from 0,18 to 0,91 below the RMSE of INX3.

4 PROCEDURE AND RESULTS

Overall, the model calculations perform slightly better for the higher grid resolution of 1 m x 1 m x 1 m. The simulation results for air temperature and relative humidity of both models show a strong positive linear relationship with the actual measured values. For the high-resolution model, the calculated values deviate on average slightly less from the measured values.

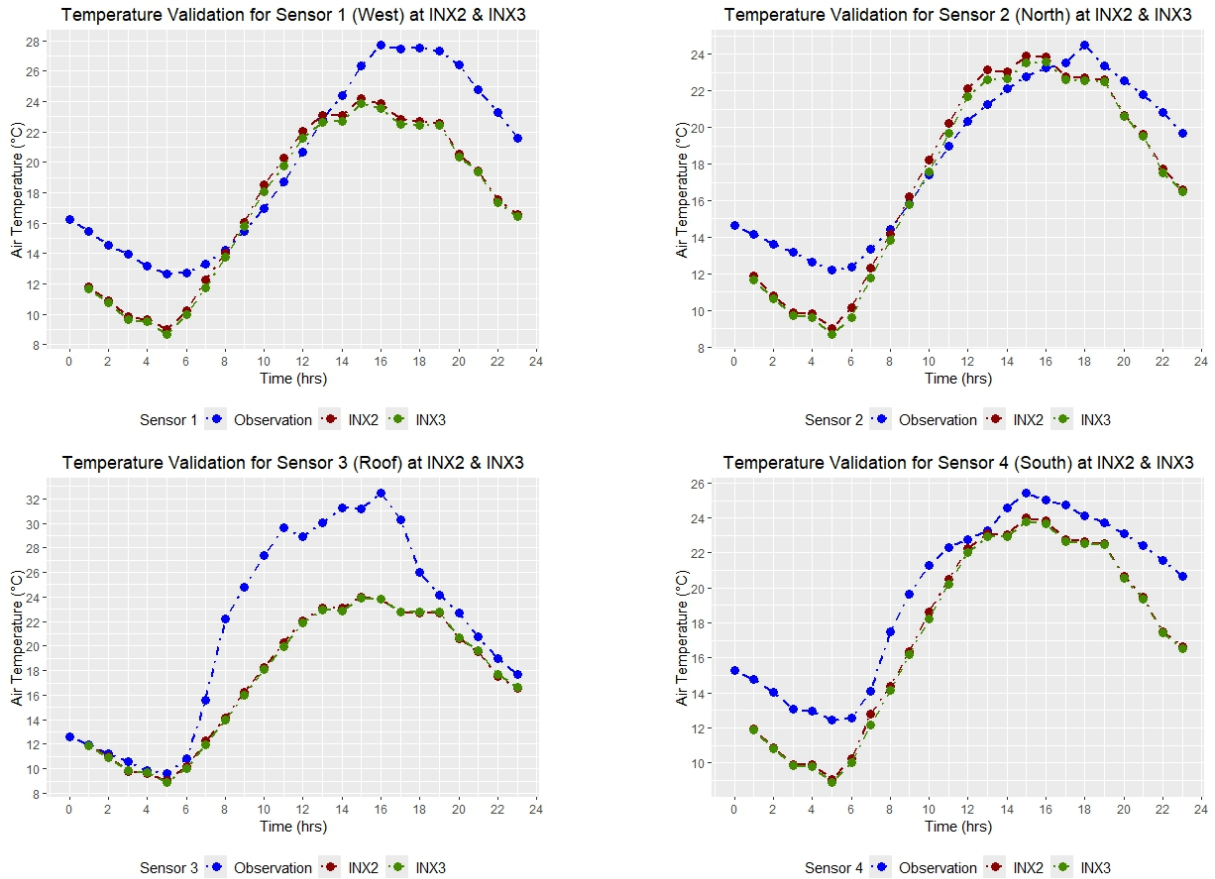


Figure 55: Influence of the Grid Resolution of 1 m x 1 m x 1 m (INX2) vs. 5 m x m 5 m x m 5 (INX3) on the Simulation of Air Temperature, Compared to the Measured Values of All Four Sensors

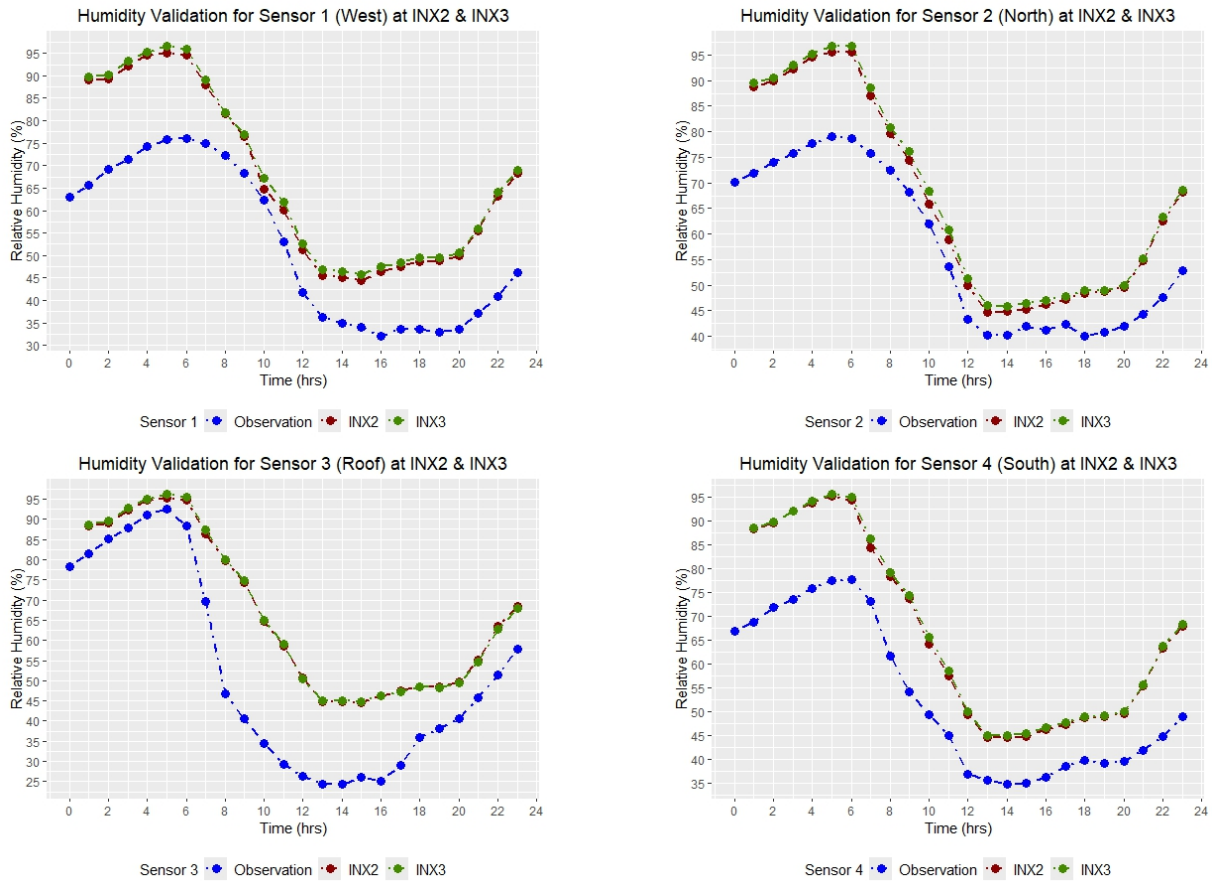


Figure 56: Influence of the Grid Resolution of 1 m x 1 m x 1 m (INX2) vs. 5 m x 5 m x 5 m (INX3) on the Simulation of Relative Humidity, Compared to the Measured Values of All Four Sensors (own illustration)

The comparison based on the extended study area again shows very similar curves for the calculated air temperature (Figure 57) and relative humidity (Figure 58) for both models. For the most part, the curves are so close that the curve of INX5 is overlapped by that of INX4. For air temperature, the linear correlation of each model with the measured values is high, with some values better for one model and some better for the other. The differences between the R values of the two models are also relatively small, ranging from 0 to 0,04. As for the RMSE, the differences between the two models range from 0,18 to 0,63, with both models having lower values than the other for two sensors. For humidity, the situation is similar to air temperature: very similar strong positive linear correlations and slightly varying RMSE. Neither model obviously performs better than the other.

4 PROCEDURE AND RESULTS

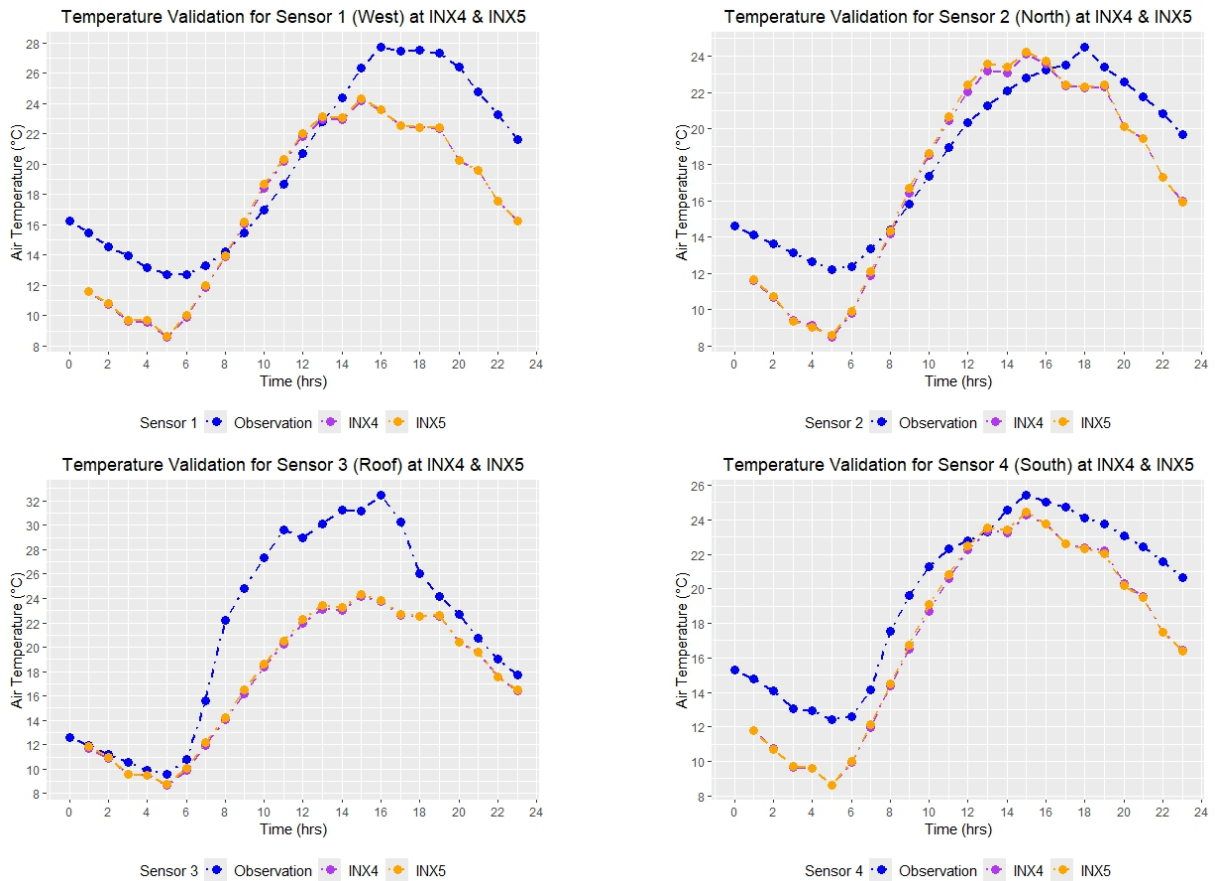


Figure 57: Influence of the Grid Resolution of 2 m x 2 m x 3 m (INX5) vs. 5 m x 5 m x 5 m (INX4) on the Simulation of Air Temperature, Compared to the Measured Values (own illustration)

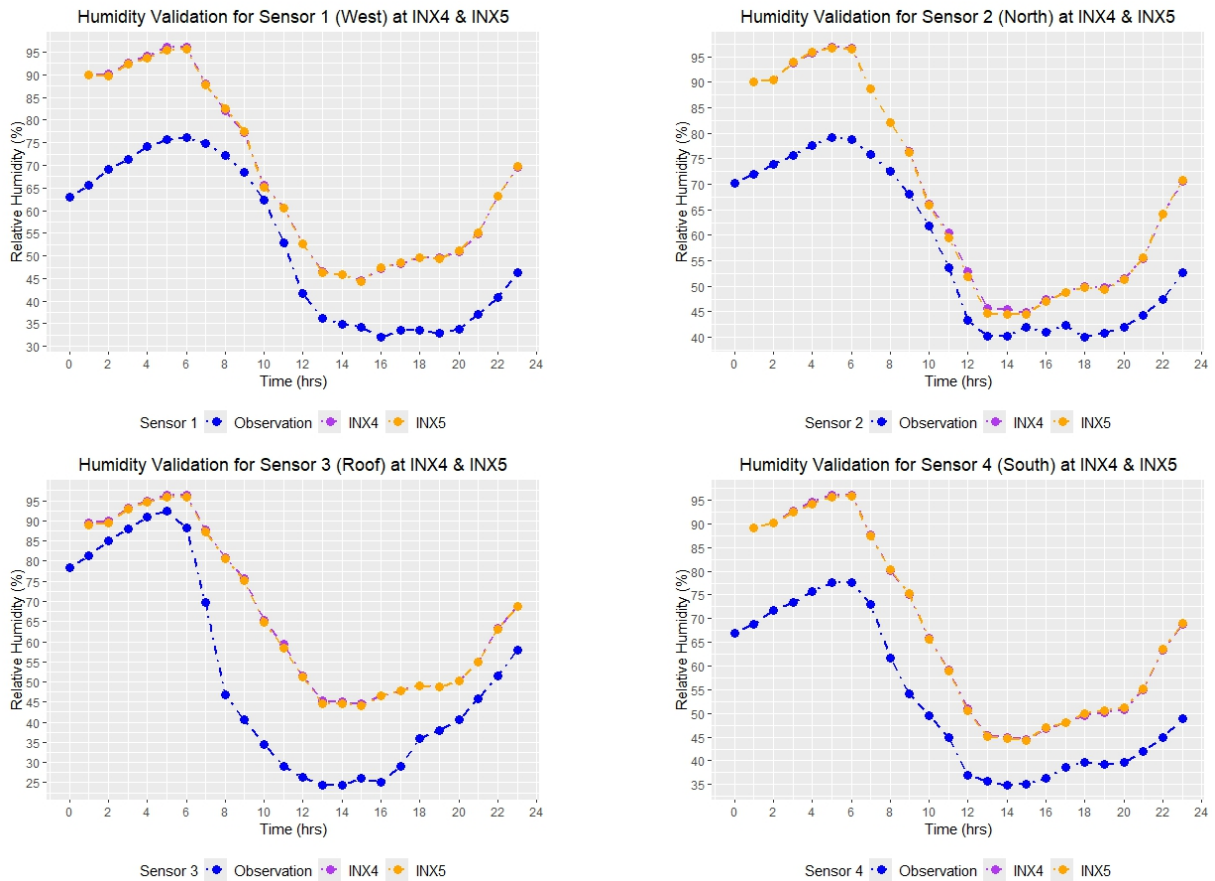


Figure 58: Influence of the Grid Resolution of 2 m x 2 m x 3 m (INX5) vs. 5 m x 5 m x 5 m (INX4) on the Simulation of Relative Humidity, Compared to the Measured Values (own illustration)

4.5. Visualization of Results

This chapter focuses on the different formats of visualization of the microclimate simulation results and the implementation of real-time weather data. First, ArcGIS Online and ArcGIS Dashboard (WP5) show a possible way to dynamically display Digital Twins in a 2D map format, while the VR application (WP6) explores the possibilities of integrating simulation results and real-time data in an immersive environment.

4.5.1. ArcGIS Online/ArcGIS Dashboard

To achieve the goal of visualizing the collected weather data from the sensors in real time, several steps are required. A FTP Server serves as the basis for all these steps. For the conversion of the data, the programming language PHP was chosen (see Chapter 4.3.2). Through a .php script, the signals from the sensors are first converted into a .txt file. This file contains the temperature and humidity as well as the id, latitude and longitude of the sensor (Figure 59). Next to the shown .txt file another .txt file specially for the use in the VR application (see Chapter 4.5.2) is created. The information in this .txt file are almost the same as in the first one, but the formatting is different due to the further use of the file (Figure 60).

```
Temperatur: 28.9
Luftfeuchtigkeit: 23.6
ID: eui-a840416d0186cb22sensor4
Breitengrad: 51.4926
Längengrad: 7.41694
```

Figure 59: Content of the .txt File (own illustration)

```
Sensor4,16:33:45,23.3,40.3
```

Figure 60: Content of the .txt File for the VR Application (own illustration)

After obtaining the .txt files, the one shown in Figure 59 is then transformed into a .geojson file. .geojson is a file format suitable for storing and sharing spatial data (Dixson et al. 2019: 3). In this .geojson file the weather data, which originates from the .txt files, are connected with the coordinates of the sensors, so that a spatial assignment of the weather data can take place (Figure 61).

The obtained .geojson file is finally to be displayed visually in a map. For this purpose the service ArcGIS Online by ESRI is used. In ArcGIS Online maps can be created and displayed with a cloud-based service. The data is stored in the company's own infrastructure so that it can always be accessed and shared with an organization or the

public (ESRI n.d.-b). ArcGIS Online provides the ability to import .geojson files and convert them into a Feature Layer. A Feature Layer is a grouping of geographic features, such as buildings, cities, or roads (ESRI n.d.-c). In the case of this work, the Feature Layers are points that symbolize the locations of weather sensors (Figure 62).

```

sensor1.geojson - Editor
Datei Bearbeiten Format Ansicht Hilfe
{
  "type": "FeatureCollection",
  "features": [
    {
      "type": "Feature",
      "properties": {
        "Temperature": 17.8999999999999857891452847979962825775146484375,
        "Humidity": 72.799999999999971578290569595992565155029296875,
        "Sensor": "Sensor 1"
      },
      "geometry": {
        "type": "Point",
        "coordinates": [
          7.41627260000000010364828995079733431339263916015625,
          51.49267650000000017380443750880658626556396484375
        ]
      }
    }
  ]
}

```

Figure 61: Weather Data of the .txt File in .geojson Format (own illustration)

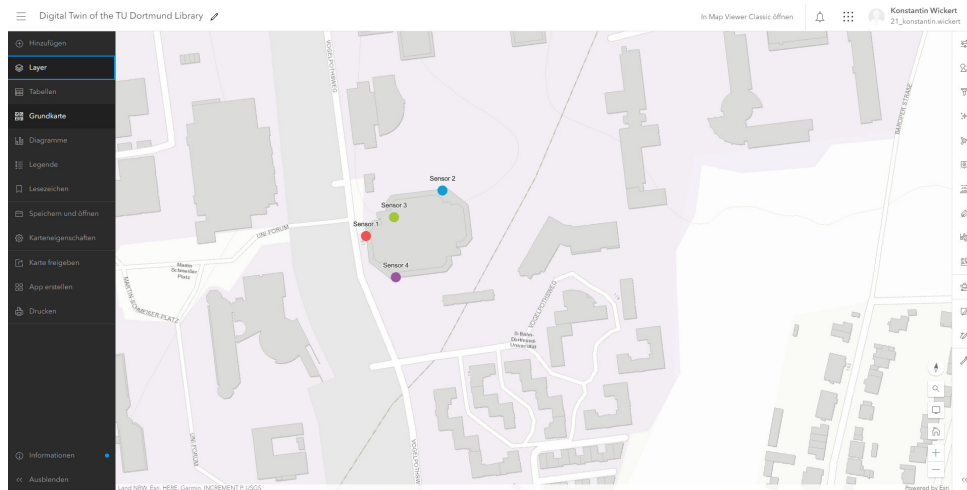


Figure 62: Sensors in ArcGIS Online (own illustration)

In order to visualize the weather data in real-time it is necessary to regularly update the Feature Layer based on the .geojson file. To implement this, ArcGIS Pro by ESRI is used. The advantage here is that data uploaded to ArcGIS Online can be easily imported into ArcGIS Pro via the cloud (ESRI n.d.-e). Within ArcGIS Pro, the Modelbuilder is used in this study. This offers the possibility to combine different geoprocessing tools in one model and thus to be able to manage spatial data (ESRI n.d.-f) (Figure 63).



Figure 63: Model Created in ArcGIS Pro (own illustration)

The Modelbuilder will update the data in ArcGIS Online based on the .geojson files. In order to always have the most recent .geojson files, they need to be provided to the Modelbuilder. To do this the .geojson files are downloaded regularly from the FTP Server to a local computer. For this purpose a .py script is used (Figure 64).

```
(arcgispro-py3) C:\xampp\htdocs\tutorial>python download2.py
Datei heruntergeladen: sensor2.geojson
Datei heruntergeladen: sensor4.geojson
Datei heruntergeladen: sensor3.geojson
Datei heruntergeladen: sensor1.geojson
Dateidownload abgeschlossen. Beende Verbindung...
Verbindung zum FTP-Server beendet.
Datei heruntergeladen: sensor2.geojson
Datei heruntergeladen: sensor4.geojson
Datei heruntergeladen: sensor3.geojson
Datei heruntergeladen: sensor1.geojson
Dateidownload abgeschlossen. Beende Verbindung...
Verbindung zum FTP-Server beendet.
```

Figure 64: Running .py Script for Downloading the .geojson Files (own illustration)

The map in ArcGIS Online with the updated Feature Layers will be integrated into ESRI's ArcGIS Dashboard application. ArcGIS Dashboard is a software that enables the visualization of spatial information with maps, diagrams or scales (ESRI n.d.-a). The Dashboard in this study includes an interactive web map as well as a list with the air temperature and the relative humidity measured by the sensors (Figure 65).

In addition to displaying the sensors with real-time data in the 2D map, a static 3D map is created that locates the sensors. For this purpose, a 3D scene is created in ArcGIS Pro and released as a web scene in ArcGIS Online (Figure 66). As the 3D model the model created in Revit is used in the webscene. For the sensors the Feature Layer used in the dynamic 2D map is extended to a 3D Feature Layer.



Figure 65: Sensors in ArcGIS Dashboard (own illustration)

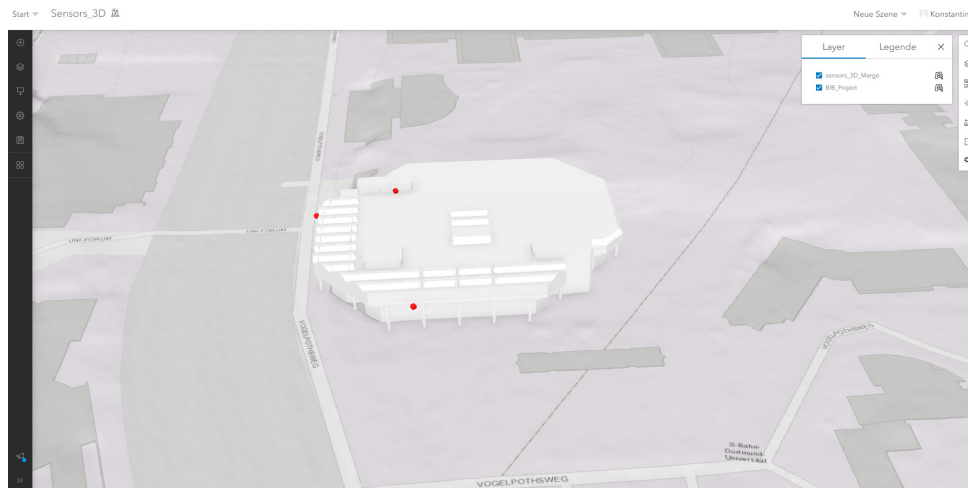


Figure 66: 3D-Visualization of the Central University Library With Sensors (own illustration)

4.5.2. VR Application

The project aimed at enriching the already existing VR application of the TU Campus South, which was developed by the M-project in winter semester 21/22 (see Gisa et al. 2022). As the library will be demolished by spring 2024, the VR application will also serve to archive the unique building of the Central University Library for posterity. For this purpose, the detailed model of the library created by laser scanning and CAD modeling was added to the existing application and enhanced by the implementation of simulation and real-time weather sensor data.

The advantages of a VR environment have already been discussed in the literature review (see Chapter 3.3). However, in order to exploit the full potential of this advanced form of dynamic visualization, certain prerequisites are necessary so that users can experience the VR application in all its depth. A key aspect of this is immersion. However, "[o]nly through a credible visual representation is full immersion possible, because visual errors and insufficient resolution of geometry and textures stand out to the user, distract him, and thus reduce immersion" (Engel & Döllner 2012: 169, own translation¹⁰).

In particular, objects and phenomena with which humans have a high level of natural visual experience therefore require a high attention to detail (Engel & Döllner 2012: 168). The factors of realism, detail and interaction level of an application that influence the creation of an immersion can be significantly increased by the tools provided by Unreal Engine. The Unreal Engine is a game engine developed by the software company Epic Games, i.e. software for developing and displaying computer games and other interactive applications (Epic Games n.d.-a).

¹⁰ „Erst durch eine glaubhafte visuelle Darstellung ist eine volle Immersion möglich, denn visuelle Fehler und zu geringe Auflösung von Geometrie und Texturen fallen dem Nutzer auf, lenken ihn ab und verringern somit die Immersion.“ (Engel und Döllner 2012: 169)

By continuing to work with the VR application created by the previous M-project (see Gisa et al. 2022), some of these immersive components are already in place. These include an approximately realistic terrain model that also contains the Campus North area, a planning office that serves as the starting point of the VR experience, a landscape panorama, and dynamic lighting. Nonetheless, the Central University Library area in particular requires its own adjustments to increase immersion and is prioritized in this regard. That includes the area of the building itself, the open space to the north of it, the Mensabrücke and, due to the high visibility, the Mensa building as well, since walkability should be made possible there (Figure 67).

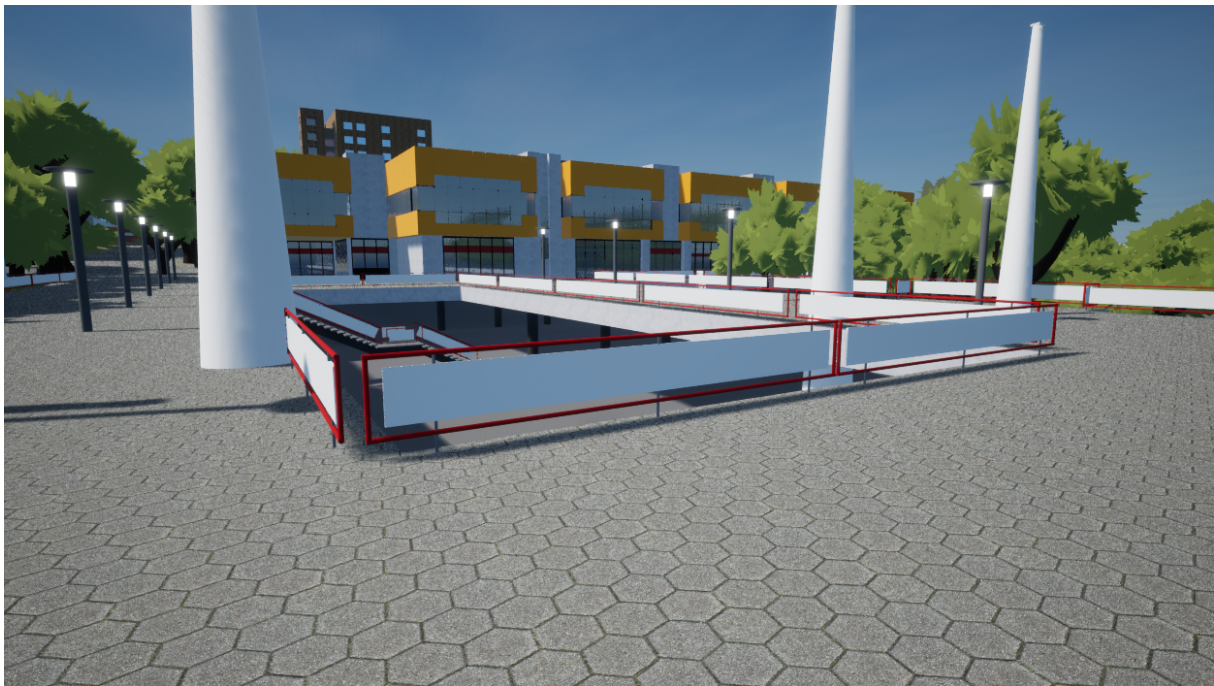


Figure 67: Mensabrücke and Mensa Building (own illustration)

Due to the use of a rough terrain mesh within the modeling process in ArcGIS CityEngine (see Gisa et al. 2022), the detail of the ground structure in the area of the Campus North is not sufficient to create immersion. For this purpose, the area of the study site is removed from the previous model and replaced with a more realistic and malleable landscape using the Unreal Engine's Landscape tool (Figure 68).

In addition, the detail and thus the realism of the model can be increased through the use of materials and the placement of props. A material is an asset that can be applied to objects and meshes to control the appearance of surfaces in the virtual world (Epic Games n.d.-c). In particular, it can be used to create realistic surfaces by assigning textures. Here, the online tool Polycam allows the free creation of 3D tileable textures using their AI Texture Generator, based on a unique text prompt (Figure 69). If the desired outcome is achieved, the file can be downloaded with one click and imported directly into Unreal Engine and other programs. The Unreal Engine Marketplace also provides a large selection

4 PROCEDURE AND RESULTS

of textures and materials, but also props like vegetation for download free of charge. The latter helps immensely in recreating reality, as people associate them with a high visual experience (Engel & Döllner 2012: 168). In this context, particularly the green space located north of the library building was improved (Figure 70).

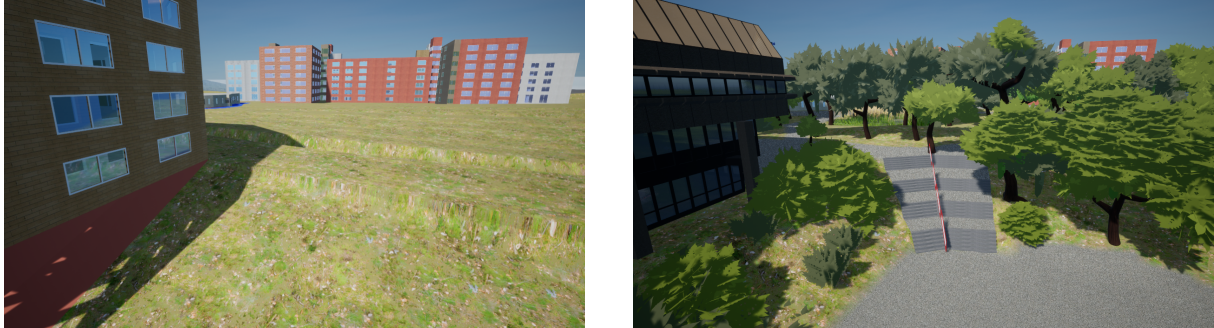


Figure 68: Before (left) and After (right) Landscape Modeling (own illustration)

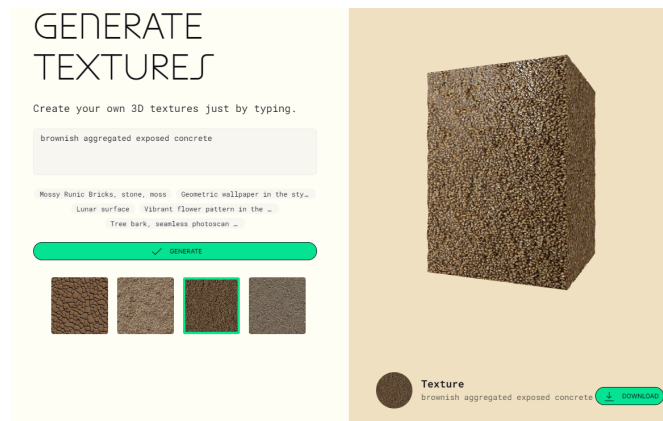


Figure 69: Example of Texture for the Library Building's Facade (Polycam 2023)

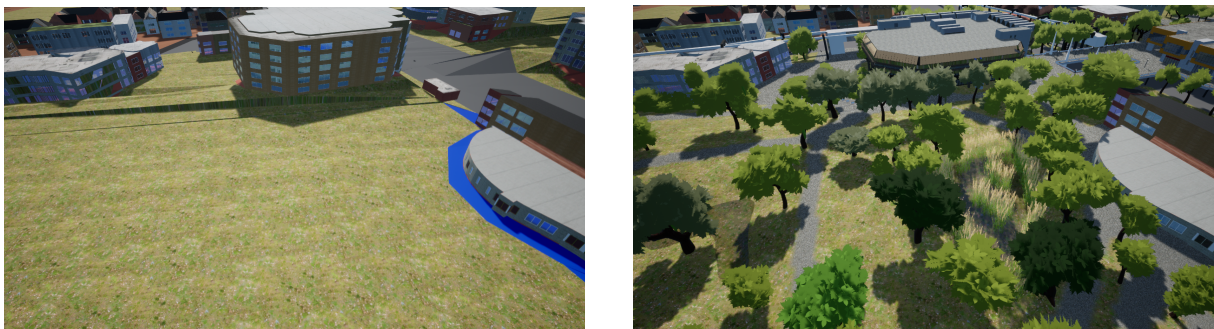


Figure 70: Before (left) and After (right) the Addition of Props to the Surroundings (own illustration)

With more detailed buildings and props added to the VR application, moreover, the project aimed to implement the collected weather data into the application. Essential prerequisites for the import and display of sensor data in the application are the .txt

files written by the .php script for each sensor (see Chapter 4.5.1). Each file contains information on the sensor name, time of measurement (hh:mm:ss), air temperature (°C) and relative humidity (%). These are split with a separator character (here a comma) (Figure 71). This is important, so that in Unreal Engine later the string can be divided into individual information blocks, which can then be saved and used.



Figure 71: Structure of the Used .txt Files (own illustration)

However, in order to reference the text files in Unreal Engine, they must first be downloaded from the FTP server to the local drive. For this purpose a .py script was written, which establishes a connection to the FTP server, then downloads the four .txt files, logs off again and repeats the same process after a given time interval (Figure 72). Thus, the data input is downloaded and also kept up to date by overwriting each file.

Since Unreal Engine does not natively support importing and reading files with its visual scripting interface (blueprints), a custom blueprint function had to be written in the programming language C++ (see Wadstein 2019). With Unreal Engine's blueprints it is possible to create gameplay elements without having to learn a programming language, as it is a visual tool, where nodes are being interconnected in certain ways to receive a desired outcome (Epic Games n.d.-b). The aforementioned created blueprint function can then be used in a blueprint, in order to repeatedly retrieve the text file in short time intervals (Figure 73). The comma-separated values contained in the .txt files are stored in different variables, which can be visualized later in the application itself at different world locations. For visualization purposes, the variables created in the blueprint refer to and control the input of text objects, which are placed onto a modeled terminal object. As the values in the .txt files change, so does the text displayed on the terminal (Figure 74). This way, the sensor data are dynamically visualized in the VR application, although the user has no way of influencing the visualization up to this point.

4 PROCEDURE AND RESULTS

```
C:\> Eingabeaufforderung - python FTPDownload.py
Microsoft Windows [Version 10.0.19044.3086]
(c) Microsoft Corporation. Alle Rechte vorbehalten.

C:\> >cd C:\          \Desktop\VR_CampusNordAdd\Content\Files\FTP

C:\          \Desktop\VR_CampusNordAdd\Content\Files\FTP>python FTPDownload.py
Datei heruntergeladen: Sensor2.txt
Datei heruntergeladen: Sensor4.txt
Datei heruntergeladen: Sensor3.txt
Datei heruntergeladen: Sensor1.txt
Dateidownload abgeschlossen. Beende Verbindung...
Verbindung zum FTP-Server beendet.
Datei heruntergeladen: Sensor2.txt
Datei heruntergeladen: Sensor4.txt
Datei heruntergeladen: Sensor3.txt
Datei heruntergeladen: Sensor1.txt
Dateidownload abgeschlossen. Beende Verbindung...
Verbindung zum FTP-Server beendet.
```

Figure 72: Running the Python Script via Cmd.exe (own illustration)

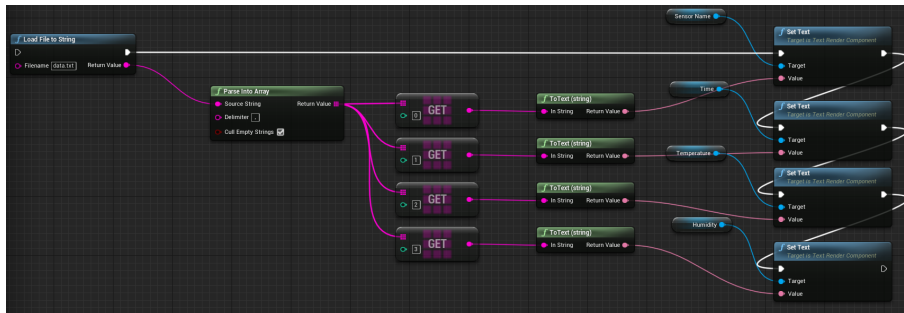


Figure 73: Basic Blueprint Design for Reading and Writing Sensor Data from a Single .txt File (own illustration)



Figure 74: Automatically Updated Display of Sensor Values in the Running VR Application (own illustration)

In addition to the implementation of sensor data, it was also an objective to implement the simulated climate into the Unreal Engine. Initially, a similar data-driven approach was pursued, in order to get the data visualized with as little work as possible and high reproducibility for other simulations. In this context, it was planned to import the voxel structured climate model with its color values as 3D objects into the Unreal Engine. However, given the time frame of the project and due to technical issues, it was not possible to do so. Instead, the simulation results were processed as single maps for each time value and subsequently put together as short video animations. These animations in turn can be imported as video files, e.g. .mp4 files, to the Unreal Engine and be portrayed in the world (Figure 75).

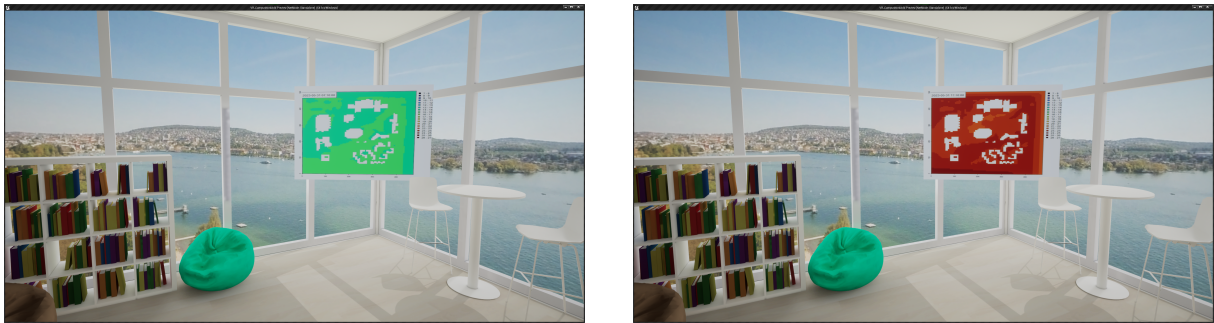


Figure 75: Automatically Played Climate Simulation Videos in the Running VR Application (own illustration)

A chance to build further resemblance with the campus environment and make the VR application more dynamic is associated with animations. Unlike video animation, which can be described as flat, Unreal Engine also allows animating 3D objects. With this, for example, the immersion created by the prominent TU letters atop the Maths Tower is further enhanced by making the letters complete a full z-axis-rotation every exact 105 seconds, just like in the real campus environment (TU Dortmund 2020) (Figure 76).



Figure 76: Rotating TU Logo in the Running VR Application (own illustration)

A believable and lively VR application is characterized, among other things, by familiar locations, requisites such as interior or trees, but also by interaction possibilities (Gisa et al. 2022). Even though dynamic components have already been integrated into the VR

4 PROCEDURE AND RESULTS

application through the previous work steps, the interaction possibility for the user was still missing. By adding user-triggered events to the VR application using Unreal Engine's blueprint capabilities, the user can activate certain processes by interacting with objects in the environment. An example of this is extending the original sensor data terminal so that the user can press a button to shift through the values of sensor 1-4 that are being displayed (Figure 77).



Figure 77: Button-Triggered Display of Sensor Values in the Running VR Application (own illustration)

5. Discussion

The following chapter consists of two parts. First, the research questions posed in Chapter 2 are answered on the basis of the results of this study. Then, the study will be critically reflected and limitations of the study, which occurred during the work process, will be highlighted.

5.1. Answering the Research Questions

To what extent are Digital Twins of buildings currently used in practice and what are possible applications in spatial planning?

The examples given in this study show that the use of a Digital Twin in urban planning is not very advanced. The prevailing understanding of a Digital Twin in practice does not coincide with the definitions provided in the literature. In practice, 3D models that are equipped with factual data are often referred to as Digital Twin. A continuous data transfer from the real object to the virtual object is not apparent. Thus often even the definition of a Digital Shadow is not fulfilled. Despite this, 3D models are used more and more in urban planning. Even if they are often only static, they are used for the simulation of environmental impacts or for the participation of citizens in planning decisions. Especially climate simulations and the effect of new buildings on the urban climate are simulated with 3D models. By using 3D models in urban planning, the first step towards the Digital Twin has been taken. For the future, the integration of real-time data is an essential topic.

What influence does the input 3D model's detail and extent have on the climate simulation and how do simulated and measured values differ at the location of the Central University Library of TU Dortmund University?

In this study, the influence of three different model characteristics on the simulation results was compared: the building resolution in LoD, the size of the study area, and the grid resolution. In general, the simulation results of air temperature and relative humidity were validated. They show a strong positive linear correlation with the measured values. The predicted air temperature values are several degrees lower than the actual measured values. The average deviations in relative humidity are even larger. However, the average deviation is within the range of other experimental studies. Overall, the five models provided similar simulation results. Differences in the examined characteristics had a small effect on the predicted values. Summing up, a smaller study area and a higher grid resolution showed slightly better results. The results related to LoD do not allow a clear conclusion and are subject to the limitation that the simulation was canceled and

therefore there is little availability of data for comparison. It is noticeable that the differences in correlation and average deviation between the studied variables and between the sensor locations were larger than the differences between the models. Due to the only small differences, it should be decided in consideration of the research interest and further criteria like modeling effort and computation time, to what extent the simulation of higher grid resolutions or LoDs is worthwhile.

What are possible options for a dynamic visualization of simulated and measured climate data at the location of the Central University Library of TU Dortmund University?

The study identified several ways to visualize the data of weather sensors and microclimate simulations using the Central Library as a case study. The collected weather data were visualized within the ArcGIS environment (ArcGIS Online and Dashboard), while additionally the simulated climate data were visually embedded in the VR application. Although the tools used in this part of the study open up a lot of possibilities, they also pose certain hurdles, especially for spatial planners. On the one hand, they require a certain level of knowledge, in order to be able to implement the desired results. Although the availability of AI such as ChatGPT has lowered this hurdle to some extent, users of the tools still need a lot of practice, a certain affinity for solving complex problems and a willingness to learn. On the other hand, it was found that interoperability between the tools is currently not always given. Although some vendors do offer solutions in some areas, they have been developed primarily for the business sector and cannot be used in research (e.g. ArcGIS Enterprise), or can only be used to a limited extent, due to expensive licensing fees. In turn, proprietary solutions often require knowledge of programming languages, which then leads back to the first hurdle.

5.2. Reflecting on this Study's Findings

As shown in Chapter 3.1, Digital Twins are currently a widely discussed topic. However, the path to the Digital Twin can be difficult. This is the case, for example, when its implementation requires communication and data exchange between multiple applications (especially against the backdrop of the IoT), which can quickly become a very complex task. Tangible practical obstacles for spatial planners include the knowledge and understanding of programming languages that may be required at a specific stage (e.g. PHP, Python, C++).

The topic of artificial intelligence currently also seems to be of great interest (see Chapter 1), not only for research, business and planning, but also in the field of education and society at large. Especially OpenAI's free to use artificial intelligence-based chatbot ChatGPT seems to hold a disruptive potential. Facilitating the way information can be

obtained, through a cohesive human-like conversation style interaction and access to a vast amount of information, it has the potential to assist with specific complex tasks and accelerate workflows (Lo 2023). In this project, ChatGPT was used for complex technical tasks, in order to overcome the above mentioned lack of programming language skills. Although it helped to achieve specific goals, the AI deployment still presented certain problems, as will be discussed in this chapter. The use of an AI has contributed a lot to the technical success of this study, as the implementation of the scripts requires knowledge of programming languages that a spatial planner often does not have. An AI is capable of translating a task given to it into a desired programming language. However, this translation does not work on the first try, nor does it work error-free. So it is important to specify exactly which script the AI should provide. As many input parameters as possible are needed, like which data should serve as a starting point for the script, what should come out at the end of the script and how exactly the data should be handled.

In addition, the code must be executed often and the results need to be checked. If the results do not fit, the AI has to edit the code again and the code has to be executed and checked again. This procedure must be repeated until the desired result is achieved. Another factor to consider is the technical implementation of a script. In this study, only simple scripts were needed, but for more complex problems it is important that a script is built as well and efficiently as possible so that it does not require an unnecessary amount of computing power. Whether a script created by the AI meets these requirements is questionable and cannot be answered without expertise in this area.

Moreover, it is important to know what the subsequent workflow should look like. While the AI is able to formulate semantically correct scripts in a programming language, it does not know what should happen before and what should happen after the script. It is therefore essential for the user to know the technical infrastructure and the platforms that are important for the workflow in order to be able to give the AI the appropriate instructions. This basic knowledge is especially needed, when AI makes something up (repeatedly happened in the study with e.g. certain blueprint functions in Unreal Engine) so the results can be critically evaluated and the error loop can be avoided (Shahriar & Hayawi 2023: 10f).

The conflict between the term Digital Twin and the term Digital Shadow have already been pointed out in Chapter 3.1. In this study, the concept of the Digital Twin could not be implemented in practice, as time and resources are lacking. Therefore, the Digital Twin created in this study actually represents only a Digital Shadow. However, there are possibilities how the Digital Shadow created in this study could be extended to a Digital Twin. For this extension, a data flow from the Digital Shadow to the real object is necessary and the real object would have to adapt itself based on the data of the Digital Shadow.

The implementation of data transmission in real-time in this study can be improved.

ESRI's product range offers possibilities to create a Digital Twin almost completely within the company's environment. A promising tool for this purpose is the ArcGIS GeoEvent Server. This allows real-time data to be optimally integrated into ArcGIS. Also the management and processing of the data can be done with the ArcGIS GeoEvent Server (ESRI n.d.-d). However, the ArcGIS GeoEvent Server is part of ArcGIS Enterprise, for which no license is available for this study. Accordingly, a way had to be chosen that can be implemented with the available resources.

In this study the update of the datasets in ArcGIS Online is done via a local PC. Although ESRI offers the possibility to implement many ArcGIS functions in Python with the ArcGIS API for Python, various errors occurred during the attempt to set up the API. For this study, the original plan was to have the data update run entirely through a cloud and not require a local computer. However, it proved impossible to install the ArcGIS API for Python on a cloud server that supports Python without in-depth knowledge of Python. This was primarily due to compatibility issues of the respective Python version with the versions of the API. To work around this problem the model builder in ArcGIS Pro was used. This is also based on Python, but by installing ArcGIS Pro on a computer, a version of Python compatible with ArcGIS is already provided. Unfortunately, by using a local computer, there is no way to completely update the data in real-time via the cloud.

As already described in Chapter 4.2.2, the study's individual point clouds were essentially assembled manually in a time-consuming process, with the automatic registration tool of CloudCompare being used successfully only once. Accordingly, it can be assumed that the assembled point cloud contains certain inaccuracies. As a result, the 3D model of the library building based on it could also have inaccuracies. However, as the application of CloudCompare's automatic registration tool showed in the case of the five facade parts, even its application would not have completely eliminated the inaccuracies. On the other hand, the tool did well in matching the two roof scans, probably due to the lower number of scans and a higher degree of overlap. This varying, point cloud dependent, performance of CloudCompare's automatic registration tool was also observed by Rajendra et al. (2014: 895) when they compared it to other algorithms. As for the concerns about inaccuracies in the study's 3D model, a comparison with the library floor plans showed that their representation was essentially the same, with only minor deviations (see Chapter 4.2.3).

One goal of the study was to explore the visualization capabilities of the collected and simulated climate data in different application environments. In order to use the collected sensor data, it was necessary to send it beyond the boundaries of The Things Network. For this purpose, several webhooks were configured during the course of the project, which helped to distribute the latest data to different destinations. Once there, the data were processed for various application purposes, such as displaying it in the ArcGIS environment or the VR application. However, at a certain point in time, individual

webhooks were repeatedly failing, resulting in missing entries in the MySQL database (see Chapter 4.3.2). The cause of these failures could not be determined. However, it is suspected that the webhooks may be in conflict with each other. For example, they all try to forward the data at the same time (right after receiving the data uplink from the sensor). For the work in this study, this was not a major problem because a suitable day for the climate simulation could be found for which all sensor values were also recorded in the MySQL database. In other cases, such as those that also rely on multiple webhooks for multiple applications, but where the climate simulation is run over a longer period of time, missing data values in the database would have had much more serious consequences.

For the verification of the climate simulation itself, this focus was the microclimate around the library building. For such a micro-scale climate model a dense array of locations with flawless instruments would be ideal (Schatzmann & Leitl 2011: 172). The verification of the simulation results was done with a limited amount of data points in both the temporal and the spatial scale. Due to the limited availability of sensors, the actual temperature could only be measured at four locations at the library building. Since there is an inherent variability to the climate even at this time scale, usually simulations have to be evaluated over a long period of time for a complete picture (ibid.: 185). Further verification methods like wind tunnel experiments that are employed to verify the wind data were beyond the scope of this project (ibid.: 178). Nevertheless, a basic verification is an important step in any simulation and can point to some over- and underestimates of the model.

Furthermore, the simulation results are influenced by a variety of factors. Since the atmospheric model has the greatest influence on the results (Salvati & Kolokotroni 2019: 3367), the choice of weather data is particularly important. In this study, weather data from the nearest weather station was used. All that is known of this station is that it is located on the North Campus of the TU Dortmund University and is managed by DTN. For example, the elevation at which the station is installed and the roughness of the terrain are not known. The simulation was only performed for one day, so only one set of atmospheric boundary conditions was estimated. To assess the quality of the simulation across different meteorological conditions, multiple days would have to be simulated (Schatzmann & Leitl 2011: 172) which was not done here because of time limitations. One weather station can also never possibly cover the entirety of the atmospheric boundary conditions (ibid.).

In addition, the assignment of materials to the 3D objects in the model is important. The materials, including the wall constructions, were not specified on the basis of official data, but were estimated as best as possible using information from site visits and aerial photographs. The materials have less influence on the result than the data on the parameters of the atmospheric model (Salvati & Kolokotroni 2019: 3367). Nevertheless, they do have an influence, especially on surface temperature, and may have biased the results

5 DISCUSSION

(*ibid.*).

Some difficulties have been encountered during the model generation and simulations, e.g. error messages and aborts. The influence of the LoD on the results could only be assessed in a limited way due to the aborted simulation, because the climate was calculated only until 08:26 model time. Then an error occurred due to unstable climate parameters. Due to time constraints and limited hardware access, the simulation could not be repeated. In addition, the error could not be identified in the model.

6. Conclusion and Further Research

The aim of this project was to explore the application potential of a Digital Twin of a building in the context of spatial planning, microclimate simulation and dynamic visualization of results using the Central University Library as a case study. To achieve this objective, the project group conducted a literature review on the topics of Digital Twins, microclimate simulation, and dynamic visualization. This served as a basis for the complex workflow that included the creation of a 3D model of the library building, the installation of weather sensors, the microclimate simulations, and the dynamic visualization of the results.

Based on the literature review, the project group found that the concept of the Digital Twin is still in its early stages in current spatial planning practice. Furthermore, the practical understanding of a Digital Twin differs from its literature definition. In practice, it often refers to 3D models with factual data, but lacks continuous real-time data transfer and often does not even meet the criteria of a Digital Shadow.

Next, three model characteristics were compared for their effect on simulation results: LoD resolution, study area size, and grid resolution. The narrow study area compared to the extended area as well as the higher resolution grid, but only when compared to a much lower resolution grid, resulted in slightly more accurate outcomes. The assessment of a higher LoD was restricted due to an error. The verification process showed a strong positive linear correlation with the measured values. However, the predicted temperature level is on average several degrees below the actual measured values, and the average deviations for relative humidity are even larger.

Finally, multiple suitable tools were used to visualize the climate data from the sensors and the microclimate simulation. However, the project group identified several barriers that could prevent a wider use of dynamic visualization in planning practice and research. Technical requirements and know-how being among the most prominent. This work shows the implementation of real-time data in a freely accessible online dashboard and extended VR application that now includes detailed parts of both the Campus South and Campus North. In addition, the documentation of the work processes in the working guide provides a helpful tool to assist such projects in the future.

Although beyond the scope of this project, one possible transformation of the Digital Shadow to a Digital Twin would be the control of the temperature inside the Central University Library based on the temperatures detected by the sensors. For example, the air conditioning, if integrated into the IoT, could be automatically turned up or down depending on the outside temperature. Another possibility would be to control windows or shutters, provided they are also integrated into the IoT. The shutters could be lowered when the temperature measured by the sensors is higher, or the windows could be closed when the interior of the building needs to be cooled. However, this extension requires

more time and resources than were available in this study. One way to easily implement this extension is the ESRI product suite, which could not be used for this study due to lack of licenses. The already mentioned ArcGIS Enterprise with the ArcGIS GeoEvent Server offers many possibilities to integrate, analyze and display real-time data. ESRI's ArcGIS Velocity application also provides a wide range of options for advancing the development of a Digital Twin. ArcGIS Velocity is an extension to ArcGIS Online that can integrate IoT data from a variety of sources into ArcGIS Online. This data can then be analyzed and specific actions can be triggered in other applications based on the results (ESRI n.d.c).

Climate simulations can be run over longer time periods by using a lower grid resolution and a smaller study area. This can reduce the computational cost of the simulation while still providing accurate results for the specific research question. Over a longer period of time, probability density functions can be generated that more accurately describe the predictive qualities of a simulation. This can help scientists better understand the range of possible outcomes for a given climate scenario. Climate simulations can be used to inform architectural and spatial planning solutions. For example, climate simulations can be used to identify areas suitable for cold air corridors or facade/roof greening. By combining climate simulation results with real-time weather data, architects and urban planners can design buildings and cities that are more comfortable, efficient, and resilient to the impacts of climate change.

For future projects, the campus model can be extended by merging the interior of the library building into the current model to achieve a comprehensive archive of the library. In addition, the vast campus environment offers numerous other buildings, objects, and areas that can be modeled in greater detail, providing exciting opportunities for data integration and creating a digital campus experience. The library's Digital Shadow and its spatial expansion opens up opportunities to extend its reach to the entire campus. This, for example, may allow for the management and monitoring of the newly planned photovoltaic panels and wind turbine (TU Dortmund 2023), leveraging the digital infrastructure for sustainable energy initiatives. In addition, the VR application can be further developed to include various elements of the campus. For example, the H-Bahn, a unique feature of the TU Dortmund in the Ruhr region, can be integrated into the VR application with the support of IT cooperation. This integration is an exciting prospect, especially with the upcoming extension of the H-Bahn to the Barop Parkhaus station or towards the Dortmund Harbor and the Smart Rhino area. As the VR application evolves, it could be made available for online download. However, this requires that the VR Gear is not a prerequisite and that the application is controllable using a mouse and keyboard in a first-person perspective. This makes the VR experience accessible to a wider audience, including prospective students and first-year students from abroad or remote locations in Germany. Such an initiative allows them to gain an immersive impression and overview

of the campus environment, facilitating a better connection and engagement with TU Dortmund's offerings.

In conclusion, this project not only explores the emerging field of Digital Twins in spatial planning, but also provides valuable insights into their practical application, particularly in the context of microclimate simulation and dynamic visualization. The challenges identified in aligning theoretical concepts with real-world implementation underscore the evolving nature of this technology in spatial planning practice. With the demolition of the current Central University Library set to begin in the spring of 2024, this work stands as a testament to the innovative use of technology to preserve and experience the legacy of a significant architectural landmark. By providing a tangible link between the past and the future, this project not only enriches our understanding of Digital Twins, but also ensures that the essence of the Central University Library will endure beyond its physical existence.

References

- Al-Ali, A. R., Gupta, R., Zaman Batool, T., Landolsi, T., Aloul, F., & Al Nabulsi, A. (2020). Digital Twin Conceptual Model within the Context of Internet of Things. *Future Internet*, 12 (10). p. 163.
- American Meteorological Society. (2012a). Glossary of Meteorology. Microclimate. Accessed on 01.07.2023 on: <https://glossary.ametsoc.org/wiki/Microclimate>
- American Meteorological Society. (2012b). Glossary of Meteorology. Microscale. Accessed on 01.07.2023 on: <https://glossary.ametsoc.org/wiki/Microclimate>
- Barnston, A. G. (1992). Correspondence among the Correlation, RMSE, and Heidke Forecast Verification Measures; Refinement of the Heidke Score. *Weather and Forecasting*, 7 (4). p. 699–709.
- Barrero, J. M., Bloom, N., & Davis, S. (2021). Why Working from Home will Stick. Working Paper 28731. National Bureau of Economic Research, Cambridge MA.
- Batty, M. (2018). Digital twins. *Environment and Planning B: Urban Analytics and City Science*, 45 (5). p. 817–820.
- Bhushan, A. (1972). The File Transfer Protocol. RFC 354. Network Working Group.
- Bick, A., Blandin, A., & Mertens, K. (2021). Work from Home Before and After the COVID-19 Outbreak. Working Paper 2017. Federal Reserve Bank of Dallas.
- Biljecki, F., Zhao, J., Stoter, J., & Ledoux, H. (2013). Revisiting the Concept of Level of Detail in 3D City Modelling. *ISPRS Annals of the Photogrammetry, Remote Sensing and Spatial Information Sciences*, 2, 63–74.
- BMZ–Bundesministerium für wirtschaftliche Zusammenarbeit und Entwicklung. (n.d.). Stadtentwicklung. Hintergrund: Das Zeitalter der Städte. Accessed on 23.07.2023 on: <https://www.bmz.de/de/themen/stadtentwicklung/hintergrund-18138>
- bplaced. (n.d.). PHP-Einstellungen. Accessed on 22.07.2023 on: <https://wiki.bplaced.net/php-version-einstellen#:~:text=PHP%2DEinstellungen&text=Bei%20bplaced%20stehen%20jeweils%20mehrere,welche%20zur%20Zeit%20zur%20Verf%C3%BCgung>
- Bruse, M. (2000). Anwendung von mikroskaligen Simulationsmodellen in der Stadtplanung. In L. Bernard (Ed.), *Simulation raumbezogener Prozesse: Methoden und Anwendungen*. Natur und Wissenschaft.
- Bruse, M. (2004). Envi-met 3.0: Updated Model Overview.
- Bruse, M., & Fleer, H. (1998). Simulating surface–plant–air interactions inside urban environments with a three dimensional numerical model. *Environmental Modelling & Software*, 13(3-4), 373–384.
- Bryson, S. (1993). Symposium Considers Applications of Virtual Reality. *Computers in Physics*, 7(5), 495.

REFERENCES

- Caprari, G., Castelli, G., Montuori, M., Camardelli, M., & Malvezzi, R. (2022). Digital Twin for Urban Planning in the Green Deal Era: A State of the Art and Future Perspectives. *Sustainability*, *14*(10), 6263.
- Chen, T.-J. (2023). ChatGPT and other artificial intelligence applications speed up scientific writing. *Journal of the Chinese Medical Association*, *86*(4), 351–353.
- Cheng, L., Chen, S., Liu, X., Xu, H., Wu, Y., Li, M., & Chen, Y. (2018). Registration of Laser Scanning Point Clouds: A Review. *Sensors*, *18*(5), 1641.
- Choi, G. Y., Kim, H. S., Kim, H., & Lee, J. S. (2021). How do paving and planting strategies affect microclimate conditions and thermal comfort in apartment complexes? *International Journal of Climate Change Strategies and Management*, *13*(2), 97–119.
- Cisco. (2014). IoE-Driven Smart Street Lighting Project Allows Oslo to Reduce Costs, Save Energy, Provide Better Service.
- City of Helsinki. (n.d.). Energy and Climate Atlas. Accessed on 22.07.2023 on: <https://kartta.hel.fi/3d/atlas/#/settings>
- City of Helsinki. (n.d.b.). Estimated Heating Energy Consumption of Buildings. Accessed on 22.07.2023 on: <https://kartta.hel.fi/3d/heating/Apps/Helsinki/view.html>
- City of Helsinki. (n.d.c.). Helsinki 3D Mesh. Accessed on 22.07.2023 on: <https://kartta.hel.fi/3d/mesh/>
- City of Zurich. (n.d.). Klimamodell: Klimaanalysekarte. Accessed on 22.07.2023 on:
- Climate-Data.org. (n.d.). Dortmund Climate (Germany): Data and Graphs for weather and climate in Dortmund. Accessed on 22.07.2023 on: <https://en.climate-data.org/europe/germany/north-rhine-westphalia/dortmund-147/>
- CloudCompare. (2015). Alignment and Registration. Accessed on 22.07.2023 on: https://www.cloudcompare.org/doc/wiki/index.php/Alignment_and_Registration
- CloudCompare. (n.d.). Cloud Compare: 3D point cloud and mesh processing software. Accessed on 22.07.2023 on: <http://www.cloudcompare.org/>
- Dembski, F., Wössner, U., Letzgus, M., Ruddat, M., & Yamu, C. (2020). Urban Digital Twins for Smart Cities and Citizens: The Case Study of Herrenberg, Germany. *Sustainability*, *12*(6), 2307.
- Deutscher Städtetag. (2017). 3D-Geodaten in der integrierten Stadtentwicklung: Handreichung des Deutschen Städtetages.
- Dhiman, R., VishnuRadhan, R., Eldho, T. I., & Inamdar, A. (2019). Flood risk and adaptation in Indian coastal cities: Recent scenarios. *Applied Water Science*, *9*, 5.
- Di Nunzio, A. (2022). Envimet INX: 1. Sketchup plugin. Accessed on 09.07.2023 on: <https://github.com/ENVI-coding/Envimet-INX/wiki/1.-Sketchup-plugin#important>
- Dixson, N., Milliken, G., & Mukanda, Keshav, Murray, Reina, Starry, Rachel. (2019). GeoJSON Data Primer. university of minnesota digital conservancy.

- Dong, Z., Liang, F., Yang, B., Xu, Y., Zang, Y., Li, J., Wang, Y., Dai, W., Fan, H., Hyypä, J., & Stilla, U. (2020). Registration of large-scale terrestrial laser scanner point clouds: A review and benchmark. *ISPRS Journal of Photogrammetry and Remote Sensing*, 163, 327–342.
- Dortmund, T. (n.d.). Universitätsbibliothek der TU Dortmund: Lesen und Lernen. Accessed on 22.07.2023 on: <https://www.tu-dortmund.de/studierende/im-studium/bibliothek/#:~:text=Die%20Universit%C3%A4tsbibliothek%20bietet%20einen%20umfassenden,die%20die%20Bibliothek%20lizenziert%20hat>.
- Dortmunder Statistik. (2023). Bevölkerung in Zahlen 2022: Bevölkerungsstand. accessed on 20.07.2023 on. <https://statistikportal.dortmund.de/bevoelkerung/bevoelkerunginzahlen/#download>
- Dragino. (2023). LSN50v2-S31-S31B LoRaWAN Temperature & Humidity Sensor User Manual. Accessed on 22.07.2023 on: <http://wiki.dragino.com/xwiki/bin/view/Main/User%20Manual%20for%20LoRaWAN%20End%20Nodes/LSN50v2-S31-S31B%20LoRaWAN%20Temperature%20%26%20Humidity%20Sensor%20User%20Manual/>
- DTN/MeteoGroup Nederland. (2023). Monatsstatistik Juni 2023: Station: Dortmund- Uni. Accessed on 18.07.2023 on: <https://wetterstationen.meteoedia.de/index.php?station=104170&wahl=rueckblick>
- Duarte, D. H., Shinzato, P., Gusson, C. d. S., & Alves, C. A. (2015). The impact of vegetation on urban microclimate to counterbalance built density in a subtropical changing climate. *Urban Climate*, 14, 224–239.
- DWD–Deutscher Wetterdienst. (n.d.). Urban climate - urban heat islands. Accessed on 19.07.2023 on: https://www.dwd.de/EN/research/climateenvironment/climate_impact/urbanism/urban_heat_island/urbanheatisland_node.html
- Egger, A. (2021). LHT65 TTN Webapp. Accessed on 23.07.2023 on: <https://www.aeq-web.com/lht65-ttn-v3-webhook-http-integration-php-webapp/>
- Engel, J., & Döllner, J. (2012). Immersive Visualisierung von virtuellen 3D-Stadtmodellen und ihr Einsatz in der Stadtplanung. In: Seyfert, Eckhardt (ed.): Vorträge. 32. Wissenschaftlich-Technische Jahrestagung der DGPF. Deutsche Gesellschaft für Photogrammetrie, Fernerkundung und Geoinformation, Oldenburg. p. 165–172.
- ENVI-met. (2017a). Configuration File - Basic Settings. Accessed on 01.07.2023 on: [https://envi-met.info/doku.php?id=basic_settings&s\[\]=location](https://envi-met.info/doku.php?id=basic_settings&s[]=location)
- ENVI-met. (2017b). Decoding Urban Nature. Accessed on 01.07.2023 on: <https://www.envi-met.com/wp-content/uploads/2021/08/ENVI-met-brochure.pdf>
- ENVI-met. (2017c). Lateral Boundary Conditions. Accessed on 01.07.2023 on: [https://envi-met.info/doku.php?id=kb:lbc&s\[\]=full&s\[\]=forcing](https://envi-met.info/doku.php?id=kb:lbc&s[]=full&s[]=forcing)
- ENVI-met. (2018). Digitalization with SPACES: 2.5D and 3D mode. Accessed on 01.07.2023 on: <https://www.youtube.com/watch?v=Xbxn1e70pK0>

REFERENCES

- ENVI-met. (2021a). ENVI-met. a holistic Microclimate Modelling System. Accessed on 01.07.2023 on: <https://envi-met.info/doku.php?id=root:start>
- ENVI-met. (2021b). Vertical Grid Layout. Accessed on 01.07.2023 on: [https://envi-met.info/doku.php?id=kb:verticalgrid&s\[\]=vertical&s\[\]=gridding](https://envi-met.info/doku.php?id=kb:verticalgrid&s[]=vertical&s[]=gridding)
- ENVI-met. (2022). Headquarter. Accessed on 01.07.2023 on: <https://envi-met.info/doku.php?id=apps:headquarter>
- ENVI-met. (2023a). ENVI-met Model Architecture. Accessed on 01.07.2023 on: <https://envi-met.info/doku.php?id=intro:modelconcept>
- ENVI-met. (2023b). ENVI-met Update History: ENVI-met updates for version 5.5.1 (Summer 23). Accessed on 01.07.2023 on: <https://envi-met.info/doku.php?id=apps:updates>
- ENVI-met. (2023c). QGIS Plugin. Accessed on 01.07.2023 on: <https://envi-met.info/doku.php?id=apps:gis4envi-met>
- ENVI-met. (n. d.). Software: ENVI-met Simulationssoftware für das Mikroklima. Accessed on 23.07.2023 on: <https://www.envi-met.com/de/software/>
- ENVI-met Admin Tim. (2020). Start Telescope Height: Online forum post. Accessed on 23.07.2023 on: (ENVI-met, Ed.). <http://www.envi-hq.com/viewtopic.php?f=31&t=3573&p=11774&hilit=telescope+grid&sid=2bc2d9c00930d2c9bf2c9905afb928e2#p11774>
- ENVI-met Admin Tim. (2023). Topography/ Terrain - 2023: Online forum post. Accessed on 23.07.2023 on: (ENVI-met, Ed.). <http://www.envi-hq.com/viewtopic.php?f=3&t=5073&p=18893&hilit=terrain+dem&sid=6ed2ed71b15bfd39adb0cea25dae7a1c#p18893>
- Epic Games. (n.d.-a). Get Ahead: Learn Unreal Engine. Accessed on 23.07.2023 on: <https://www.unrealengine.com/en-US/learn>
- Epic Games. (n.d.-b). Introduction to Blueprints. Accessed on 23.07.2023 on: <https://docs.unrealengine.com/4.27/en-US/ProgrammingAndScripting/Blueprints/GettingStarted/>
- Epic Games. (n.d.-c). Unreal Engine: Frequently Asked Questions (faqs). Accessed on 20.07.2023 on: <https://www.unrealengine.com/en-US/faq?active=general>
- ESRI. (n.d.-a). ArcGIS Dashboards. Accessed on 23.07.2023 on: <https://www.esri.com/de-de/arcgis/products/arcgis-dashboards/overview#:~:text=Mithilfe%20von%20ArcGIS%20Dashboards%20k%C3%B6nnen,einem%20einzelnen%20Bildschirm%20pr%C3%A4sentiert%20werden.>
- ESRI. (n.d.-b). Einführung in ArcGIS Online. Accessed on 23.07.2023 on: <https://doc.arcgis.com/en/arcgis-online/get-started/what-is-agol.htm>
- ESRI. (n.d.-c). Feature-Layer. Accessed on 23.07.2023 on: <https://enterprise.arcgis.com/de/portal/latest/use/feature-layers.htm#:~:text=ArcGIS%20Server%20Server>

- 2DFeature%2DLayer%3A,Store%2DElementen%20im%20Portal%20ver%20C3%B6ffentlicht.
- ESRI. (n.d.-d). Introduction to ArcGIS GeoEvent Server. Accessed on 23.07.2023 on: <https://enterprise.arcgis.com/de/geoevent/latest/get-started/what-is-arcgis-geoevent-server.htm>
- ESRI. (n.d.-e). Portal-Verbindungen in ArcGIS Pro verwalten. Accessed on 23.07.2023 on: <https://pro.arcgis.com/de/pro-app/latest/help/projects/manage-portal-connections-from-arcgis-pro.htm>
- ESRI. (n.d.-f). Was ist Modelbuilder?. Accessed on 23.07.2023 on: <https://pro.arcgis.com/de/pro-app/latest/help/analysis/geoprocessing/modelbuilder/what-is-modelbuilder-.htm>
- Felstead, A., & Reuschke, D. (2020). Homeworking in the UK: Before and during the 2020 lockdown. WISERD Report. Wales Institute of Social and Economic Research, Cardiff.
- fluxguide. (n.d.). GLARA Kick-off in der Bernardgasse 1070 Wien. Accessed on 20.07.2023 on: <https://www.fluxguide.com/puls/glara-kick-off-in-der-bernardgasse/>
- Geobasis NRW. (2023a). Digitale Orthophotos NW. Accessed on 28.05.2023 on: <https://open.nrw/dataset/56fb584b-10cf-4009-a405-0bef06bb3e00>
- Geobasis NRW. (2023b). Digitales Geländemodell NW Gitterweite 1m. Accessed on 28.05.2023 on: <https://open.nrw/dataset/0c6796e5-9eca-4ae6-8b32-1fcc5ae5c481>
- GeoSLAM. (2020). ZEB-HORIZON User Manual v1.3. Accessed on 23.07.2023 on: <https://geoslam.com/wp-content/uploads/2021/02/ZEB-Horizon-User-Manual-v1.3.pdf>
- Gisa, D., Karakus, S., Schartmann, M., Simon, J., & Wittig, M. (2022). Opportunities and limitations of VR in spatial planning. Accessed on 17.07.2023 on: <https://storymaps.arcgis.com/stories/672324a377524889bc725a03f2e57237>
- Gollob, C., Ritter, T., & Nothdurft, A. (2020). Forest Inventory with Long Range and High-Speed Personal Laser Scanning (PLS) and Simultaneous Localization and Mapping (SLAM) Technology. *Remote Sensing*, 12(9), 1509.
- Gordijn, B., & ten Have, H. (2023). ChatGPT: Evolution or revolution? *Medicine, Health Care and Philosophy*, 26(1), 1–2.
- Gröger, G., Kolbe, T. H., & Czerwinski, A. (Eds.). (2006). Candidate OpenGIS CityGML Implementation Specification: (City Geography Markup Language. open geospatial consortium inc.
- Großmann, K. (2020). Gebäude-Energieeffizienz als Katalysator residentieller Segregation. *sub\urban. zeitschrift für kritische stadtforschung*, 8(1/2), 199–210.
- Grützner, U. (2022). Uav-footage.
- H-Bahn21. (n.d.). H-Bahn Dortmund Streckennetz. Accessed on 20.07.2023 on: <https://h-bahn.info/streckennetz/>

REFERENCES

- Hedquist, B. C., & Brazel, A. J. (2014). Seasonal variability of temperatures and outdoor human comfort in Phoenix, Arizona, U.S.A. *Building and Environment*, *72*, 377–388.
- Hegarty, M. (2004). Dynamic visualizations and learning: Getting to the difficult questions. *Learning and Instruction*, *14*(3), 343–351.
- Herath, H., Halwatura, R. U., & Jayasinghe, G. Y. (2018). Evaluation of green infrastructure effects on tropical Sri Lankan urban context as an urban heat island adaptation strategy. *Urban Forestry & Urban Greening*, *29*, 212–222.
- Huttner, S. (2012). Further development and application of the 3D microclimate simulation ENVI-met. Dissertation. Johannes Gutenberg-Universität, Mainz.
- Imottesjo, H., & Kain, J.-H. (2022). The Urban CoCreation Lab—An Integrated Platform for Remote and Simultaneous Collaborative Urban Planning and Design through Web-Based Desktop 3D Modeling, Head-Mounted Virtual Reality and Mobile Augmented Reality: Prototyping a Minimum Viable Product and Developing Specifications for a Minimum Marketable Product. *Applied Sciences*, *12*(2), 797.
- Jänicke, B., Meier, F., Hoelscher, M.-T., & Scherer, D. (2015). Evaluating the Effects of Façade Greening on Human Bioclimate in a Complex Urban Environment. *Advances in Meteorology*, *2015*, 1–15.
- Khoa, T. A., Man, M. M., Nguyen, T.-Y., Nguyen, V., & Nam, N. H. (2019). Smart Agriculture Using IoT Multi-Sensors: A Novel Watering Management System. *Journal of Sensor and Actuator Networks*, *8*(3), 45.
- Kim, H. H. (1992). Urban heat island. *International Journal of Remote Sensing*, *13*(12), 2319–2336.
- Kitchin, R. (2013). The real-time city? Big data and smart urbanism. *GeoJournal*, *79*(1), 1–14.
- Kite-Powell, J. (2022). Can Digital Twins Drive A Climate Change Agenda? Accessed on 23.07.2023 on: <https://www.forbes.com/sites/jenniferhicks/2022/05/16/can-digital-twins-drive-a-climate-change-agenda/>
- Klostermeier, R., Haag, S., & Benlian, A. (2018). Digitale Zwillinge: Eine explorative Fallstudie zur Untersuchung von Geschäftsmodellen. *HMD Praxis der Wirtschaftsinformatik*, *55*(2), 297–311.
- Kraus, H. (2004). *Die Atmosphäre der Erde: Eine Einführung in die Meteorologie*. Springer.
- Kurian, N., Cherian, J. M., Sudharson, N. A., Varghese, K. G., & Wadhwa, S. (2023). AI is now everywhere. *British Dental Journal*, *234*(2), 72.
- Lee, H., Mayer, H., & Chen, L. (2016). Contribution of trees and grasslands to the mitigation of human heat stress in a residential district of Freiburg, Southwest Germany. *Landscape and Urban Planning*, *148*, 37–50.
- Lewis, S. (n.d.). Dynamic and Static: Definition. Accessed on 20.07.2023 on:

- Lippmann, D. (2015). 50 Jahre Universitätsbibliothek: Drei Jahre vor der TU Dortmund feiert die UB ihr Gründungsjubiläum. *In: Unizet, Nr. 443(443)*, 2.
- Liu, M., Fang, S., Dong, H., & Xu, C. (2021). Review of digital twin about concepts, technologies, and industrial applications. *Journal of Manufacturing Systems*, 58, 346–361.
- Lo, C. K. (2023). What is the Impact of ChatGPT on Education? A Rapid Review of the Literature.
- Lowe, R. (2004). Interrogation of a dynamic visualization during learning. *Learning and Instruction*, 14(3), 257–274.
- Madakam, S., Ramaswamy, R., & Tripathi, S. (2015). Internet of Things (IoT): A Literature Review. *Journal of Computer and Communications*, 3(5), 164–173.
- Malberg, H. (2007). *Meteorologie und Klimatologie: Eine Einführung* (4th ed.). Springer.
- Mclean, Douglas J. (2012). *Understanding Aerodynamics: Arguing from the real physics*. John Wiley & Sons.
- Middel, A., Hüb, K., Brazel, A. J., Martin, C. A., & Guhathakurta, S. (2014). Impact of urban form and design on mid-afternoon microclimate in Phoenix Local Climate Zones. *Landscape and Urban Planning*, 122, 16–28.
- MySQL. (n.d.). MySQL. Accessed on 17.07.2023 on: <https://www.mysql.com/>
- Nguyen, M.-T., Nguyen, H.-K., Vo-Lam, K.-D., Nguyen, X.-G., & Tran, M.-T. (2016). Applying virtual reality in city planning. In S. Lackey & R. Shumaker (Eds.), *Virtual, augmented and mixed reality* (pp. 724–735, Vol. 9740). Springer. https://link.springer.com/chapter/10.1007/978-3-319-39907-2_69
- Nijhuis, S., Sun, Y., & Lange, E. (2023). Introduction: Adaptive urban transformation in the pearl river delta, china. In S. Nijhuis, Y. Sun, & E. Lange (Eds.), *Adaptive urban transformation* (pp. 3–19). Springer International Publishing.
- NVIDIA Developer. (2020). Cinematic Climate Visualization with NVIDIA Omniverse. youtube, 11.11.2020. Accessed on 20.07.2023 on: <https://www.youtube.com/watch?v=xJtKd2bDS3M>
- Pénard, T., & Coulanges, N. (2020). Le télétravail au temps du COVID: Les enseignements de l'enquête marsouin sur les usages numériques des travailleurs bretons pendant le confinement. Enquête CAPUNI crise. GIS Marsouin.
- phpMyAdmin. (n.d.). Bringing MySQL to the web. Accessed on 17.07.2023 on: <https://www.phpmyadmin.net/>
- Polycam. (2023). Generate Textures: Create your own 3D textures just by typing. Accessed on 20.07.2023 on: <https://poly.cam/material-generator>
- Powers, D. (2022). *PHP 8 Solutions*. Berkeley, Ca.
- Psyllidis, A., Bozzon, A., Bocconi, S., & Titos Bolivar, C. (2015). A Platform for Urban Analytics and Semantic Data Integration in City Planning. In G. Celani, D. M.

REFERENCES

- Sperling, & J. M. S. Franco (Eds.), *Computer-Aided Architectural Design Futures* (pp. 21–36, Vol. 527). Springer. Berlin, Heidelberg.
- Rajendra, Y. D., Mehrotra, S. C., Kale, K. V., Manza, R. R., Dhumal, R. K., Nagne, A. D., & Vibhute, A. D. (2014). Evaluation of Partially Overlapping 3D Point Cloud's Registration by using ICP variant and CloudCompare. *The International Archives of the Photogrammetry, Remote Sensing and Spatial Information Sciences, XL-8*, 891–897.
- Rau, C. (2017). Was der Umbau der Bib für Studierende bedeutet. Accessed on 20.07.2023 on: <http://www.pflichtlektuere.com/08/02/2017/was-der-umbau-der-bib-fuer-studierende-bedeutet/>
- Rheingans, P. (2002). Are we there yet? Exploring with dynamic visualization. *IEEE Computer Graphics and Applications*, 22(1), 6–10.
- Rohland, H. (2008). Der SQL-Standard. Accessed on 17.07.2023 on: https://elearn.inf.tu-dresden.de/sqlkurs/lektion01/01_02_sql%20standard.html
- RVR–Regionalverband Ruhr. (2022). Luftbilder. Accessed on 28.05.2023 on: <https://luftbilder.geoportal.ruhr/?#4541@7.41672/51.49180r0@EPSG:25832>
- Salata, F., Golasi, I., de Lieto Vollaro, R., & de Lieto Vollaro, A. (2016). Urban microclimate and outdoor thermal comfort. A proper procedure to fit ENVI-met simulation outputs to experimental data. *Sustainable Cities and Society*, 26, 318–343.
- Salvati, A., & Kolokotroni, M. (2019). Microclimate Data for Building Energy Modelling: Study On ENVI-met Forcing Data. In V. Corrado, E. Fabrizio, A. Gasparella, & F. Patuzzi (Eds.), *16th international conference of the international building performance simulation association (building simulation 2019)* (pp. 3361–3368). Curran Associates Inc.
- Sanchez, V., & Zakhor, A. (2012). Planar 3D modeling of building interiors from point cloud data. *2012 19th IEEE International Conference on Image Processing (ICIP 2012)*, 1777–1780.
- Schaefer, M. (2022). Between vision and action: The predicted effects of co-designed green infrastructure solutions on environmental burdens. *Urban Ecosystems*, 25(6), 1805–1824.
- Schatzmann, M., & Leitl, B. (2011). Issues with validation of urban flow and dispersion CFD models. *Journal of Wind Engineering and Industrial Aerodynamics*, 99(4), 169–186.
- Schrotter, G., & Hürzeler, C. (2020). The Digital Twin of the City of Zurich for Urban Planning. *Journal of Photogrammetry, Remote Sensing and Geoinformation Science*, 88(1), 99–112.
- Sepasgozar, S. M. E. (2021). Differentiating Digital Twin from Digital Shadow: Elucidating a Paradigm Shift to Expedite a Smart, Sustainable Built Environment. *Buildings*, 11(4), 151.

- Shahriar, S., & Hayawi, K. (2023). Let's have a chat! a Conversation with ChatGPT: Technology, Applications, and Limitations.
- Song, B., & Park, K. (2015). Contribution of Greening and High-Albedo Coatings to Improvements in the Thermal Environment in Complex Urban Areas. *Advances in Meteorology*, 2015, 1–14.
- Souch, C., & Grimmond, S. (2006). Applied climatology: Urban climate. *Progress in Physical Geography*, 30(2), 270–279.
- Stadt Dortmund. (n.d.). Leben in Hombruch: Barop, Bittermark, Brüninghausen, Eichlinghofen, Großholthausen, Hombruch, Kirchhörde, Kleinholthausen, Kruckel, Löttringhausen, Lücklemburg, Menglinghausen, Persebeck, Renninghausen, Salingen, Schanze, Schnee, Schönau. Accessed on 27.05.2023 on: https://www.dortmund.de/de/leben_in_dortmund/stadtbezirke/stbzportal_hombruch/leben_in_hombruch/index.html
- STATEC. (n.d.). Le télétravail expose: Une expérience jugée positive par la majorité des travailleurs. STATNEWS 15.
- Statistisches Bundesamt (Destatis). (2022). Einwohnerzahl der größten Städte in Deutschland am 31. Dezember 2021, cited as in Statista. Accessed on 20.07.2023 on: <https://de.statista.com/statistik/daten/studie/1353/umfrage/einwohnerzahlen-der-grossstaedte-deutschlands/>
- Statistisches Bundesamt (Destatis). (2023). Erwerbstätige, die von zu Hause aus arbeiten: Qualität der Arbeit. Accessed on 20.07.2023 on: <https://www.destatis.de/DE/Themen/Arbeit/Arbeitsmarkt/Qualitaet-Arbeit/Dimension-3/home-office.html>
- Stock, T. (2019). Klimaanalyse Stadt Dortmund. Regionalverband Ruhr - Referat Geoinformation und Raumbewertung, Essen.
- Tang, P., Anil, E. B., Akinci, B., & Huber, D. (2011). Efficient and Effective Quality Assessment of As-Is Building Information Models and 3D Laser-Scanned Data. In Y. Zhu & R. R. Issa (Eds.), *Computing in civil engineering (2011)* (pp. 486–493). American Society of Civil Engineers.
- Tchana, Y., Ducellier, G., & Remy, S. (2019). Designing a unique Digital Twin for linear infrastructures lifecycle management. *Procedia CIRP*, 84, 545–549.
- The Things Industries. (n.d.-a). The Things Stack. Accessed on 22.07.2023 on: <https://www.thethingsindustries.com/stack/>
- The Things Industries. (n.d.-b). Webhooks. Accessed on 22.07.2023 on: <https://www.thethingsindustries.com/docs/integrations/webhooks/#:~:text=Webhooks%20can%20be%20used%20to,visualized%20in%20an%20external%20dashboard>
- Thinh, N. X. (2022). Virtual Reality in der Raumplanung: Entwicklung und Demonstration eines in VR erlebbaren digitalen Zwillings des Campus Süd der TU Dortmund. In R. Bill & M. L. Zehner (Eds.), *Geoforum MV 2022* (pp. 95–104). tredition, Hamburg.

REFERENCES

- Tomkins, A., & Lange, E. (2020). Bridging the Analog-Digital Divide: Enhancing Urban Models with Augmented Reality. *Journal of Digital Landscape Architecture*, (5), 366–373.
- Tommasi, C., Achille, C., Fassi, F., et al. (2016). From point cloud to BIM: A modelling challenge in the cultural heritage field. *International Archives of the Photogrammetry, Remote Sensing and Spatial Information Sciences*, XLI-B5, 429–436.
- Toparlar, Y., Blocken, B., Maiheu, B., & van Heijst, G. (2017). A review on the CFD analysis of urban microclimate. *Renewable and Sustainable Energy Reviews*, 80, 1613–1640.
- TU Dortmund. (2020). TU-Logo auf dem Mathetower wird zehn. Accessed on 22.07.2023 on: <https://www.tu-dortmund.de/nachrichtendetail/detail/tu-logo-auf-dem-mathetower-wird-zehn-5407/>
- TU Dortmund. (n.d.-a). Neubau Bibliothek: Aktuelles rund um Umzug, Standorte und Bestände. Accessed on 20.07.2023 on: <https://baublog.ub.tu-dortmund.de/>
- TU Dortmund. (n.d.-b). Neubau der Universitätsbibliothek. Accessed on 22.07.2023 on: <https://www.tu-dortmund.de/beschaefigte/campus/bauprojekte/neubau-der-universitaetsbibliothek/>
- TU Dortmund. (n.d.-c). Statistics: Students. Accessed on 27.05.2023 on: <https://www.tu-dortmund.de/en/university/information-material-downloads/statistics/students/?tabindex=1&cHash=4805cf4a8fbbe1620db87175814173d6>
- van Heerden, N. (2021). *BIM and 3D City Models as Input for Microclimate Simulation*. [Masterthesis]. Delft University of Technology.
- von der Hude, M. (2020). *Predictive analytics und data mining: Eine Einführung mit R*. Springer Vieweg.
- Vosselman, G., Gorte, B., Sithole, G., & Rabbani, T. (2004). Recognising structure in laser scanner point clouds. *International Archives of the Photogrammetry, Remote Sensing and Spatial Information Sciences*, 46(8), 33–38.
- Wadstein, M. (2019). Unreal Concepts - Updating Data From a Text File at Runtime (UE4). youtube, 26.11.2019. Accessed on 17.07.2023 on: <https://www.youtube.com/watch?v=zuJ2tjZW770>
- Wang, B., Xiangsheng, L., & Zhang, Y. (2022). *Internet of things and bds application*. Springer Nature Singapore Pte Ltd.
- Ward, K., Lauf, S., Kleinschmit, B., & Endlicher, W. (2016). Heat waves and urban heat islands in Europe: A review of relevant drivers. *The Science of The Total Environment*, 569-570, 527–539.
- Wiener Stadtwerke. (2011). Smart City: Begriff, Charakteristika und Beispiele. materialien der Wiener Stadtwerke zur nachhaltigen Entwicklung Nummer 7, Wien.

Ye, X., Du, J., Han, Y., Newman, G., Retchless, D., Zou, L., Ham, Y., & Cai, Z. (2023). Developing Human-Centered Urban Digital Twins for Community Infrastructure Resilience: A Research Agenda. *Journal of Planning Literature*, 38(2), 187–199.

A. LoRaWAN and Weather Sensors

A.1. Photos of Exact Gateway and Sensor Positions



Sensor 1 at the library's west facade



Sensor 2 at the library's north facade



Sensor 3 on the rooftop of the library



Sensor 4 at the library's south facade



Gateway on the library's rooftop

Installation of Gateway and End Devices (own illustration)

B. ENVI-met Input Data

B.1. ENVI-met Grid Rotation

Create Telescope Grid

Num Z cells: 74

Dim X(m): 1.0

Dim Y(m): 1.0

Dim Z(m): 1.0

Start Telescope Height: 60

Telescope: 20

Rotation(0°-360° anticlockwise) [0.0 North]: 349.1

OK Abbrechen

ENVI-met Counterclockwise Grid Rotation in Envimet INX plugin for SketchUp (Envimet INX plugin)

B.2. Facade and Roof Materials of the Basic Model (DB Manager)

Building IDs and Materials (own illustration)

Building ID	Building	ID Wall Construction	ID Wall Construction (Roof)
1	FoodFakultät+Gebäude	0251BG Burned Brick to Glass Ratio 50 to 50	0201ST Steel
3	Audimax	0200G4 Clear Float Glass	0202ST Steel
4	Bib	0200C6 Concrete to Glass Ratio 50 to 50	0200CO Default Concrete
(5)	CampusTreff+Gebäude	0230PG Plaster to Glass Ratio 70 to 30	0202ST Steel
6	CampusTreff	0200G4 Clear Float Glass	0200CO Default Concrete
7	EF50	0252CG Concrete to Glass 50 to 50	0200CO Default Concrete
8	FH-Dortmund	0252CG Concrete to Glass 50 to 50	0202ST Steel
9	FoodFakultät	0200G4 Clear Float Glass	0201ST Steel

Building IDs and Materials (own illustration)			
Building ID	Building	ID Wall Construction	ID Wall Construction (Roof)
11	H-Bahn-Nord	0200G4 Clear Float Glass	0200CO Default Concrete
12	H-Bahn-S	0200G4 Clear Float Glass	0202ST Steel
13	Journalistik	0230BG Burned Brick to Glass Ratio 70 to 30	0200CO Default Concrete
14	Mathetower	0251CG Concrete to Glass 50 to 50	0200CO Default Concrete
15	Mensabrücke	0200CO Default Concret	0200CO Default Concrete
16	Mensgebäude	0253CG Concrete to Glass 50 to 50	0200CO Default Concrete
17	Wohngebäude	0230BG Burned Brick to Glass Ratio 70 to 30	0200R1 Roofing: Tile
(18)	Wohnheim	0230PG Plaster to Glass Ratio 70 to 30	0200R1 Roofing: Tile
19	ZHB/CDI	0230PG Plaster to Glass Ratio 70 to 30	0202ST Steel
(20)	H-Bahn-Linie	0202ST Steel	0202ST Steel
21	Campus Treff Wohnhaus	like 5	like 5
22	Vogelpothsweg 118	like 5	like 5
23	Vogelpothsweg 108	like 18	like 18
24	Vogelpothsweg 114	like 18	like 18
25	Vogelpothsweg 94	like 18	like 18
26	Vogelpothsweg 100	like 18	like 18
27	Vogelpothsweg	like 18	like 18

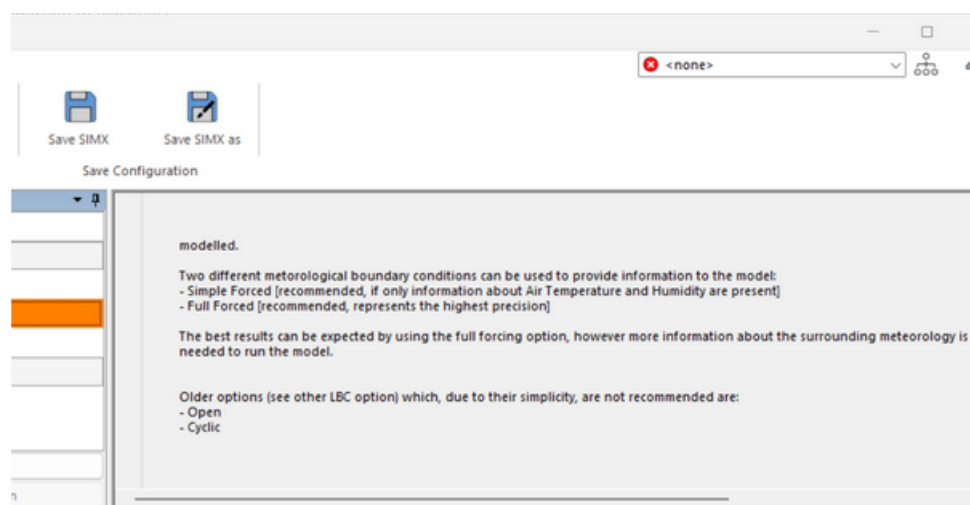
B.3. Soil Materials (DB Manager)

Soil Materials (own illustration)	
Soil	Material
Wege	0100PP LEGACY Pavement Concrete used/dirty
Asphalt	0100ST Asphalt Road

B.4. Simple Plants (DB Manager)

Plants (own illustration)	
Plant	Material
Grass	000001
Conifer 10m	0010SK
Conifer 12,5m	0011SK
Tree 5m very dense	0001SK
Tree 7,5m very dense	0002SK
Tree 10m very dense	0003SK
Tree 12,5m very dense	0004SK
Tree 15m very dense	0005SK
Tree 17,5m very dense	0006SK
Tree 20m very dense	0007SK
Tree 22,5m very dense	0008SK
Tree 25m very dense	0009SK

B.5. ENVI-guide Forcing Precision



Information on Meteorological Boundary Conditions in ENVI-guide V5.5.1 (ENVI-guide V5.5.1)

B.6. Local Weather Data

Weather Data (own illustration based on DTN data)

Date	Time	Clouds	Abs. Air Temperature [K]	Rel. Humidity [%]	Wind Speed [m/s]	Wind Direction [°]	Precipi- tation [mm]
31.05.2023	00:00:00		285	86	2,1	60	0
31.05.2023	00:30:00		285	87	2,1	60	0
31.05.2023	01:00:00		285	89	2,1	53	0
31.05.2023	01:30:00		284	89	2,1	57	0
31.05.2023	02:00:00		284	90	2,1	60	0
31.05.2023	02:30:00		284	92	2,1	53	0
31.05.2023	03:00:00		283	93	1,7	47	0
31.05.2023	03:30:00		283	95	1,7	40	0
31.05.2023	04:00:00		283	95	1,7	33	0
31.05.2023	04:30:00		282	96	1,7	33	0
31.05.2023	05:00:00		282	97	1,7	43	0
31.05.2023	05:30:00		282	97	1,7	50	0
31.05.2023	06:00:00		283	97	1,3	53	0
31.05.2023	06:30:00		284	92	1,3	47	0
31.05.2023	07:00:00		285	88	1,3	43	0
31.05.2023	07:30:00		286	85	2,1	47	0
31.05.2023	08:00:00		287	80	2,4	40	0
31.05.2023	08:30:00		288	78	2,8	43	0
31.05.2023	09:00:00		289	75	2,4	43	0
31.05.2023	09:30:00		290	70	2,8	57	0
31.05.2023	10:00:00		291	66	2,4	63	0
31.05.2023	10:30:00		292	63	2,4	50	0
31.05.2023	11:00:00		293	59	2,4	50	0
31.05.2023	11:30:00		294	55	2,4	53	0
31.05.2023	12:00:00		295	50	2,8	40	0
31.05.2023	12:30:00		295	45	3,3	53	0
31.05.2023	13:00:00		296	45	3,3	47	0
31.05.2023	13:30:00		296	43	3,6	57	0
31.05.2023	14:00:00		296	45	3,6	47	0
31.05.2023	14:30:00		296	45	3,1	60	0
31.05.2023	15:00:00		297	45	3,3	60	0
31.05.2023	15:30:00		297	46	3,1	43	0

Weather Data (own illustration based on DTN data)

Date	Time	Clouds	Abs. Air Temperature [K]	Rel. Humidity [%]	Wind Speed [m/s]	Wind Direction [°]	Precipi- tation [mm]
31.05.2023	16:00:00		297	46	3,3	47	0
31.05.2023	16:30:00		297	46	3,3	57	0
31.05.2023	17:00:00		296	47	3,3	43	0
31.05.2023	17:30:00		297	47	3,6	40	0
31.05.2023	18:00:00		296	48	3,3	43	0
31.05.2023	18:30:00		296	49	3,3	30	0
31.05.2023	19:00:00		296	48	3,3	50	0
31.05.2023	19:30:00		295	48	3,3	40	0
31.05.2023	20:00:00		294	49	3,3	40	0
31.05.2023	20:30:00		294	50	3,1	43	0
31.05.2023	21:00:00		293	54	2,4	40	0
31.05.2023	21:30:00		292	57	2,4	33	0
31.05.2023	22:00:00		291	62	2,1	37	0
31.05.2023	22:30:00		290	66	2,1	30	0
31.05.2023	23:00:00		290	67	2,4	27	0
31.05.2023	23:30:00		290	67	2,8	30	0

C. Grid Cell Coordinates for Verification

Grid Coordinates of estimated sensor locations in the model

Grid Coordinates of Sensor Locations in INX1 (own illustration)

Sensor	Grid Cell (x-y-z)	Height [m]
1	53-89-17	13,5
2	113-114-17	13,5
3	72-96-23	19,5
4	73-52-17	13,5

Grid Coordinates of Sensor Locations in INX2 (own illustration)

Sensor	Grid Cell (x-y-z)	Height [m]
1	54-89-17	13,5
2	113-114-17	13,5
3	72-96-23	14,5
4	73-52-17	13,5

Grid Coordinates of Sensor Locations in INX3 (own illustration)

Sensor	Grid Cell (x-y-z)	Height [m]
1	10-18-6	12,5
2	23-23-6	12,5
3	14-19-8	12,5
4	14-10-6	12,5

Grid Coordinates of Sensor Locations in INX4 (own illustration)

Sensor	Grid Cell (x-y-z)	Height [m]
1	35-51-6	12,5
2	47-56-6	12,5
3	38-52-8	22,5
4	39-43-6	12,5

Grid Coordinates of Sensor Locations in INX5 (own illustration)

Sensor	Grid Cell (x-y-z)	Height [m]
1	95-131-8	13,5
2	125-143-8	13,5
3	104-134-10	19,5
4	105-111-8	13,5

D. ENVI-met Simulation Results

Results of INX1 (narrow area, 1x1x1, LoD3) (own illustration)

Datetime	S1_West T (°C)	S1_West RH (%)	S2_Nord T (°C)	S2_Nord RH (%)	S3_Roof T (°C)	S3_Roof RH (%)	S4_South T (°C)	S4_South RH (%)
0 2023-05-31 01:00:00	11,84	88,68	11,86	88,77	11,93	88,27	12,06	87,62
1 2023-05-31 02:00:00	11,05	88,47	10,81	89,94	11,01	88,98	10,97	88,91
2 2023-05-31 03:00:00	9,90	91,60	9,88	92,41	9,79	92,30	10,25	89,85
3 2023-05-31 04:00:00	9,65	94,46	9,77	94,87	9,64	94,74	10,22	91,59
4 2023-05-31 05:00:00	9,07	94,53	8,98	95,89	9,01	95,20	9,38	93,01
5 2023-05-31 06:00:00	10,54	93,15	10,15	95,66	10,24	94,60	10,54	92,30
6 2023-05-31 07:00:00	12,40	87,41	12,32	87,41	12,44	85,90	13,35	81,54
7 2023-05-31 08:00:00	14,09	81,37	14,18	81,37	14,34	79,14	14,56	77,31

D ENVI-MET SIMULATION RESULTS

Results of INX2 (narrow area, 1x1x1, LoD2) (own illustration)

	Datetime	S1_West T (°C)	S1_West RH (%)	S2_Nord T (°C)	S2_Nord RH (%)	S3_Roof T (°C)	S3_Roof RH (%)	S4_South T (°C)	S4_South RH (%)
0	2023-05-31 01:00:00	11,78	89,02	11,86	88,74	11,91	88,37	11,94	88,37
1	2023-05-31 02:00:00	10,92	89,22	10,83	89,85	11,00	89,04	10,87	89,59
2	2023-05-31 03:00:00	9,83	91,10	9,91	92,22	9,81	92,27	9,91	91,99
3	2023-05-31 04:00:00	9,63	94,62	9,81	94,69	9,66	94,68	9,90	93,72
4	2023-05-31 05:00:00	8,99	95,10	9,01	95,61	9,02	95,23	9,04	95,13
5	2023-05-31 06:00:00	10,23	94,59	10,18	95,50	10,20	94,84	10,23	94,29
6	2023-05-31 07:00:00	12,29	87,99	12,31	86,97	12,29	86,44	12,80	84,42
7	2023-05-31 08:00:00	14,05	81,58	14,18	79,59	14,17	79,78	14,38	78,34
8	2023-05-31 09:00:00	16,04	76,54	16,22	74,50	16,24	74,24	16,35	73,67
9	2023-05-31 10:00:00	18,53	64,70	18,23	65,89	18,23	64,65	18,66	64,09
10	2023-05-31 11:00:00	20,27	60,09	20,24	58,95	20,25	58,52	20,151	57,59
11	2023-05-31 12:00:00	22,05	51,32	22,11	49,91	22,08	50,64	22,27	49,36
12	2023-05-31 13:00:00	23,06	45,42	23,12	44,75	23,13	44,76	23,13	44,63
13	2023-05-31 14:00:00	23,06	45,08	23,04	44,82	23,08	44,74	23,06	44,70
14	2023-05-31 15:00:00	24,23	44,41	23,89	45,26	24,02	44,63	23,99	44,88
15	2023-05-31 16:00:00	23,90	46,32	23,84	46,82	23,86	46,29	23,85	46,20
16	2023-05-31 17:00:00	22,81	47,41	22,79	47,28	22,78	47,44	22,76	47,41
17	2023-05-31 18:00:00	22,68	48,65	22,72	48,46	22,70	48,54	22,65	48,69
18	2023-05-31 19:00:00	22,58	48,83	22,61	48,73	22,73	48,38	22,56	48,89
19	2023-05-31 20:00:00	20,55	49,97	20,67	49,59	20,61	49,78	20,65	49,67
20	2023-05-31 21:00:00	19,45	55,44	19,64	54,74	19,53	55,14	19,46	55,40
21	2023-05-31 22:00:00	17,55	63,25	17,71	62,56	17,50	63,44	17,50	63,44
22	2023-05-31 23:00:00	16,54	68,39	16,59	68,15	16,55	68,34	16,63	67,98

Results of INX3 (narrow area, 5x5x5, LoD2) (own illustration)

	Datetime	S1_West T (°C)	S1_West RH (%)	S2_Nord T (°C)	S2_Nord RH (%)	S3_Roof T (°C)	S3_Roof RH (%)	S4_South T (°C)	S4_South RH (%)
0	2023-05-31 01:00:00	11,67	89,71	11,7	89,53	11,70	88,71	11,91	88,48
1	2023-05-31 02:00:00	10,75	90,23	10,66	90,6	10,66	89,47	10,83	89,70
2	2023-05-31 03:00:00	9,63	93,29	9,7	93,12	9,70	92,67	9,86	92,09
3	2023-05-31 04:00:00	9,55	95,35	9,62	95,19	9,62	94,98	9,79	94,07
4	2023-05-31 05:00:00	8,69	96,62	8,7	96,71	8,70	96,24	8,90	95,59
5	2023-05-31 06:00:00	9,96	95,87	9,63	96,77	9,63	95,56	10,00	94,94
6	2023-05-31 07:00:00	11,73	89,07	11,76	88,56	11,76	87,40	12,20	86,14
7	2023-05-31 08:00:00	13,79	81,82	13,82	80,92	13,82	79,96	14,18	79,06
8	2023-05-31 09:00:00	15,79	77,00	15,81	76,1	15,81	74,85	16,18	74,29
9	2023-05-31 10:00:00	18,09	67,30	17,58	68,36	17,58	65,09	18,23	65,58
10	2023-05-31 11:00:00	19,75	61,80	19,66	60,77	19,66	58,96	20,24	58,53
11	2023-05-31 12:00:00	21,56	52,65	21,67	51,34	21,67	45,44	22,96	50,00
12	2023-05-31 13:00:00	22,64	46,80	22,61	46,05	22,61	46,06	22,96	45,07
13	2023-05-31 14:00:00	22,67	46,44	22,64	45,9	22,65	45,07	22,91	45,07
14	2023-05-31 15:00:00	23,84	45,80	23,5	46,36	23,50	44,83	23,77	45,44
15	2023-05-31 16:00:00	23,54	47,49	23,56	47,03	23,56	46,24	23,65	46,70
16	2023-05-31 17:00:00	22,51	48,40	22,6	47,85	22,60	47,32	22,65	47,70
17	2023-05-31 18:00:00	22,43	49,54	22,56	48,94	22,56	48,38	22,54	49,02
18	2023-05-31 19:00:00	22,42	49,46	22,51	49,04	22,51	48,35	22,47	49,20
19	2023-05-31 20:00:00	20,56	50,65	20,59	49,86	20,59	49,54	20,56	49,94
20	2023-05-31 21:00:00	19,38	55,88	19,49	55,27	19,49	54,70	19,38	55,69
21	2023-05-31 22:00:00	17,42	64,09	17,52	63,35	17,52	62,80	17,42	63,79
22	2023-05-31 23:00:00	16,42	68,97	16,48	68,63	16,48	67,96	16,55	68,35

D ENVI-MET SIMULATION RESULTS

Results of INX4 (extended area, 5x5x5, LoD2) (own illustration)

	Datetime	S1_West T (°C)	S1_West RH (%)	S2_Nord T (°C)	S2_Nord RH (%)	S3_Roof T (°C)	S3_Roof RH (%)	S4_South T (°C)	S4_South RH (%)
0	2023-05-31 01:00:00	11,57	89,92	11,62	90,13	11,73	89,42	11,80	89,11
1	2023-05-31 02:00:00	10,73	90,12	10,70	90,54	10,85	89,84	10,74	90,12
2	2023-05-31 03:00:00	9,63	92,66	9,41	93,73	9,60	93,12	9,67	92,80
3	2023-05-31 04:00:00	9,59	94,24	9,16	95,69	9,53	94,85	9,59	94,50
4	2023-05-31 05:00:00	8,58	96,05	8,49	96,89	8,70	96,39	8,62	96,08
5	2023-05-31 06:00:00	9,90	96,13	9,80	96,63	9,92	96,27	9,93	96,05
6	2023-05-31 07:00:00	11,83	88,03	11,87	88,64	11,95	87,80	11,97	87,69
7	2023-05-31 08:00:00	13,90	82,14	14,19	81,99	14,06	80,85	14,35	80,22
8	2023-05-31 09:00:00	16,03	77,16	16,44	76,42	16,19	75,60	16,52	75,14
9	2023-05-31 10:00:00	18,43	65,51	18,53	66,21	18,41	65,27	18,70	65,90
10	2023-05-31 11:00:00	20,19	60,59	20,42	60,43	20,29	59,39	20,57	59,23
11	2023-05-31 12:00:00	21,84	52,72	22,01	52,79	21,97	51,60	22,28	50,97
12	2023-05-31 13:00:00	22,91	46,55	23,19	45,76	23,09	45,35	23,33	45,26
13	2023-05-31 14:00:00	22,93	45,92	23,10	45,42	23,05	45,15	23,25	44,86
14	2023-05-31 15:00:00	24,18	44,58	24,10	44,94	24,14	44,51	24,29	44,57
15	2023-05-31 16:00:00	23,62	47,26	23,57	47,38	23,74	46,68	23,76	46,81
16	2023-05-31 17:00:00	22,53	48,27	22,33	48,85	22,61	47,90	22,60	48,04
17	2023-05-31 18:00:00	22,40	49,51	22,23	50,01	22,54	49,04	22,37	49,58
18	2023-05-31 19:00:00	22,37	49,51	22,3	49,72	22,57	48,89	22,19	50,08
19	2023-05-31 20:00:00	20,26	50,93	20,11	51,43	20,45	50,31	20,28	50,88
20	2023-05-31 21:00:00	19,59	54,96	19,43	55,49	19,59	54,95	19,58	55,00
21	2023-05-31 22:00:00	17,57	63,18	17,31	64,21	17,56	63,21	17,50	63,44
22	2023-05-31 23:00:00	16,24	69,66	15,99	70,69	16,45	68,74	16,43	68,83

Results of INX5 (extended area, 2x2x3, LoD2) (own illustration)

	Datetime	S1_West T (°C)	S1_West RH (%)	S2_Nord T (°C)	S2_Nord RH (%)	S3_Roof T (°C)	S3_Roof RH (%)	S4_South T (°C)	S4_South RH (%)
0	2023-05-31 01:00:00	11,57	89,89	11,68	90,07	11,83	89,02	11,79	89,11
1	2023-05-31 02:00:00	10,80	89,72	10,74	90,47	10,94	89,39	10,70	90,17
2	2023-05-31 03:00:00	9,66	92,28	9,38	93,87	9,60	92,94	9,69	92,46
3	2023-05-31 04:00:00	9,68	93,75	9,05	95,94	9,54	94,69	9,61	94,11
4	2023-05-31 05:00:00	8,67	95,51	8,58	96,77	8,79	95,90	8,63	95,73
5	2023-05-31 06:00:00	10,03	95,62	9,93	96,44	10,05	95,79	10,01	95,78
6	2023-05-31 07:00:00	12,02	87,79	12,09	88,62	12,16	87,32	12,15	87,48
7	2023-05-31 08:00:00	13,96	82,42	14,37	82,03	14,22	80,71	14,48	80,41
8	2023-05-31 09:00:00	16,17	77,45	16,70	76,20	16,47	75,12	16,71	75,30
9	2023-05-31 10:00:00	18,65	65,27	18,64	65,95	18,60	64,86	19,07	65,58
10	2023-05-31 11:00:00	20,31	60,50	20,68	59,50	20,53	58,47	20,84	59,00
11	2023-05-31 12:00:00	22,03	52,64	22,42	52,00	21,26	51,21	22,47	50,65
12	2023-05-31 13:00:00	23,13	46,38	23,55	44,72	23,40	44,59	23,50	45,10
13	2023-05-31 14:00:00	23,09	45,87	23,41	44,55	23,30	44,50	23,40	44,68
14	2023-05-31 15:00:00	24,32	44,30	24,24	44,49	24,31	44,06	24,47	44,39
15	2023-05-31 16:00:00	23,60	47,48	23,72	46,98	23,83	46,47	23,78	46,93
16	2023-05-31 17:00:00	22,51	48,44	22,42	48,71	22,66	47,86	22,63	48,10
17	2023-05-31 18:00:00	22,38	49,65	22,31	49,82	22,56	49,01	22,32	49,85
18	2023-05-31 19:00:00	22,39	49,65	22,40	49,41	22,63	48,70	22,05	50,54
19	2023-05-31 20:00:00	20,22	51,07	20,13	51,36	20,44	50,40	20,16	51,28
20	2023-05-31 21:00:00	19,57	55,03	19,43	55,52	19,59	54,96	19,52	55,19
21	2023-05-31 22:00:00	17,57	63,17	17,33	64,10	17,57	63,15	17,47	63,58
22	2023-05-31 23:00:00	16,22	69,75	15,96	70,81	16,46	68,66	16,38	69,06

D ENVI-MET SIMULATION RESULTS

Sensor data used for verification (own illustration)

	Datetime	Sensor	Air Temperature (°C)	Relative Humidity (%)
Sensor 1 (West facade)				
0	2023-05-31 00:00:00	Sensor1_West	16.23	62.97
1	2023-05-31 01:00:00	Sensor1_West	15.43	65.67
2	2023-05-31 02:00:00	Sensor1_West	14.52	69.17
3	2023-05-31 03:00:00	Sensor1_West	13.95	71.4
4	2023-05-31 04:00:00	Sensor1_West	13.15	74.2
5	2023-05-31 05:00:00	Sensor1_West	12.68	75.72
6	2023-05-31 06:00:00	Sensor1_West	12.73	76.07
7	2023-05-31 07:00:00	Sensor1_West	13.32	74.87
8	2023-05-31 08:00:00	Sensor1_West	14.23	72.2
9	2023-05-31 09:00:00	Sensor1_West	15.45	68.38
10	2023-05-31 10:00:00	Sensor1_West	16.98	62.33
11	2023-05-31 11:00:00	Sensor1_West	18.7	52.93
12	2023-05-31 12:00:00	Sensor1_West	20.7	41.67
13	2023-05-31 13:00:00	Sensor1_West	22.8	36.13
14	2023-05-31 14:00:00	Sensor1_West	24.37	34.93
15	2023-05-31 15:00:00	Sensor1_West	26.33	34.12
16	2023-05-31 16:00:00	Sensor1_West	27.72	32.05
17	2023-05-31 17:00:00	Sensor1_West	27.48	33.55
18	2023-05-31 18:00:00	Sensor1_West	27.53	33.48
19	2023-05-31 19:00:00	Sensor1_West	27.32	32.85
20	2023-05-31 20:00:00	Sensor1_West	26.38	33.68
21	2023-05-31 21:00:00	Sensor1_West	24.77	37.15
22	2023-05-31 22:00:00	Sensor1_West	23.25	40.78
23	2023-05-31 23:00:00	Sensor1_West	21.62	46.28
Sensor 2 (North facade)				
0	2023-05-31 00:00:00	Sensor2_North	14.63	70.23
1	2023-05-31 01:00:00	Sensor2_North	14.15	71.92
2	2023-05-31 02:00:00	Sensor2_North	13.63	73.98
3	2023-05-31 03:00:00	Sensor2_North	13.17	75.68
4	2023-05-31 04:00:00	Sensor2_North	12.65	77.68
5	2023-05-31 05:00:00	Sensor2_North	12.22	79.12
6	2023-05-31 06:00:00	Sensor2_North	12.37	78.78
7	2023-05-31 07:00:00	Sensor2_North	13.35	75.82

8	2023-05-31 08:00:00	Sensor2_North	14.43	72.47
9	2023-05-31 09:00:00	Sensor2_North	15.82	68.15
10	2023-05-31 10:00:00	Sensor2_North	17.38	61.92
11	2023-05-31 11:00:00	Sensor2_North	18.98	53.57
12	2023-05-31 12:00:00	Sensor2_North	20.35	43.42
13	2023-05-31 13:00:00	Sensor2_North	21.27	40.23
14	2023-05-31 14:00:00	Sensor2_North	22.1	40.23
15	2023-05-31 15:00:00	Sensor2_North	22.78	42.02
16	2023-05-31 16:00:00	Sensor2_North	23.25	41.1
17	2023-05-31 17:00:00	Sensor2_North	23.52	42.33
18	2023-05-31 18:00:00	Sensor2_North	24.5	40.05
19	2023-05-31 19:00:00	Sensor2_North	23.38	40.88
20	2023-05-31 20:00:00	Sensor2_North	22.57	41.93
21	2023-05-31 21:00:00	Sensor2_North	21.77	44.28
22	2023-05-31 22:00:00	Sensor2_North	20.82	47.52
23	2023-05-31 23:00:00	Sensor2_North	19.68	52.78
0	2023-05-31 00:00:00	Sensor3_Roof	12.62	78.37

Sensor 3 (Roof)

0	2023-05-31 01:00:00	Sensor3_Roof	11.97	81.43
1	2023-05-31 02:00:00	Sensor3_Roof	11.2	85.15
2	2023-05-31 03:00:00	Sensor3_Roof	10.6	87.97
3	2023-05-31 04:00:00	Sensor3_Roof	9.87	91.03
4	2023-05-31 05:00:00	Sensor3_Roof	9.6	92.5
5	2023-05-31 06:00:00	Sensor3_Roof	10.83	88.23
6	2023-05-31 07:00:00	Sensor3_Roof	15.58	69.63
7	2023-05-31 08:00:00	Sensor3_Roof	22.18	46.8
8	2023-05-31 09:00:00	Sensor3_Roof	24.83	40.57
9	2023-05-31 10:00:00	Sensor3_Roof	27.37	34.55
10	2023-05-31 11:00:00	Sensor3_Roof	29.65	29.18
11	2023-05-31 12:00:00	Sensor3_Roof	28.93	26.37
12	2023-05-31 13:00:00	Sensor3_Roof	30.08	24.43
13	2023-05-31 14:00:00	Sensor3_Roof	31.27	24.4
14	2023-05-31 15:00:00	Sensor3_Roof	31.17	26.03
15	2023-05-31 16:00:00	Sensor3_Roof	32.47	25
16	2023-05-31 17:00:00	Sensor3_Roof	30.25	29.02
17	2023-05-31 18:00:00	Sensor3_Roof	26.02	35.9
18	2023-05-31 19:00:00	Sensor3_Roof	24.12	38.05
19	2023-05-31 20:00:00	Sensor3_Roof	22.72	40.6

D ENVI-MET SIMULATION RESULTS

20	2023-05-31 21:00:00	Sensor3_Roof	20.75	45.72
21	2023-05-31 22:00:00	Sensor3_Roof	19	51.52
22	2023-05-31 23:00:00	Sensor3_Roof	17.7	57.93

Sensor 4 (South facade)

0	2023-05-31 00:00:00	Sensor4_South	15.27	66.88
1	2023-05-31 01:00:00	Sensor4_South	14.78	68.77
2	2023-05-31 02:00:00	Sensor4_South	14.07	71.82
3	2023-05-31 03:00:00	Sensor4_South	13.6	73.45
4	2023-05-31 04:00:00	Sensor4_South	12.95	75.83
5	2023-05-31 05:00:00	Sensor4_South	12.44	77.54
6	2023-05-31 06:00:00	Sensor4_South	12.58	77.7
7	2023-05-31 07:00:00	Sensor4_South	14.12	73.06
8	2023-05-31 08:00:00	Sensor4_South	17.52	61.6
9	2023-05-31 09:00:00	Sensor4_South	19.63	54.2
10	2023-05-31 10:00:00	Sensor4_South	21.28	49.5
11	2023-05-31 11:00:00	Sensor4_South	22.32	44.98
12	2023-05-31 12:00:00	Sensor4_South	22.77	36.98
13	2023-05-31 13:00:00	Sensor4_South	23.27	35.63
14	2023-05-31 14:00:00	Sensor4_South	24.58	34.88
15	2023-05-31 15:00:00	Sensor4_South	25.43	34.98
16	2023-05-31 16:00:00	Sensor4_South	25.02	36.4
17	2023-05-31 17:00:00	Sensor4_South	24.75	38.62
18	2023-05-31 18:00:00	Sensor4_South	24.1	39.75
19	2023-05-31 19:00:00	Sensor4_South	23.75	39.25
20	2023-05-31 20:00:00	Sensor4_South	23.08	39.68
21	2023-05-31 21:00:00	Sensor4_South	22.45	41.97
22	2023-05-31 22:00:00	Sensor4_South	21.55	44.88
23	2023-05-31 23:00:00	Sensor4_South	20.66	49
